CR-158934

DESIGN DEFINITION STUDY OF THE EARTH RADIATION BUDGET SATELLITE SYSTEM

FINAL REPORT
contract no.
NAS 1-14538

DEPARTMENT OF ATMOSPHERIC SCIENCE
COLORADO STATE UNIVERSITY
FORT COLLINS, COLORADO

ERRATA TO CR-158934

1. P. 3-10, 3-12

The quantity Ω should be replaced by the quantity H* where H* is the normalized irradiance at the entrance aperture from a Lambertian scene, the radiance from which has been arbitrarily set to unity. The conclusions regarding the signal ratios on p. 3-12 are, however, correct.

2. P. 3-24 Change "target height" to "tangent height"

3. P. 3-27 Para. 3.2.3, item (1) spelling,
Change Pycheliometer to Pyrheliometer

4. P. 3-55 Para. 3.3.6 Change "with specular reflectance....."
to "without specular reflectance....."

5. P. 4-2 Table 4-1 Linearity component (see pp. 4-28, 29) omitted. This should be $\pm$ 0.7 W/M^2. The totals are correct.

NASA CR-158934

FINAL REPORT

DESIGN DEFINITION STUDY OF THE EARTH RADIATION BUDGET SATELLITE SYSTEM

by

T.H. Vonder Haar, Principal Investigator
Department of Atmospheric Science
Colorado State University

and

W.H. Wallschlaeger
Ball Aerospace Systems Division

Contract NAS 1-14538
NASA, Langley Research Center
J. Cooper, Technical Monitor

August, 1978

With contributions by co-investigators of Contract NAS 1-14538, J. Hickey, Eppley Laboratories, Inc., D. Hilleary, H. Jacobowitz, W. Smith and L. Stowe, National Oceanographic and Atmospheric Administration, and E. Vande Noord, Ball Aerospace Systems Division.

PREFACE

This report is the culmination of a study effort for the design definition of an Earth Radiation Budget Satellite System (ERBSS) instrument concept which began in 1976. This effort has undergone redirection on several occasions on the basis of new inputs, mission redefinitions, and modified constraints and requirements. The objective of this report is to present the results of approximately two years of work. Included are the instrument design concept, present mission objectives, the design constraints and requirements which have evolved, analyses pertaining to error budgets, and a consideration of instrument testing requirements.

In addition to those listed on the title page, the authors would like to gratefully acknowledge the assistance of Mr. C. Woerner, Mr. R. Babcock, Mr. J. Cooper, Dr. G.L. Smith and Mr. E. Harrison of NASA, Langley, Mr. M. Luther of LTV, Dr. R. Willson of NASA, JPL, Dr. R. Curran of NASA, Goddard, Mr. R. Maschhoff of Gulton and the rest of the participating BASD staff.

During this study, our colleague Don Hilleary of NOAA, NESS passed away. His contributions to the instrument configurations were major and we have missed having the benefits of his experience and expertise. This report is dedicated to his memory.

TABLE OF CONTENTS

ILLUSTRATIONS

ILLUSTRATIONS (continued)

TABLES

TABLES (continued)

Section 1
INTRODUCTION

Of the solar energy incident upon Earth, a portion is reflected to space while the remainder is absorbed by the Earth and its atmosphere. The absorbed energy provides the bulk of the thermal energy to the Earth and its atmospheric system and ultimately returns to space as emitted or infrared radiation. To maintain the thermal equilibrium of the Earth, these incident, reflected and emitted components of the Earth's radiation budget must be in balance. Meteorologists and climatologists agree that the spatial distributions of the Earth radiant energy budget and the temporal variations in these distributions are the fundamental physical drivers of climate. The mission for the Earth Radiation Budget Satellite System (ERBSS) instruments then is the measurement of the radiation budget components, i.e., the incoming solar radiation, terrestrially reflected shortwave radiation, and the terrestrially emitted longwave radiation. Measurements made by the ERBSS instruments from a three satellite system* will provide monthly averages of the radiation components on various spatial and temporal scales. Areas of localized warming (positive net radiation) or cooling (negative net radiation) represent the energy sources and sinks that drive the atmospheric and oceanic circulations. These measurements are expected to provide improved understanding of climate and possible projections of climate trends leading to improved management, planning, and utilization of food supplies and natural resources.

The major portion of the studies necessary to characterize instrument system concepts have now been accomplished. Under the direction of the NASA Langley Research Center, Colorado State University and its subcontractor, Ball Aerospace Systems Division (BASD), have completed design definition studies of the ERBSS instrument system. The results of these studies, which provide a basis for the generation of the conceptual instrument design, are contained in this report. Section 2 of this report is a review of the overall mission requirements, guidelines and constraints imposed on a scientific or a practical

*"Sampling Analysis for the Earth Radiation Budget Satellite System Mission Based on Orbital Coverage and Cloud Variability", E.F. Harrison, NASA Langley Research Center.

basis. The focus of the report, i.e., the description of the conceptual instrument systems design, is found in Section 3. The results of various instrument analyses are found in Section 4, while Section 5 includes system or component level testing guidelines, recommendations, or considerations.

The basic ERBSS instrument concept which has emerged from the studies contains eight sensor channels included in two instrument assemblies as illustrated by Figures 1-1 and 1-2. The two assemblies, referred to as the Non-Scanning Instrument and the Scanning Instrument, will be included in the payloads of three orbiting satellites. Two of these will be in the TIROS-N series, probably those designated NOAA-F and NOAA-G, and will operate in sun-synchronous, 98° inclined orbits with equatorial crossings at 0730 and 1530 hours. The orbital altitudes of the two TIROS-N spacecraft will be 833 KM while the third spacecraft, designated ERBS-A, will fly the ERBSS instruments in a lower 600 KM orbit at a lower inclination angle; probably about 56°. This spacecraft will be a version of the AEM series, modified for Shuttle launch. Figure 1-3 illustrates the three satellite mission coverage while Figure 1-4 is an artist's concept of the ERBS-A/AEM spacecraft.

Two of the four Earth viewing channels in the Non-Scanning Assembly have a wide field of view (WFOV) for viewing the Earth disc from limb to limb. The other two channels have a medium field of view (MFOV) for viewing a 10° Earth central angle (ECA). The WFOV channels measure an area of the Earth's surface with a diameter of approximately 5000 to 6000 KM, while the MFOV channels measure an area 1100 KM in diameter; a footprint approximately the size of Texas. One of the WFOV channels and one of the MFOV channels are filtered for response only to shortwave, i.e., 0.2 to 5 micrometers, radiation. The other two channels are unfiltered and measure the total of the emitted and reflected radiation. The emitted component is determined by subtraction of the shortwave measurement from the total measurement. A feature of the design is the ability of the four Earth looking channels to be periodically rotated for a solar calibration or calibration of the total channels by internal blackbody targets.

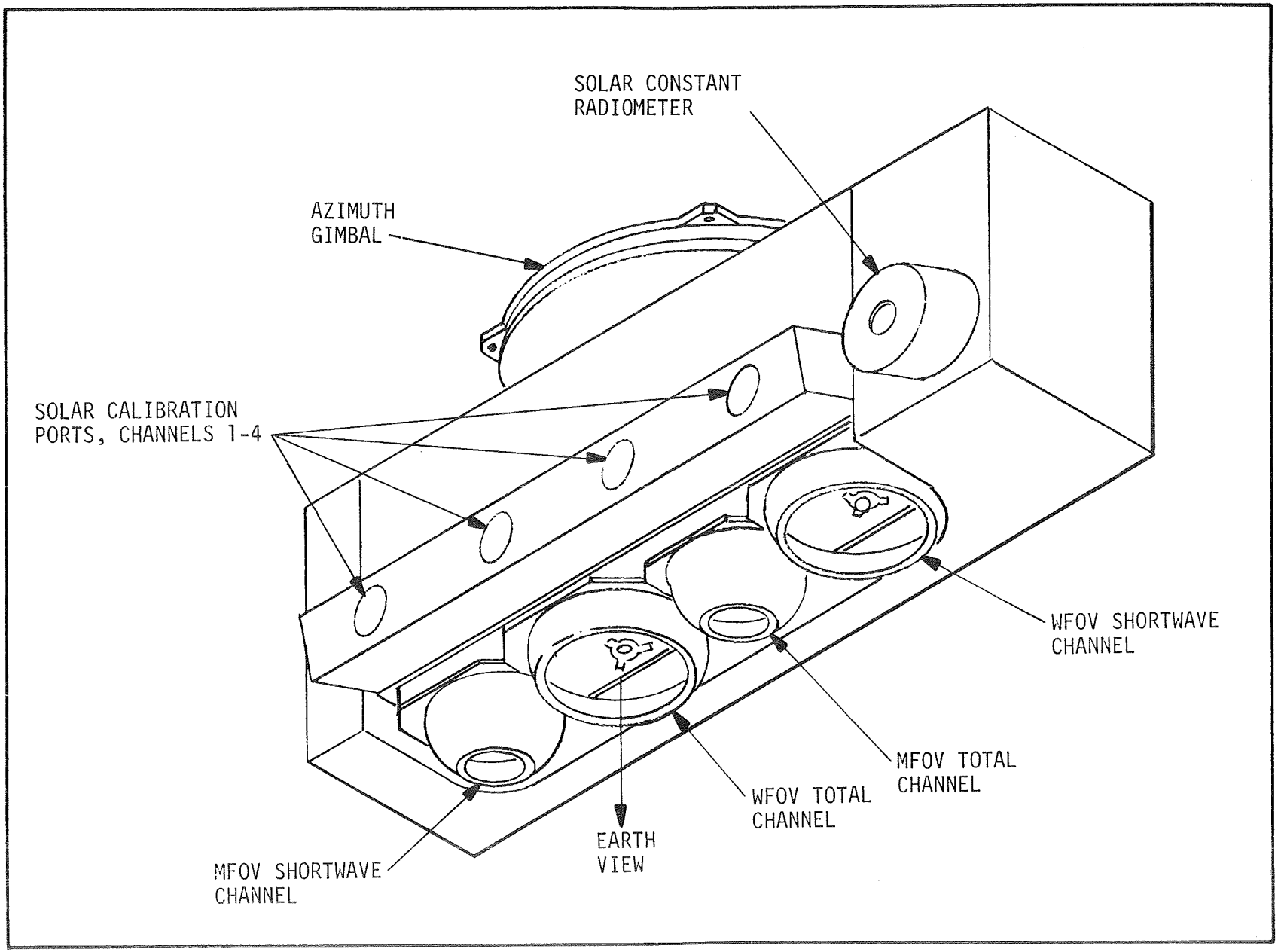

FIGURE 1-1 ERBSS NON-SCANNING INSTRUMENT

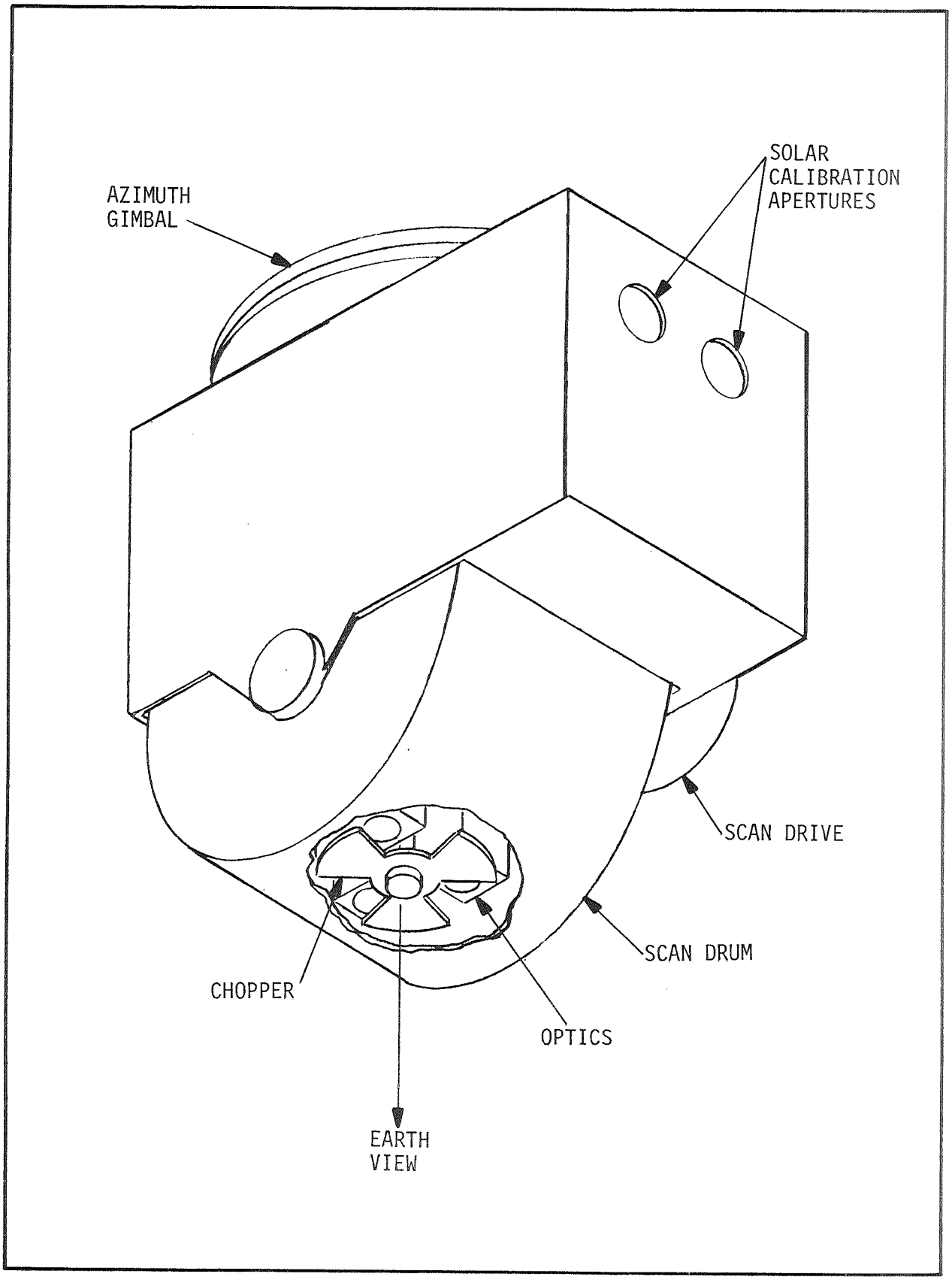

FIGURE 1-2 ERBSS SCANNING INSTRUMENT

Figure 1-3 ERBSS THREE SATELLITE SIMULTANEOUS EARTH COVERAGE

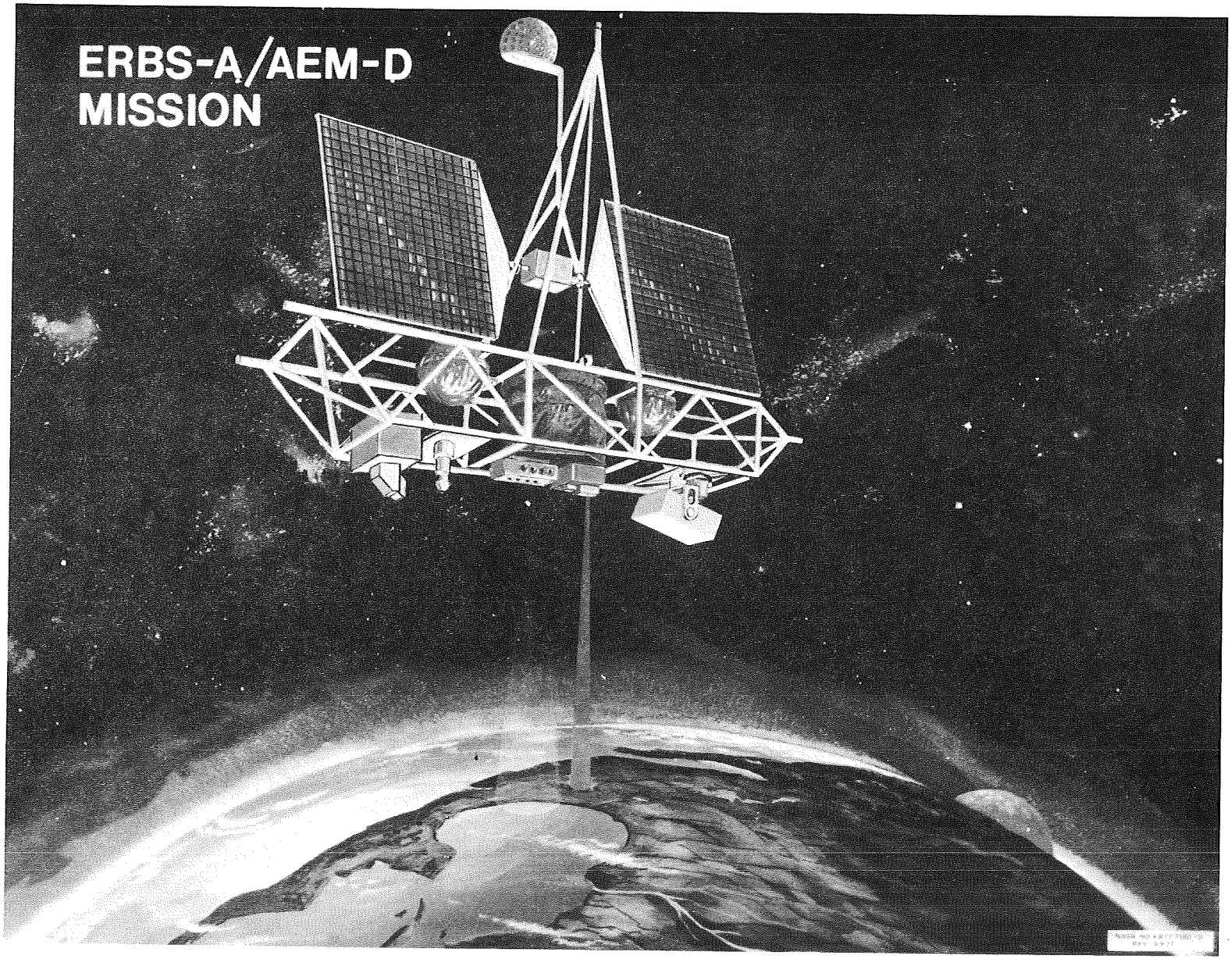

Figure 1-4 ERBSS-A/AEM SPACECRAFT

During solar calibration the four Earth looking channels have a common field of view with the fifth channel, the solar constant radiometer. This channel is a cavity radiometer which may be operated in the active mode. It serves as a reference for the other ERBSS channels during solar calibration. Channels 6, 7, and 8 are contained in the cross track Scanning Instrument. The three-degree field of view of these channels has an Earth footprint (at nadir) of an approximately 45 kilometer diameter for localized measurements. Channel 6 responds to shortwave energy (0.2 to 5 micrometers), while co-registered Channel 7 measures longwave energy (approximately 5 μm and beyond). The eighth channel* responds to radiation at 1.64 micrometers and is used for discrimination of clouds from snow or ice fields. However, the optimum spectral interval for Channel 8 is still under study (see "System Implementation for Earth Radiation Budget Satellite System", Cooper and Woerner, Third Conference on Atmospheric Radiation of the American Meteorological Society, June 28-30, 1978.

This instrument design definition study has directly benefited from previous studies conducted by the Langley Research Center of NASA. An experiment definition study of a concept called Radiation Climate Radiometer (RCR) or Solar and Earth Radiation Monitor (SERM) under Contract NAS 1-13501 with Colorado State University was conducted by a team of scientists and engineers from CSU, NOAA/NESS, Eppley Laboratories, Inc., and BASD. Additionally, the ERB instrument, flown on Nimbus-6 and to be flown on Nimbus-G, provided concepts and results useful in formulating the ERBSS requirements, design concepts and test requirements contained in this report.

*Channel 8 as baselined for this study.

Section 2
ERBSS MISSION REQUIREMENTS

The mission requirements for ERBSS can be categorized as scientific inputs concerning accuracy, reproducibility, and periodicity; instrument requirements based on the statement of work for this study; and spacecraft interface constraints. Scientific requirements for ERBSS have been accumulated in numerous publications. Significant to this report are NASA CR-132407, "An Experiment Definition Study for a Radiation Climate Radiometer", November 1975; NASA TMS-72776, "Earth Radiation Budget Satellite System Studies", May, 1977; and the "Proposed NASA Contribution to the Climate Program", July, 1977. Instrument configuration requirements such as channel selections are largely based on the statement of work requirements which have been influenced by previous studies and the ERB instrument. Changes to the statement of work have evolved on the basis of improving instrument definition and scientific requirements. The spacecraft interface constraints are largely based on TIROS-N interface requirements as the AEM Spacecraft for this mission is not well defined as this report is being completed.

2.1 RADIATION BUDGET MEASUREMENT REQUIREMENTS

Current studies have focused on the development of a satellite/sensor system approach for the determination of Earth radiation budget parameters at the top of the atmosphere on monthly and larger time scales for the following area resolutions:

- 250 by 250 KM regions
- 1000 by 1000 KM regions in the Tropics
- 10° Latitudinal Zones
- Equator to Pole Gradient
- Global

Values for Earth albedo or shortwave radiation, longwave radiation and net radiation, i.e., incoming solar radiation minus shortwave and longwave radiation, will be determined for the regional and zonal spatial scales. The net

radiation will be determined for the equator to pole gradients and global spatial scales. Realization of these goals and the accuracies with which the components can be measured are a function of the data interpretation and analysis methods, orbital coverage or sampling and instrument design. Since the instrument measures only that energy at the Earth's surface directed at the satellite, other components directed away from the satellite must be accounted for by the use of computer directional models. One purpose of the ERB instruments flown on Nimbus 6 and 7 was the improvement of the currently used directional models for various scenes. Sampling studies and analysis considerations have resulted in the recommendation for the three satellite missions mentioned in Section 1.0 and for the instrument fields of view. The required minimum useful ERBSS mission accuracies for monthly averages at the top of the atmosphere have been compiled from various science studies for the various spatial scales and are shown in Table 2-1.

Table 2-1
ERBSS Minimum Useful Accuracy Requirements

Spatial Scale	Minimum Useful Requirement--W/M^2		
	Longwave	Shortwave	Net
250 x 250 KM Regions	14	14	
1000 x 1000 KM Regions in Tropics	15	15	
10° Latitudinal Zones	12	12	
Equator to Pole Gradient			4
Global			1

Inaccuracies associated with sampling, data interpretation and analysis, and instrument factors all have to be included in the error budget. From these mission requirements, the instrument uncertainty allocations have been formulated. The medium and wide field of view channels have a requirement for a single sample uncertainty of ± 4 W/M^2. Included in the ± 4 W/M^2 are a bias component of ± 1 W/M^2 and a random component of ± 3.0 W/M^2.

The overall mission requirement for the solar constant measurement is an accuracy of ± 1.5 W/M^2 with a reproducibility of ± 0.3 W/M^2. The design goal for the solar

solar constant radiometer (Channel 5) is an accuracy of ±0.1 percent of full scale (equivalent of ±1.37 W/M^2) with a reproducibility of ±0.02 percent.

Scanner data multiplied by influence coefficients from the directional models are summed and averaged to provide monthly averages for the 250 by 250 kilometer regions. The noise equivalent radiance (NEN) requirements for Channels 6 (shortwave) and 7 (longwave) are 0.11 W/M^2-SR and 0.13 W/M^2-SR respectively. Channel 8, used for cloud discrimination to aid in data analysis for Channels 6 and 7, is required to have a signal to noise ratio (SNR) of 300:1 at λo = 1.639 μm, $\Delta\lambda$ = 0.1 μm, a surface reflectance of 0.1 and a solar zenith angle of 45°.*

In addition to the accuracy, and temporal and spatial scanning requirements, the ERBSS has related lifetime and field of view requirements. As a major experiment in the United States climate program, the ERBSS must perform in space for several years while yielding a stable data output. Simplicity is a key word for the ERBSS mission for achievement of the lifetime goal. The extensive time and space sampling studies which led to the selection of the three satellites and their orbits also led to the spatial coverage or field of view requirements summarized by Table 2-2.

Table 2-2
ERBSS SPATIAL COVERAGE REQUIREMENTS

Channel Type	Spatial Coverage	Field Of View Requirement
Wide FOV	Limb to Limb	132° AEM**, 125° TIROS**
Medium FOV	10° Earth Central Angle ~1000 KM diameter	88° AEM, 66° TIROS
Scanner	250 to 500 KM averaged from 30-50 KM image at nadir	3°

*Dr. Robert Curran, NASA, GSFC.
**Does not include spacecraft attitude errors.

Spectral responses and filters identical in concept to those used for the ERB instrument are suggested for the ERBSS mission instrument channels. Approximately 99.5% of the solar radiance is included in wavelengths between 0.2 μm and 5.0 μm. Because of the wide angles involved for the medium and wide field of view channels, flat or planar filters are not appropriate and a hemispheric dome of Suprasil-W quartz provides shortwave response filtering for the appropriate MFOV and WFOV channels. One MFOV channel and one WFOV channel are not filtered and measure irradiance over the entire spectrum from approximately 0.2 μm to beyond 50 μm. The long wave or emitted component is the difference between the total and shortwave channel radiance measurement. The scanner shortwave channel also uses a quartz filter while the longwave channel filter substrate is Type II diamond. An interference type bandpass filter is suggested for Channel 8. Table 2-3 summarizes the channel spectral responses and the suggested filter materials.

Table 2-3
ERBSS SPECTRAL RESPONSES

Channel Type	Spectral Response	Purpose
Shortwave; MFOV, WFOV and Scanner	0.2-5 μm, Suprasil-W Quartz Filter	Albedo measurement
Total; MFOV and WFOV	0.2-50+ μm, unfiltered	Total radiance measurement
Longwave; Scanner	5-50+ μm, Type II Diamond filter with absorbing shortwave coating	Emitted radiance measurement
Cloud; Scanner	1.589-1.689 μm, Interference type bandpass filter	Cloud discrimination

Solar measurements are made by the Channel 5 cavity radiometer which has a 10° field of view. These measurements are planned to be made on a monthly basis at an appropriate time in the orbit by rotating the non-scanning assembly with its azimuth gimbal to allow solar acquisition by the Channel 5 field of view. The medium and wide field of view channels are rotated at the same time to their solar

viewing ports which are coregistered with the Channel 5 field of view. These MFOV and WFOV solar calibrations are thereby referenced to the Channel 5 cavity radiometer response providing traceability to other standard cavities developed for the ERBSS program. The infrequent solar calibrations also limit exposure of the quartz domes to solar irradiance, thus minimizing UV exposure and subsequent transmission degradation.

2.2 INSTRUMENT DESIGN GUIDELINES AND CONSIDERATIONS

Other than scientific requirements and spacecraft interface constraints, a set of requirements which we choose to call design guidelines and constraints have been imposed. These have been split into two categories for the non-scanning and scanning instrument assemblies.

2.2.1 Design Guidelines and Considerations for the Non-Scanning Assembly

To provide a better basis for the design of the non-scanning instrument assembly the following guidelines have been used.

Detectors. Circular wire-wound thermopiles of the type used on the ERB experiment are suggested for use on the medium and wide field of view channels. The solar constant sensor, on the other hand, will be a cavity-type radiometer probably operated in the active mode.

Apertures. The apertures used for setting the fields of view in the medium and wide field of view channels are as shown in Figure 2-1. They are truncated hemispheres having a low emittance specular finish on the inner surface. The angle $2\delta_1$, as indicated, is the total unobscured field of view and has a cosine response. The total field of view, $2\delta_2$, includes that portion of the field extremes in which the detector is being obscured by the aperture. It is a requirement that the signal defined by $2\delta_1$ be equal to or greater than 75 percent of the entire signal (assuming a uniform target).

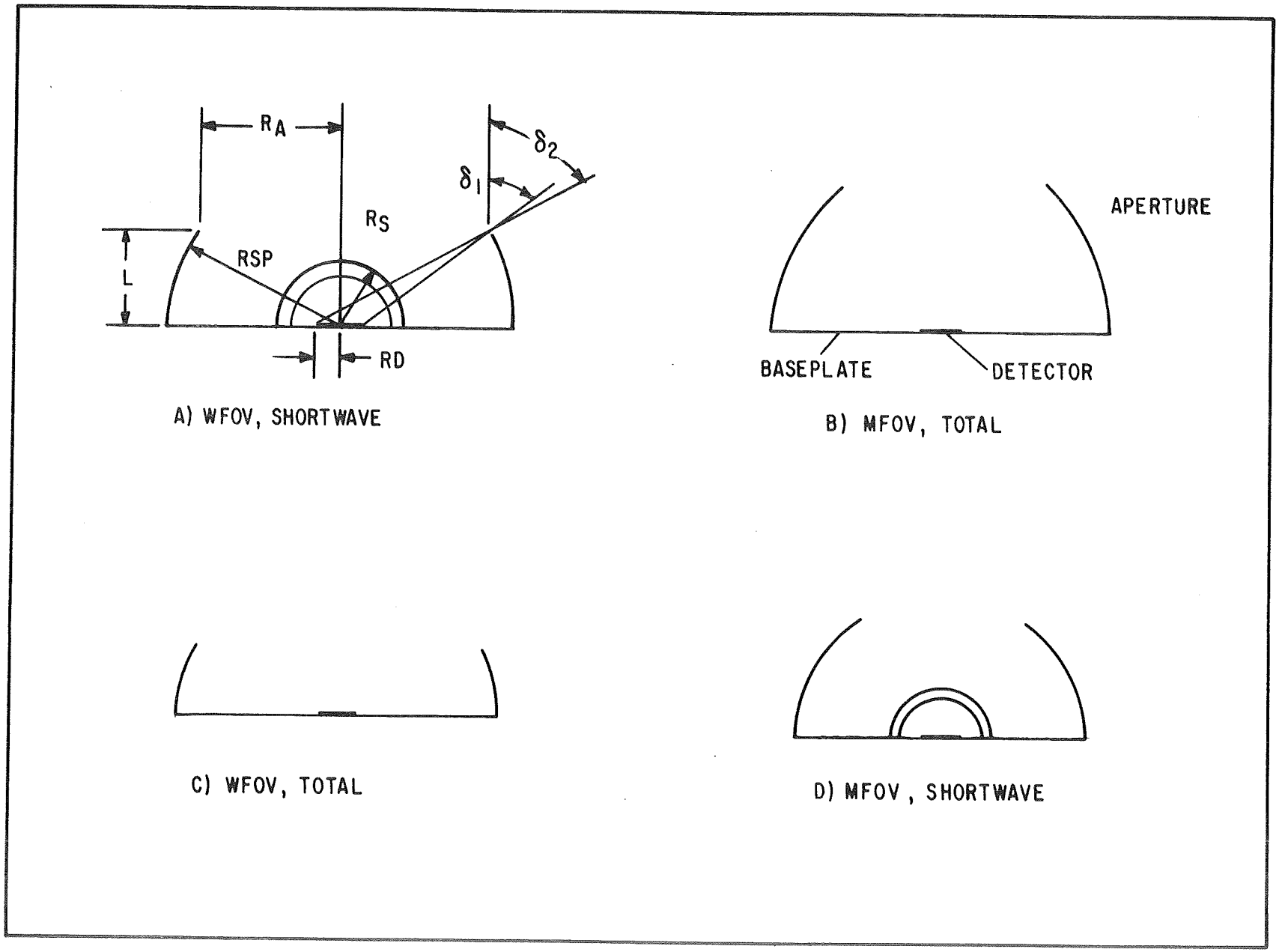

Figure 2-1 MFOV/WFOV Apertures

In-flight Calibration and Solar Viewing. The four medium and wide field of view detectors which look at the Earth are gimballed for rotation to blackbody targets for the total channels and to a solar viewing position for all channels. As the field of view apertures do not rotate with the detectors, special solar viewing apertures have to be used for this application. The solar calibration apertures set the fields of view with the following constraints:

- The total field, i.e., $2\delta_2$ for solar viewing shall not include the spacecraft and shall be tangent to the spacecraft mounting surface.
- The total field of solar viewing shall not include the Earth or its atmosphere. The extreme of the field shall not exceed the tangent with the Earth's atmosphere at an altitude of 450 kilometers above the Earth's surface. This is to avoid emitted or scattered radiance from the Earth limb during solar calibration.

With the TIROS orbital and launch parameters, there is, potentially, a large variation in the angle between the sun and the orbit normal. To have solar irradiance incident upon the solar calibration parts at opportune times, azimuth gimballing of approximately $\pm 35^{\circ}$ is required allowing rotation of the instrument about the nadir axis. A minimum of 90 seconds of solar viewing time is desirable during solar calibration.

Data Sampling. Sampling of the medium, wide, and solar constant channels data is done every 1.6 seconds in synchronization with the TIROS spacecraft clock.

High Contamination Launch Mode. The AEM spacecraft will be shuttle-launched in a highly contaminating environment. Protection for sensitive surfaces should be provided during this period.

Weight and Power. While no firm requirements have been formulated, the weight and power of the non-scanning assembly including the gimbal were baselined as follows:

- Weight: 25 kilograms or 55 pounds
- Power: 15 watts average, 40 watts peak.

Identical Configuration. To the extent possible, there should be no difference between instruments for the AEM or TIROS missions. Differences in configuration should be easily modifiable by a field kit to the desired configuration.

2.2.2 Design Guidelines and Considerations for the Scanning Assembly

Detectors. Detectors suggested for use in the scanner are Lithium Tantalate Pyroelectric detectors in the shortwave and longwave channels and Lead Sulphide in the cloud channel.

Chopping and Sampling. There will be three chops by the scanner optical chopper per integration or sampling period, which is 0.053 second, in synchronism with the spacecraft clock. This makes the chopping rate approximately 55 Hz. The system will be configured so that a controlled source will be reflected by the chopper to the detector during chopper closure.

In-flight Calibration and Solar Viewing. Provision for solar calibration of the shortwave and cloud channels and a blackbody calibration target for the longwave channel will be included in the design of the scanning assembly. Azimuth gimballing of approximately ±35° of the scanning assembly is required for solar viewing with the possible orbital variations.

Failure Mode Scan Position. The scan system will be designed so that the field of view can be positioned to the subsatellite or nadir position in the event there is an incipient failure. That is, the scanner can be stopped at the nadir viewing position if the telemetry indicates a failure may occur.

High Contamination Launch Mode. (Same as Section 2.2.1)

Weight and Power. Baseline weight and power of the scanning assembly including the azimuth gimbal were as follows:

- Weight: 20 kilograms or 44 pounds
- Power: 30 watts average, 45 watts peak

Identical Configuration. (Same as Section 2.2.1)

2.3 TIROS/AEM SPACECRAFT REQUIREMENTS AND CONSTRAINTS

In this section, spacecraft requirements and constraints which affect exterior or physical areas of design are considered. Various electrical interface requirements such as powerline ripple or exact command interfaces which will have to be considered for a very detailed design are not covered here. As the AEM/ERBS-A spacecraft for this mission is not as yet completely defined, most of the spacecraft requirements have been generated from TIROS documentation.

2.3.1 General Requirements and Constraints

Requirements applying to both the scanning and non-scanning instrument assemblies are included in this section.

Spacecraft Attitude Control. Control to ±1° in any axis which produces a ±1.4° error for two axes considerations, will have to be used for margin when calculating fields of view. This is an assumed AEM capability; TIROS control is somewhat better.

Spacecraft Time Scheduling. A 30-second margin has been arbitrarily assigned for factors such as orbit location errors, command priority interrupts, etc.

Spacecraft Mounting. The two instrument assemblies will be mounted on the outboard surface of the Equipment Support Module (ESM) of TIROS. Exact positions have not been established at this time. The method of mounting is to be such that the assemblies will be essentially thermally isolated (minimum thermal conductance) from the spacecraft. The exterior of the ESM is multilayer insulation with absorptance = 0.12 and emittance = 0.6.

Data Format. The TIROS Information Processor (TIP) has a major frame period of 32 seconds. It consists of 320 minor frames each containing 832 bits organized into 104, 0.9375 millisecond eight-bit words or time slots. The period for the minor

frame is 0.1 second. Data are fed into allocated time slots in synchronization with the spacecraft clock. All clocks, drive systems, etc., must be in synchronization with the spacecraft clock.

2.3.2 Tentative Spacecraft Requirements and Constraints Peculiar to the Non-Scanning Assembly

Although some of these requirements have general application, they are included here since they affect only the non-scanning assembly.

Maximum Field of View. Due to interference from other spacecraft instrumentation and solar paddles, the maximum total conical field of view allowed is 132°.

TIP Data Allocation. The non-scanning instrument is allowed three time slots or 24 bits in a minor frame every 0.1 second. This makes the allowable data rate for the non-scanning instrument 240 bits per second including processed telemetry.

Commands. The non-scanning assembly has been allocated 26 pulse discrete commands and three multilevel commands for operational purposes.

Telemetry. The non-scanning assembly has been allocated 22 analog and 13 digital B telemetry channels.

2.3.3 Tentative Spacecraft Requirements Peculiar to the Scanning Assembly

Uncompensated Angular Momentum. Uncompensated angular momentum generated by rotating mechanisms is required to be less than 0.02 in-lb-sec. Therefore, mechanisms whose angular momentum is greater than 0.02 in-lb-sec are required to have counter rotating compensating momentum.

TIP Data Allocation. The scanner is allocated nine or ten time slots, or 72 to 80 bits every 0.1 second. This constraint makes the allowable data rate 720 to 800 bits per second including processed telemetry.

Commands. Nineteen pulse discrete commands and two multilevel commands have been allocated to the scanner.

Telemetry. Twenty-two analog and ten digital telemetry channels have been allocated to the scanner.

Section 3
CONCEPTUAL DESIGN DESCRIPTION

On the basis of the requirements, constraints, baselines, and desires experienced in the previous sections, instrument concepts illustrated by Figures 1-1 and 1-2 have been developed. Figures 3-1 and 3-2 provide three views of the non-scanning and scanning assemblies. Although the two are separate assemblies for convenience and flexibility, they are required to function much as a single coregistered multi-field of view instrument.

3.1 GENERAL DESCRIPTION OF ERBSS INSTRUMENTS

The Non-Scanning Assembly has four channels for measurement of shortwave and total Earth radiation with two fields of view; and a fifth channel for measurement of the solar parameter. Two of the Earth-looking channels have a wide field of view so the radiance of the entire Earth disc is measured; one of these channels is filtered by a small hemispherical quartz dome to limit its response to the shorter wavelengths.

The other wide field of view channel is unfiltered as is one of the medium field of view channels. The field of view is set by a truncated hemispheric aperture so that a portion of the Earth disc corresponding to a ten degree Earth central angle (ECA) is measured at the proper spacecraft altitude. The other channel of the medium field of view set is filtered by a hemispheric quartz dome identical to the WFOV shortwave filter. The total response MFOV and WFOV channels measure both the emitted and reflected radiation budget components while the shortwave MFOV and WFOV measure only the reflected or shortwave component. During ground data processing, the emitted component is determined by an algorithm which subtracts the shortwave data from the total data and also corrects for data errors on the basis of housekeeping telemetry data (see Section 4.0).

To provide frequent solar calibration of these channels, gimballing is provided in two axes. One gimbal (see Figure 1-1) rotates the sensors, but not the

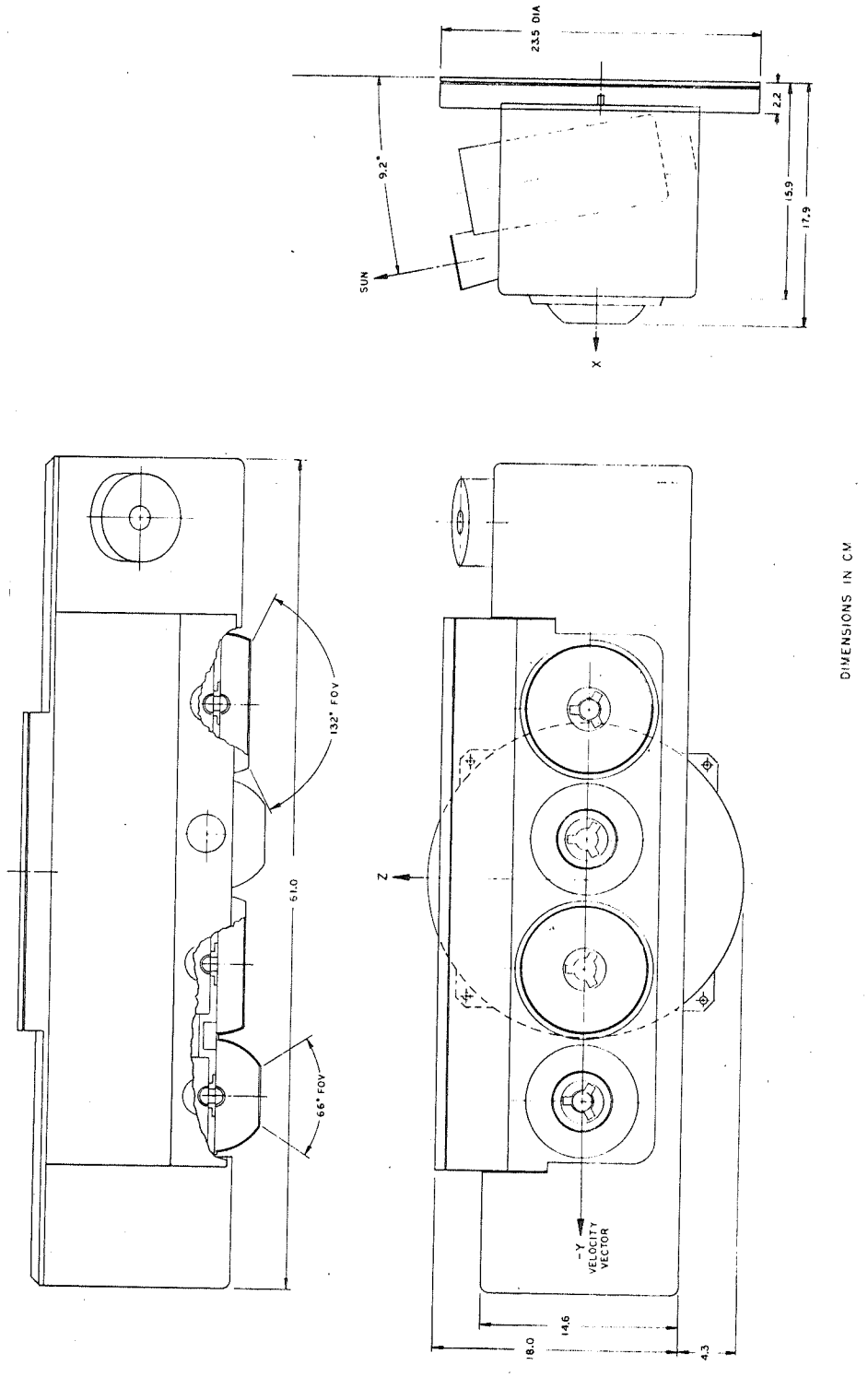

Figure 3-1 ERBSS Non-Scanning Instrument Layout

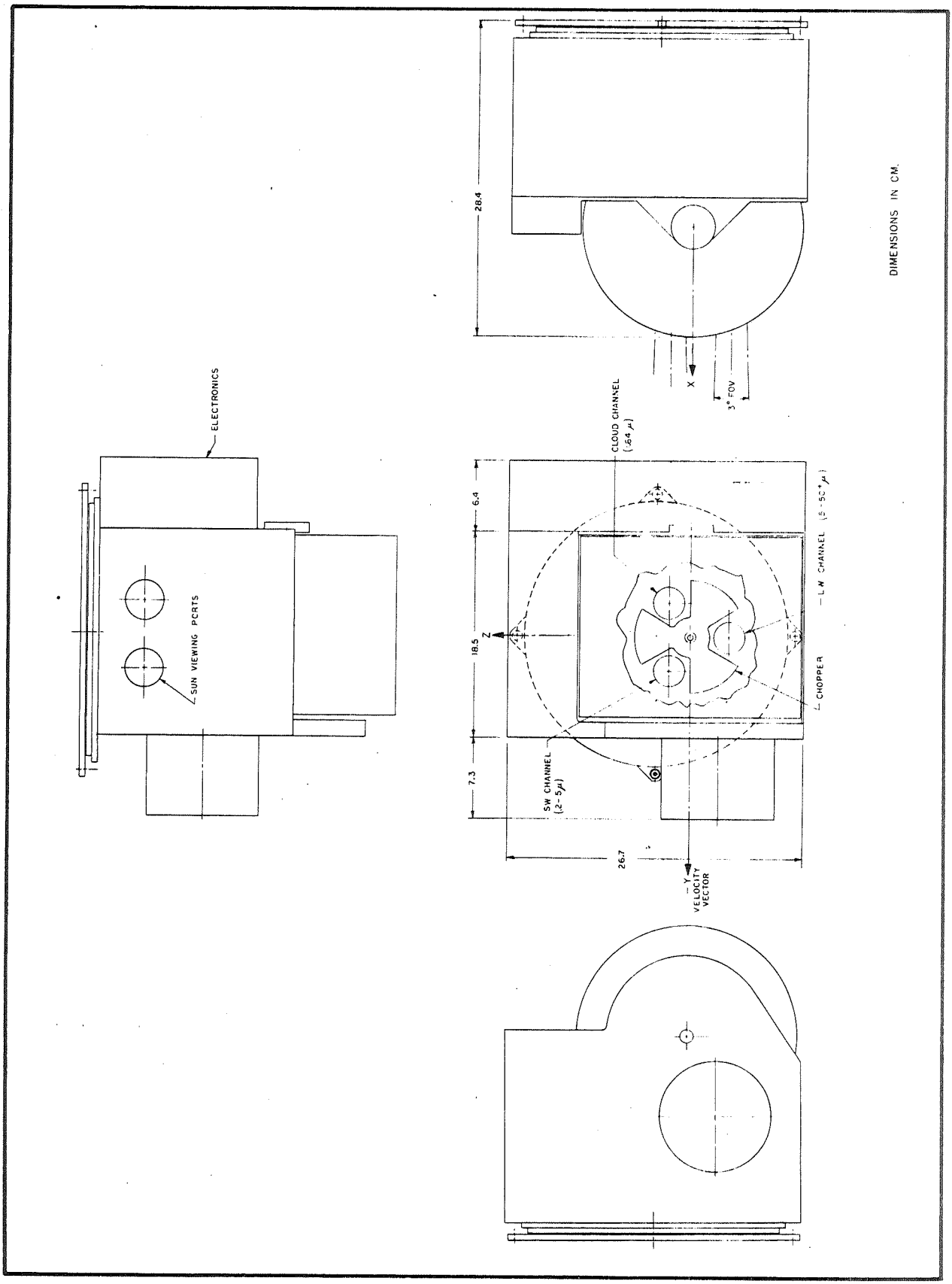

Figure 3-2 ERBSS Scanning Instrument Layout

apertures, approximately 81° from nadir where solar observations are made through more limited field of view ports. Rotation about the nadir axis is provided by an azimuth gimbal so the sun can be brought within the narrow field of the solar ports. The sensor gimbal can also rotate 180° from nadir for calibration of the total channels by controlled calibration blackbodies. The fifth channel is an electrically calibrated cavity radiometer for measurement of the solar parameter. It also functions as a reference during coregistered solar viewing with the other four channels. Earth albedo values are determined from appropriate ratios of the Earth and solar measurements. Characteristics of the non-scanning assembly are summarized and elaborated on in Section 3.2

The Scanning Assembly has three channels each of which have a circular three degree field of view. One channel responds identically spectrally to the medium and wide field of view shortwave channels. Longwave (or emitted) radiance only is measured by another scanning channel. The third channel is provided for discrimination between clouds and snow fields for proper data interpretation. Once during each rotation of the scanner drum (see Figure 1-2), the longwave channel is calibrated by a controlled blackbody source. If the sun is incident from the proper angle, the solar port is opened and the shortwave and cloud channels are calibrated by diffusely reflective targets. The scanner also can be rotated about the nadir axis so the sun can be brought within the approximate ±10° useful incidence angle on the diffuser targets. The characteristics of the scanning assembly are summarized in Section 3.3.

3.2 NON-SCANNING ASSEMBLY

Table 3-1 summarizes the important characteristics of the non-scanning assembly. In the following subsections, operation of the medium and wide field of view channels, in-flight calibration, solar constant radiometer, system electronics, thermal requirements, and weight and power budgets will be elaborated on.

Table 3-1

ERBSS NON-SCANNING ASSEMBLY CHARACTERISTICS

Field of View	Channels 1 and 3	Limb to limb, 132° cone
	Channels 2 and 4	10° Earth Central Angle; 66° Cone (TIROS), 88° Cone (AEM)
	Channel 5	10° Cone
Spectral Response	Channels 1 and 4	0.2 to 5 μm
	Channels 2 and 3	0.2 to 50+ μm
	Channel 5	0.2 to 50+ μm (solar constant)
Baseline Detector	Channels 1-4	Circular, toroidal thermopile
	Channel 5	Circular, electronically calibrated, cavity radiometer
Solar Calibration or Space Field of View	Channels 1-4	10°
Measurement Frequency (Earth)	Channels 1-4	1.6 seconds
Solar Calibration Frequency	All Channels	Monthly, every 1.6 seconds for 90 seconds or more
Orbital Altitude		600 kilometers (AEM), 833 kilometers (TIROS)
Data Rate (Maximum)		160 bits per second
Commands		28
Weight		25 KG or 55 pounds
Power		15 watts orbital average

3.2.1 Medium and Wide Field of View Channels

The differences between the four medium and wide field of view channels are, as explained earlier, the configuration of the field of view apertures and the spectral filtering employed in two of the channels. Other than that, the operation of the four channels are identical in that the detectors, amplifiers, and other signal processing electronics are exactly the same for all channels.

Figure 3-3 illustrates the electronics for a typical medium or wide field of view channel. Energy from the scene is incident on the thermopile detector with the scene limited by the field of view aperture. One side of the detector facing the source is heated and the differential thermopile output changes. That change is amplified by the chopper stabilized amplifier. Signals are integrated for 1.6 seconds by the integrator and sampled and held by the sample and hold to be multiplexed into the analog to digital converter.

3.2.1.1 Medium and Wide Field of View Apertures

The field of view limiting apertures have been designed with the requirements of Section 2 providing guidelines and limits. The apertures for the four Earth-looking channels are shown by Figure 2-1. The requirements applicable to the designs are:

- The signal due to radiance within the solid angle defined by $2\delta_1$ must be equal to or greater than 75 percent of the entire signal, i.e., due to $2\delta_2$.
- For the wide field of view channels, the angle $2\delta_1$ must be large enough to include the entire Earth disc.
- The angle $2\delta_2$ cannot exceed 132° on TIROS.
- The spacecraft attitude control is one degree in any axis or 1.4° in any direction.

Figure 3-4 shows δ_1 as a function of δ_2 for meeting the 75 percent signal requirement. On that basis, the medium field of view apertures can be sized. The

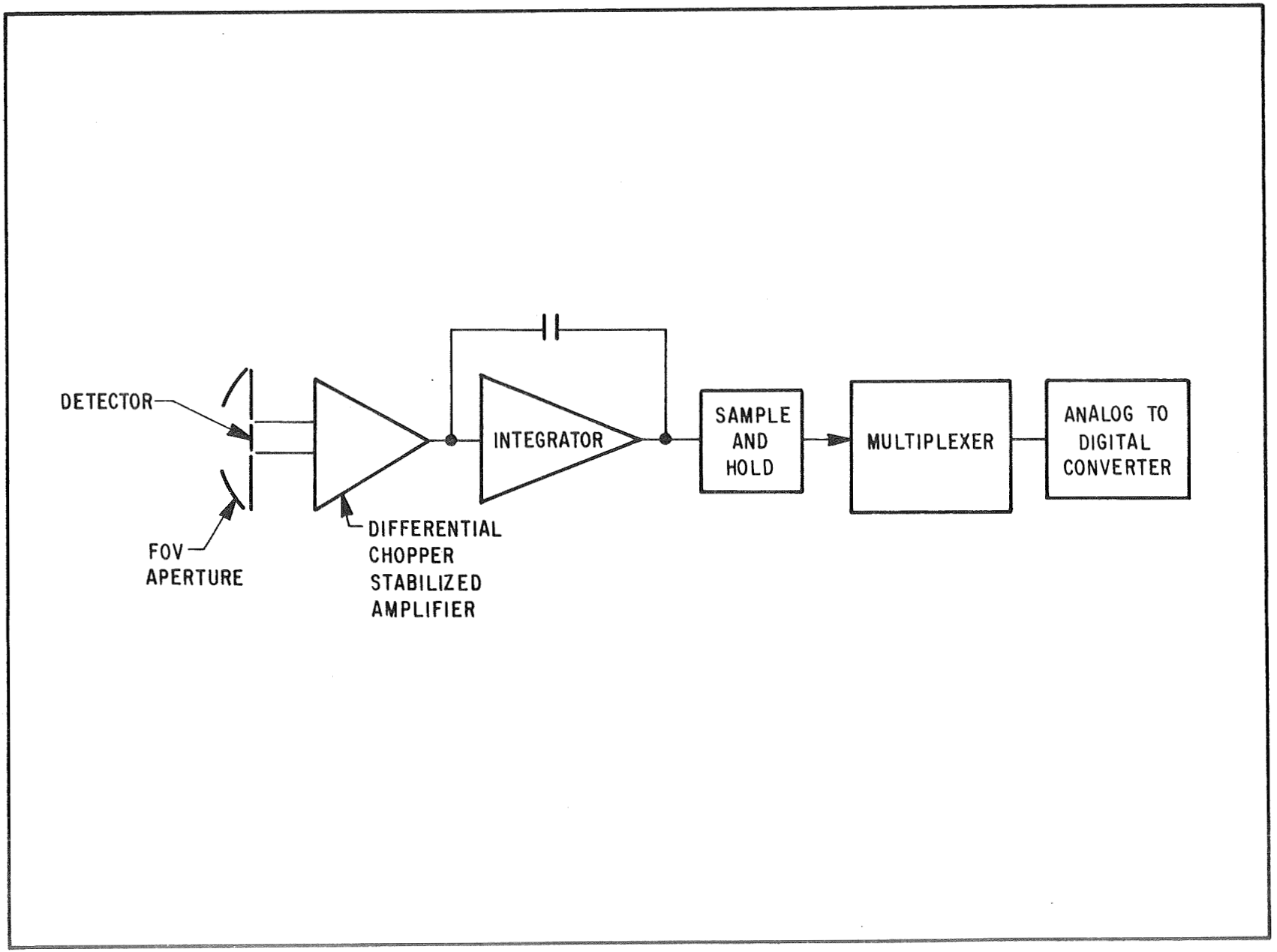

Figure 3-3 Typical MFOV/WFOV Channel

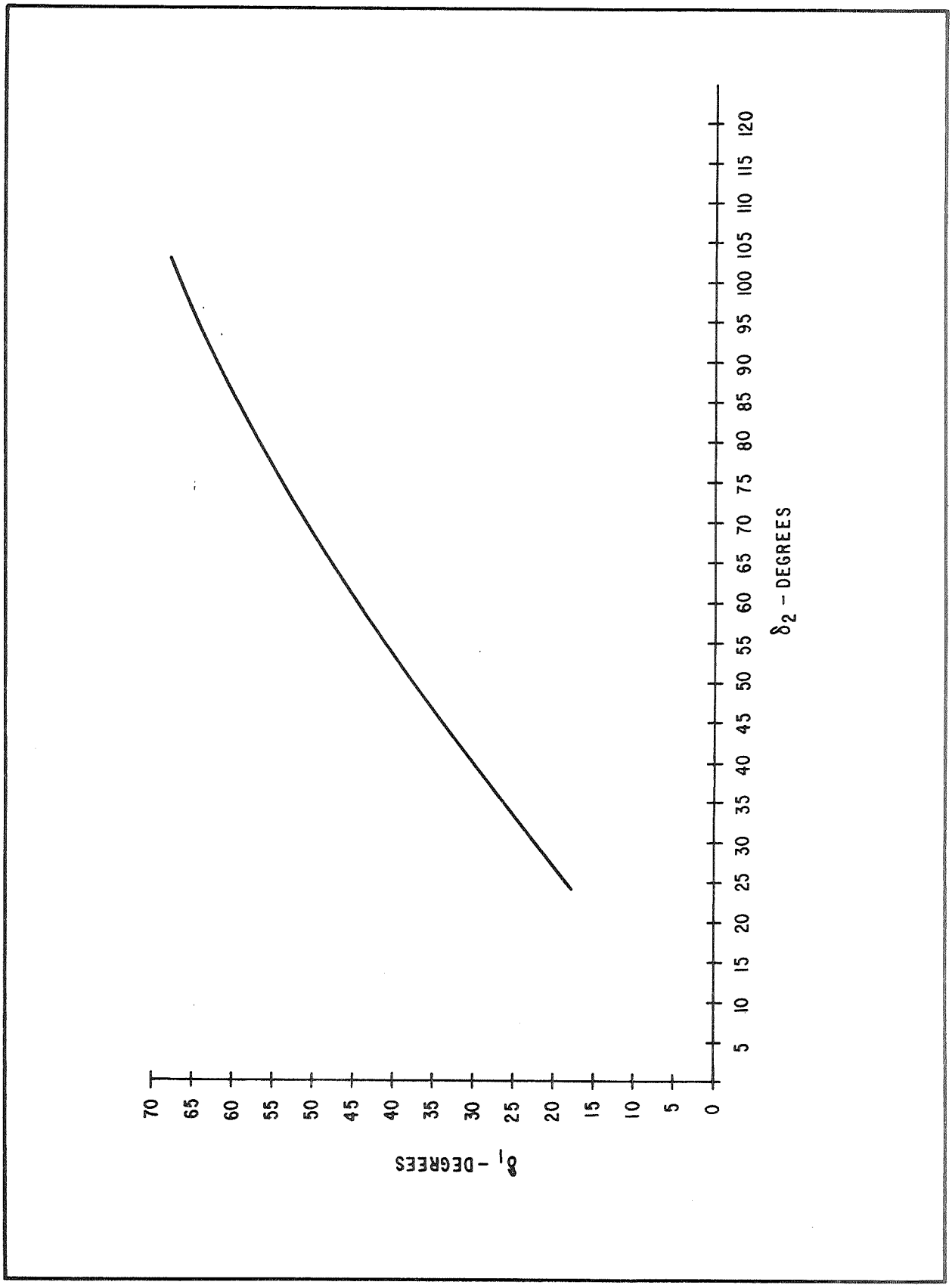

Figure 3-4 δ_1 versus δ_2 for 75 percent Signal Requirement

The equations:

$$\delta_2 = \tan^{-1} \frac{R_A+R_D}{L},$$

$$\delta_1 = \tan^{-1} \frac{R_A-R_D}{L},$$

$$R_A^2+L^2 = R_{SP}^2$$

are used to define the medium field of view aperture dimensions. The results of such calculations, using Figure 3-4 to establish δ_1 for $\delta_2 = 33°$ (TIROS) and $\delta_2 = 44°$ (AEM) show that the radius for the TIROS aperture (R_{SP}) is larger than the spherical radius for the AEM case. The sphere is sized for the larger value and the results are shown in Table 3-2.

Table 3-2
MEDIUM FIELD OF VIEW APERTURE PARAMETERS

	TIROS	AEM
δ_2	33°	44°
δ_1	25°	37°
R_D	3.175 mm	3.175 mm
R_A	19.4 mm	25.9 mm
L	34.7 mm	30.1 mm
R_{SP}	39.7 mm	39.7 mm

This allows one MFOV aperture size to be manufactured for both the TIROS and AEM flights. The resulting hemisphere is machined for the proper aperture hole radius as required by Table 3-2. For given values of R_{SP}, R_D and δ_2, R_A and L can be determined by combining the equations:

$$L \tan \delta_2 = R_A + R_D \text{ and}$$

$$R_{SP}^2 = R_A^2 + L^2$$

The value for L is determined by solution of the resulting quadratic equation and R_A is easily determined after that. A value for δ_1, is then computed from the equation:

$$\delta_1 = \tan^{-1} \frac{R_A - R_D}{L}$$

The result is that δ_1, R_A, and L and R_{SP} are determined for 75% signal purity for the TIROS flight and from the TIROS R_{SP} value for the AEM flight. The signal from the solid angle Ω_1, which corresponds to the view angle δ_1, is 75.7% of the total signal from view angle Ω_2 (which corresponds to δ_2) for TIROS. For the AEM values, $\Omega_1/\Omega_2 = 86.2\%$.

The solid angle field of view can be determined from the double integral:

$$\Omega = \int_0^{2\pi} \int_{\delta_A}^{\delta_B} f(\delta)\sin\delta d\theta d\delta$$

$$= 2\pi \int_{\delta_A}^{\delta_B} f(\delta)\sin\delta d\delta$$

As shown by Figure 3-5, the detector/aperture has a cosine response between $\delta = 0$ and $\delta = \delta_1$, while from δ_1 to δ_2 the dropoff is approximately a linear function. That is, $f(\delta)$ between 0 and δ_1 is cosine δ_1, while $f(\delta)$ between δ_1 to δ_2 is $m\delta + b$. The values for m and b are easily computed using $f(\delta_1) = \cos \delta_1$, and $f(\delta_2) = 0$. The solid angle $\Omega_1 = \pi\sin^2\delta_1$ and

$$\Omega_2 = \Omega_1 + 2\pi \int_{\delta_1}^{\delta_2} (m\delta+b)\sin\delta d\delta$$

For the TIROS MFOV values, $\Omega_1 = 0.5611$ SR and $\Omega_2 = 0.7415$ SR. For AEM, $\Omega_1 = 1.1378$ SR and $\Omega_2 = 1.3206$ SR.

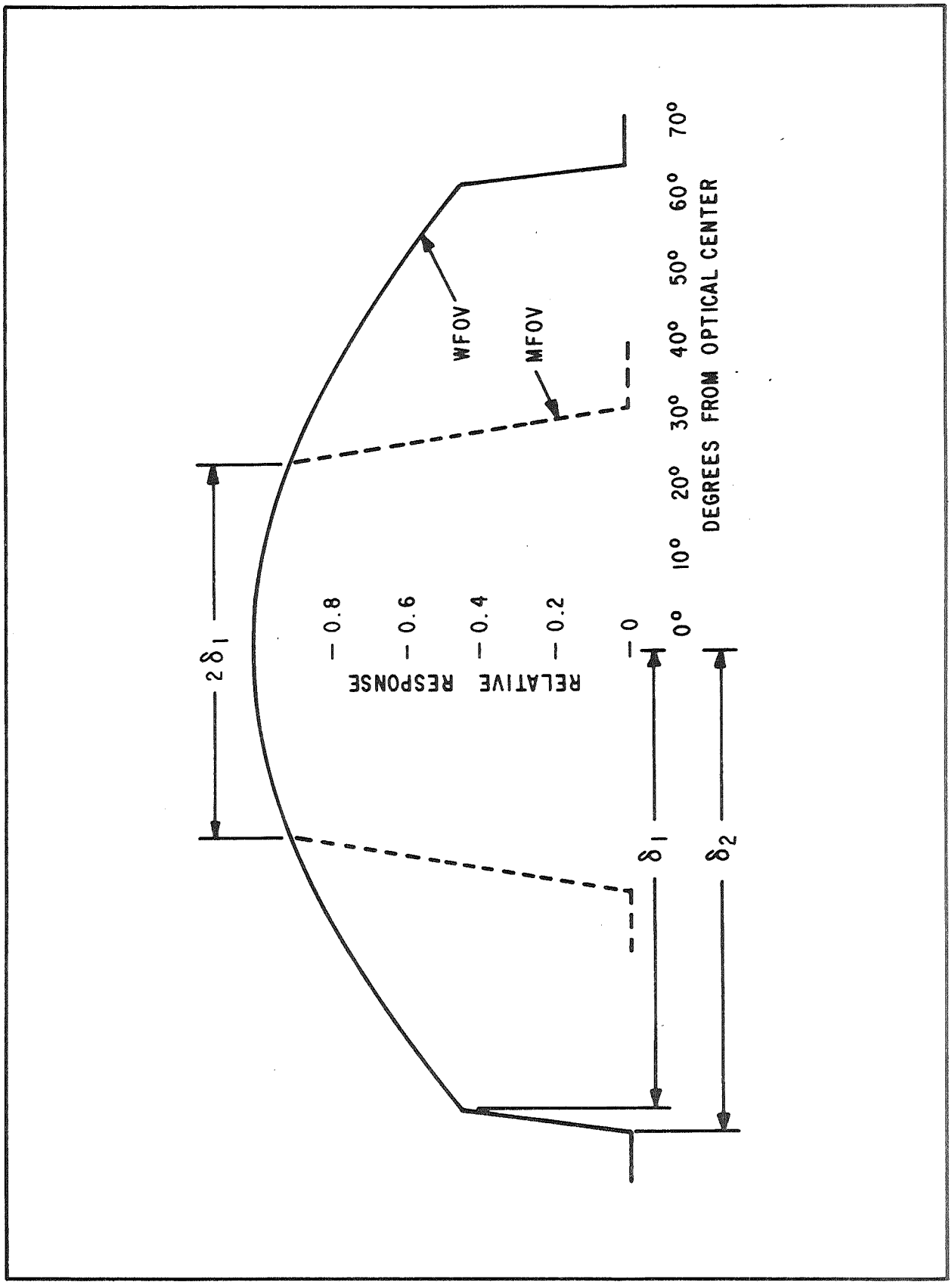

Figure 3-5 Detector Angular Response

To see the entire Earth disc within the angle $2\delta_1$ in the wide field of view channel with spacecraft attitude errors included, the $2\delta_1$ angle is 127° for TIROS and 135° for AEM. The constraint on TIROS that $2\delta_2$ be less than 132° makes the spherical radii of these apertures larger than would otherwise be necessary. If the smaller TIROS spacecraft attitude error is factored in, however, a value of $2\delta_1$ of 126° is possible for TIROS. Reducing the $2\delta_1$ value from 127° to 126° reduces the spherical radius by 10mm as shown by Figure 3-6. The aperture parameters, R_{SP} (the aperture opening radius) and L (the aperture height), were calculated for various values of δ_1 and δ_2 with the results shown in Figure 3-6 and 3-7. While decreasing $2\delta_1$ reduces the aperture, increasing $2\delta_2$ also reduces the aperture (see Figure 3-7). Calculations were made of the aperture parameters with the 126° $2\delta_1$ and 132° $2\delta_2$ for TIROS. The same spherical radius was then used to determine the same parameters for AEM. These are shown in Table 3-3.

Table 3-3
APERTURE PARAMETERS FOR THE WIDE FIELD OF VIEW APERTURES

	TIROS	AEM
δ_2	66°	70°
δ_1	63°	67.5°
R_D	3.175 mm	3.175 mm
R_A	47.2 mm	47.8 mm
L	22.4 mm	18.5 mm
R_{SP}	52.3 mm	52.3 mm

Again, a common value for R_{SP} has been established for both TIROS and AEM instruments. For the TIROS values, Ω_1 = 2.4941 SR, Ω_2 = 2.5613 SR, and Ω_1/Ω_2 = 97.4%. For AEM, Ω_1 = 2.6815 SR, Ω_2 = 2.7304 SR, and Ω_1/Ω_2 = 98.2%.

The impact of these parameters on the overall instrument size will be shown in Section 4.5. Typical field of view responses are shown for a medium and wide field of view channel by Figure 3-8. Various finishes have been considered for the apertures and the baseplate as designated by Figure 3.4. Scattering and

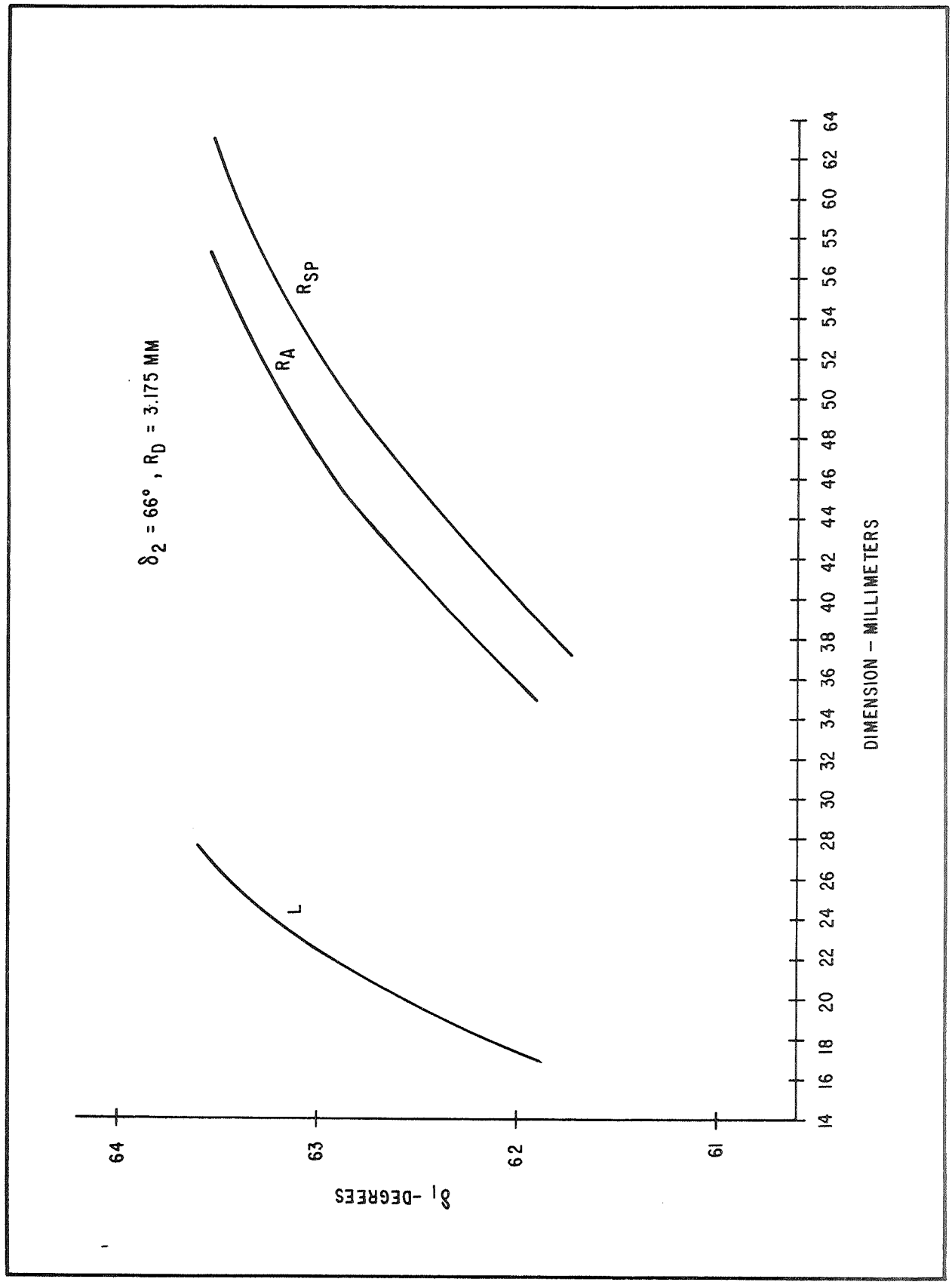

Figure 3-6 Aperture Parameters vs δ_1 with δ_2 and R_D Fixed

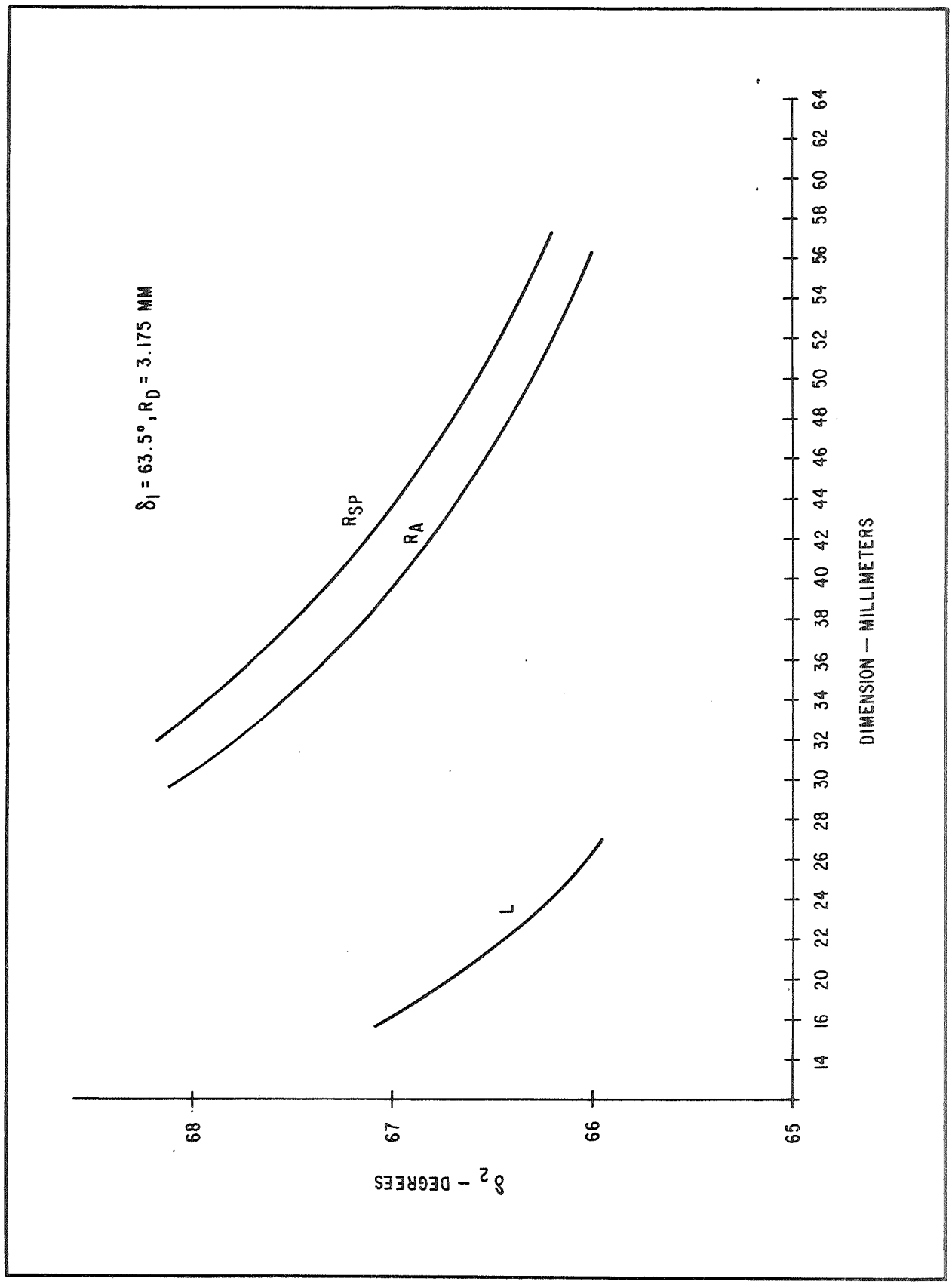

Figure 3-7 Aperture Parameters vs δ_2 with δ_1 and R_D Fixed

thermal analyses have been performed (see Section 4) to determine the best finishes. The inner surface of the aperture and the baseplate were made black or high emittance; specular low emittance and black; and specular low emittance on both. Scattering analyses indicate that the best overall configuration is a black baseplate and low emittance specular aperture. However, a low emittance specular finish on both surfaces is clearly acceptable.

Subsequent thermal analyses have indicated a preference for low emittance on both surfaces. The largest single contributor to scattering in the shortwave channels is the Suprasil-W hemispheric spectral filter. This design, a carry-over from the ERB program, has been modified to reduce the radius. This allows a larger percentage of the dome to be included in the transmission path during the solar calibration, thus reducing possible calibration inaccuracy. However, polarization analyses (see Section 4) indicate an increasing sensitivity of the shortwave channel to the state of scene radiation as the ratio of the detector to filter radii increases (see Section 4). For a detector radius of 3.175 mm and a filter radius of 6.35 mm, 14.9 percent of the filter area used for Earth viewing is involved in the solar view. As the ratio is increased by decreasing the filter radius to 5.475 mm, the common area is increased to 19.2 percent. For the latter case, the signal from a symmetrical polarized Earth scene, caused by a small zenith angle, will be 0.35 percent higher than that from an asymmetrical scene (zenith angle equals 57.5°). As this effect decreases rapidly as the detector to filter radii ratio decreases, a R_D/R_S ratio of 0.5 (R_S equals 6.35 mm) is recommended.

The spectral response of the shortwave channel is set by the natural transmission of Suprasil-W quartz as shown by Figure 3-8. Approximately 99 percent of the solar energy* is included in the spectral band defined by this material.

Darkening of this filter due to ultraviolet or particle radiation exposure is the probable cause of signal reduction observed in the ERB solar channels. Transmission changes at the shorter wavelengths (0.2 to 0.3 μm) after exposure to electron, proton, and ultraviolet radiation have been noted in tests at

*M.P. Thekaekara, Applied Optics, Volume 13, No. 3, March, 1974, p. 520.

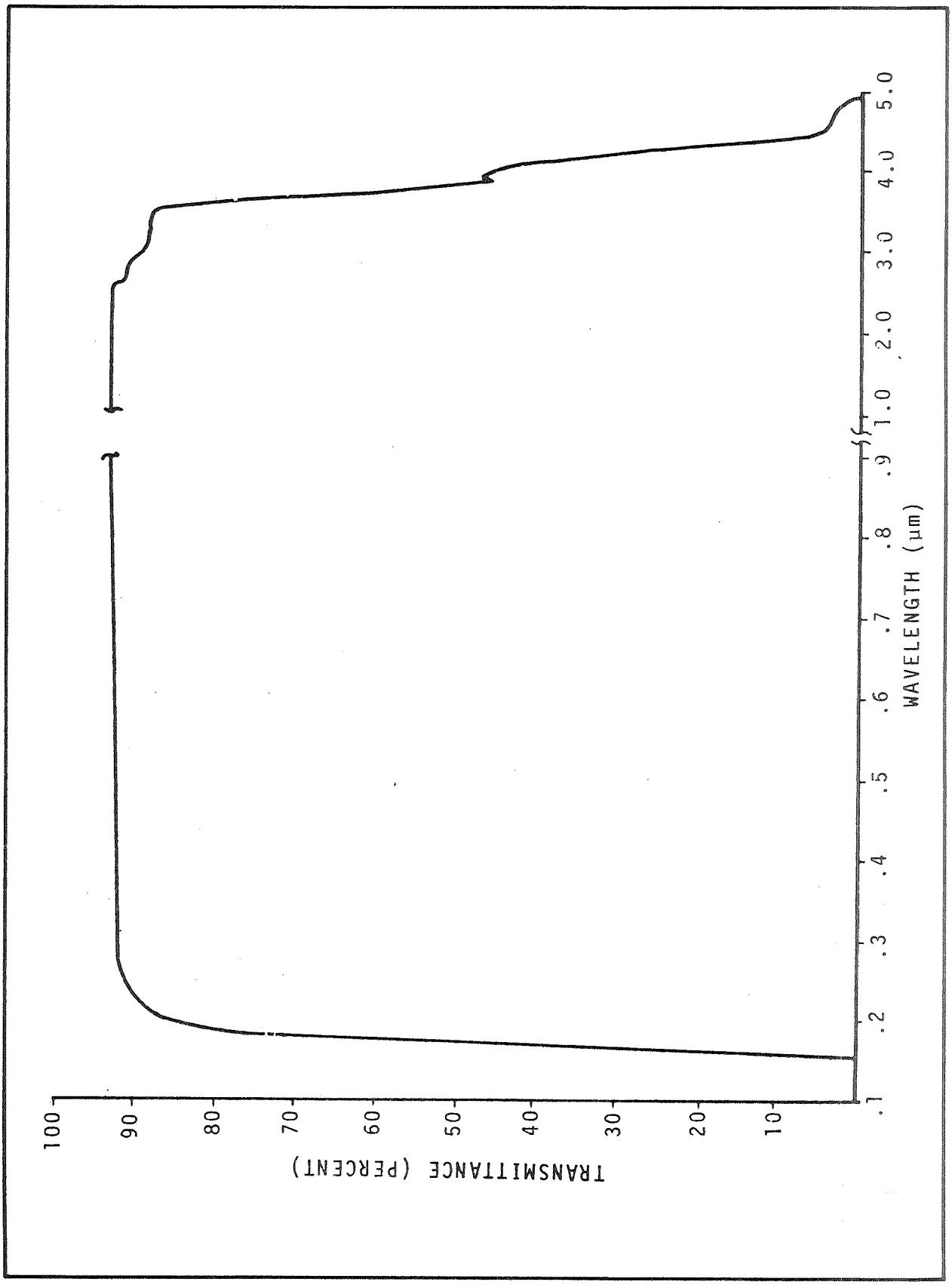

Figure 3-8 Transmittance of Suprasil-W (Thickness 2mm)

GSFC.** The exposures were similar to those expected for the ERBSS mission. Degradation appeared to level off after 1,200 equivalent ultraviolet solar hours at 3.5 ultraviolet solar constants. Preflight exposures of the filters to cause pre-calibration darkening will minimize in-flight changes. It should be noted, however, that ERB filters subjected to preflight aging and aligned for maximum solar exposure exhibited considerable (up to 20 percent) degradation after launch. Another similar channel, shuttered for only brief exposure and measurements, has shown a change of one part in 1700 over several years of operation. The secret to minimization of the filter transmission degradation would appear to be, (1) preaging by UV exposure and (2) minimizing solar exposure. Therefore, the frequency of solar calibrations should be consistent with the effects of such calibrations on filter degradation and, thereby, the calibration accuracy.

3.2.1.2 Medium and Wide Field of View Detectors

During the study, both wire-wound thermopile detectors with a flat plate or circular disc receiver, and a cavity type detector were considered for the medium and wide field of view channels. The cavity detectors for this application would be modifications of the cavities being considered for Channel 5 (see Section 3.2.3). The configuration for the medium and wide field of view channels would include the primary and secondary cavities without a view limiter except as provided by the truncated hemispheric apertures. Discussions with JPL and Eppley/Gulton indicate that there would be adequate space in the rotating sensor housing, as presently configured, for cavity detectors. The advantages of the cavity detector over the flat plate detector are:

(1) Improved receiver absorptance (hence better longwave length response), and less sensitivity to coating degradation.
(2) The cavities can be calibrated electrically. (Flat plate receivers may also incorporate this feature.)

The disadvantages of the cavity detectors are:

**C.A. Nicoletta and A.G. Bubanks, Applied Optics, Volume II, 1972, p. 1365.

(1) Volume
(2) Weight
(3) Power (depends on mode of operation)
(4) Time constant and
(5) A shutter is required (ACR-IV, JPL only)

The ACR-IV cavity radiometer made by JPL is generally operated in the active mode, i.e., the irradiance incident on the primary cavity is proportional to the difference in the electrical power applied to the secondary and primary cavities. The applied electrical power maintains a constant heat flow from each cavity to the housing or heat sink. With the shutter closed, both primary and secondary cavities are exposed to about the same irradiance and the power difference is minimized. With the shutter open, the scene irradiance incident on the primary cavity reduces the electrical heat on that cavity necessary to maintain the constant heat flow to the housing. The change in the primary cavity electrical power is then proportional to the incident irradiance. In the passive mode, nickel resistance sensors measure the temperature difference between the two cavities; that difference being proportional to the incoming scene irradiance.

The ESP (Eclectic Satellite Pyrheliometer) of Eppley/Gulton employs a toroidal wire-wound thermopile, nearly identical to the flat plate thermopile receiver, to measure the temperature difference between the two cavities. In the active mode, heat is applied to the secondary cavity to null the thermopile output. Eppley feels no shutter is necessary as the thermopile sensor is both linear and sensitive over three decades and can measure very small temperature differences.

Because of the better absorptance of the cavities, the spectral response is essentially flat to beyond 50 micrometers. This is not true of the flat disc receiver which has increased reflectance at longer wavelengths regardless of the coating used. The electrical calibration feature of the cavities allows additional calibration points when rotated to look at space, regardless of the mode of operation. A Langley funded study is now underway at JPL to determine the

potential for cavity detectors to operate in a wide field mode. Testing of a cavity detector with a wide field view limiter was performed at JPL by Kendall in 1977. These tests show a response slightly above a cosine response which was probably caused by scattering in the view limiter that was used.

In its simplest form, the thermopile detector may be considered as a two terminal device whose output is a voltage proportional to the difference in irradiances incident on the detector active receiver and reference receiver surfaces. Internally, it may be considered as an array of thermocouples. It is constructed by wrapping a coil of constantan wire around an aluminum heat sink where a portion of the constantan wire is copper plated to form the thermocouples. Incident radiation is absorbed in a blackened 0.25-inch (6.35 mm) diameter disc-shaped receiver surface, changing its temperature, and in turn, generating a proportional net output voltage from the thermocouple array.

It is to be emphasized that this type of detector is now in use, with proven performance, in the Earth Radiation Budget (ERB) experiment aboard NIMBUS-6. Flight Evaluation Report Number Four, recently published, shows that ERB Solar Channel 3, which consists of a thermopile detector exposed to the sun all of the time, has exhibited no significant degradation after two years in orbit ($<\pm 0.1\%$). Toroidal wire-wound thermpoiles with approximately the desired area have been made for use on the ESP, a version of which has been included as one of the channels of the Nimbus-7 ERB. Tests performed on the ESP with irradiance levels up to 1.2 solar constants showed a temperature change of less than 1°C and linear response over three decades (see Section 4.0). The toroidal configuration provides a highly uniform response over the disc receiver. This type of thermopile detector has a balanced reference receiver with the heat sink between the active and reference receivers. This balance and heat sinking technique minimizes the effect of any conductive thermal transients and allows a relatively fast time constant. The temperature difference, ΔT, between the active and reference receivers, is not allowed to reach high values for high incident flux levels, reducing the effects of temperature dependent responsivity non-linearities. The desirable qualities of wire-wound thermopiles are good linearity, low temperature coefficient, long-term stability, and structural integrity.

It should be noted that, for off-normal axis image points, the detector presents a cross-section which varies as the cosine of the off-axis angle. Hence, the circular wire-wound thermopile detector is said to have a cosine response characteristic.

While exact data are not available, estimates have been made of the weight and power increases associated with the use of cavity radiometers rather than the flat plat thermopile. Without a shutter, the weight of each channel will increase by 0.395 kg or 0.87 lbs. This estimate is based on use of 90 percent of the available volume by a material with the density of aluminum. The available volume is a cylinder of 5.7 cm diameter and 6.35 cm height and a volume of 162.6 cm^3. If the cavity detector can be operated in the passive mode, there is no need for additional power over that already allocated per channel. In the active mode, it is estimated that each cavity channel will require approximately 0.5 watts. Use of cavity detectors in all four Earth-looking channels will require an additional 1.58 kg or 3.48 lbs. in weight and up to 2.0 watts of power.

Since the shortwave channels do not require spectral response past 5.0 micrometers, a good compromise might be the use of passive cavity detectors for the total channels and the flat plate thermopile for the shortwave channels. This would increase the weight by 0.79 kg and not affect the power. Until further studies and tests have been made of the wide field performance of the cavity detectors, however, use of cavity detectors for the ERBSS medium and wide field of view channels cannot be recommended. At the present, flat plate thermopiles of the toroidal configuration are recommended.

3.2.1.3 Medium and Wide Field of View Signal Processing

The signal processing electronics are located in close proximity to the detectors in the gimballed assembly. The design is similar to that developed for the ERB solar channels by Gulton. The basic configuration is shown in Figure 3-9. The thermopile detectors are DC devices and electronically chopped amplification is employed to avoid offsets and temperature drift in the amplifiers.

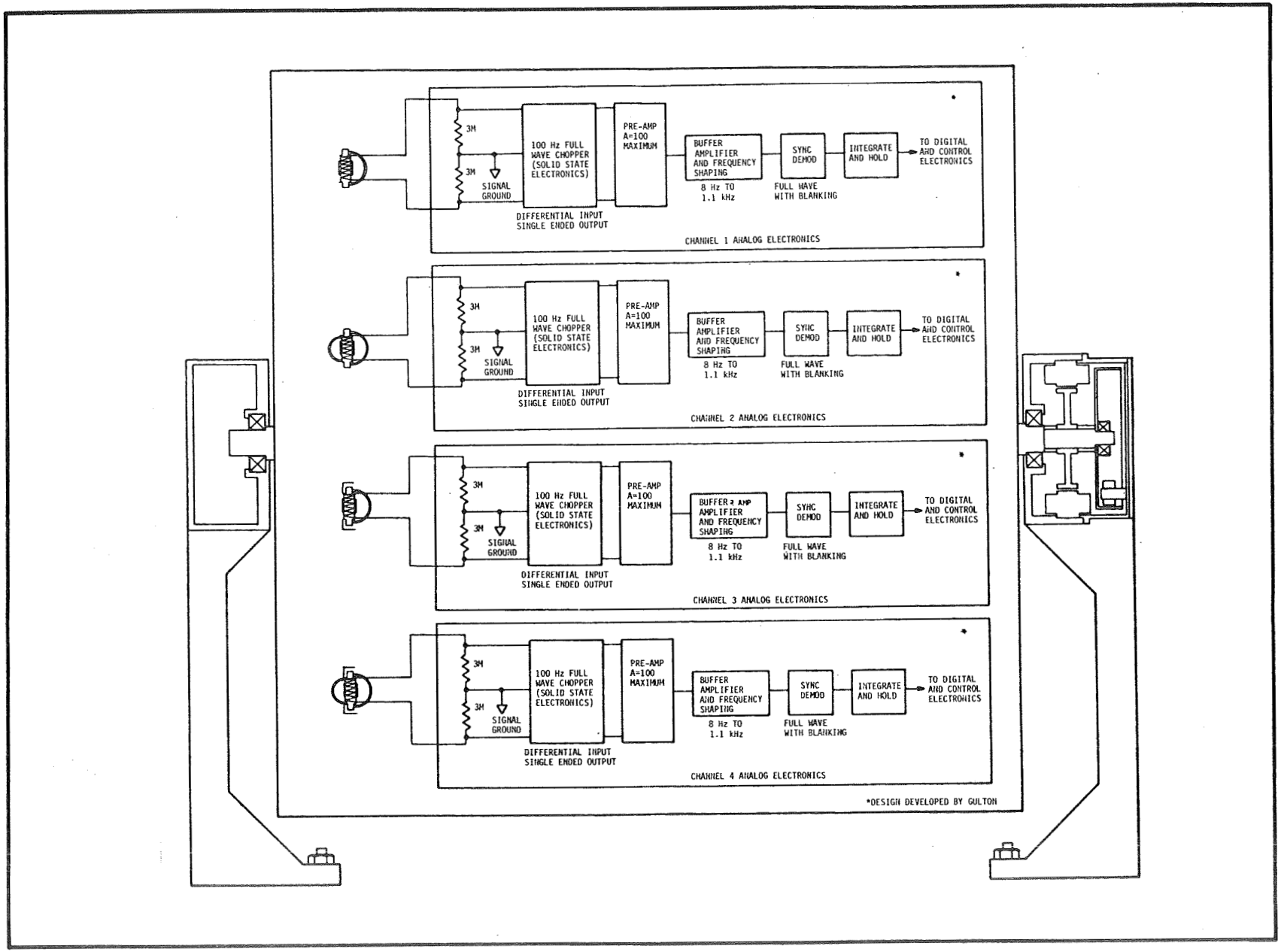

Figure 3-9 MFOV/WFOV Signal Processing Electronics

From a low level, high impedance DC signal, the amplifier provides conversion to a high level, low impedance AC signal. The post amplifier provides predemodulation filtering as well as signal amplification. The synchronous demodulator converts the signal back to DC with blanking employed at the switching crossovers to eliminate switching spikes and preserve signal linearity to low levels. The system filter is a gated integrator with an effective bandwidth equal to the reciprocal of twice the integration time. The integration time will be approximately 1.6 seconds and is synchronous with the spacecraft clock. The integrator is reset every 1.6 seconds so the output is stored by a sample and hold circuit for further processing.

To check the linearity and response of the electronics, a precision variable level voltage is gated into the input. This level should be generated by a precision digital to analog converter. The connections to the remainder of the signal processing electronics which are packaged outside the gimballed sensor assembly are provided by a shielded flex cable. Referring to Figure 3-3, the sampled and held signal level is multiplexed with the other channels and housekeeping telemetry for serial conversion by a 12-bit analog to digital converter.

3.2.2 In-Flight Calibration

In-flight calibration of the ERBSS non-scanning assembly channels will be accomplished using blackbody targets for the total channels and the sun for all channels.

3.2.2.1 In-Flight Calibration Blackbodies

Two blackbodies centrally located for instrument balance will be employed to calibrate total Channels 2 and 3. The gimballed detector assembly, which includes the hemispheric quartz filters but not the apertures, is rotated 180° to the blackbodies periodically. The blackbodies should be configured to have a field of view for the detector consistent with that of the Earth aperture. That is, the solid angle field of view should be 2.56 to 2.73 steradians for the WFOV channel and 0.56 to 1.32 steradians for the MFOV channel. In practice, these

would probably be made for the larger field of view for the AEM orbit. Wide field of view targets were provided by Eppley for the ERB in-flight calibration. A cylindrical cavity wide field of view target was fabricated for the NASA Langley Research Center under Contract NAS 1-12471 and its design should be a candidate for the ERBSS mission. It is anticipated that platinum resistance sensors will be used for control and monitoring of the blackbody temperature. A heater will raise the target to either of two controlled operating temperatures. When the heater is turned off, the blackbody should seek an equilibrium temperature at approximately the instrument temperature. The blackbody targets will, therefore, provide a three point calibration of the total channels. Control temperatures of 375K and 335K would be useful. It is estimated that each target will require 5.5 watts for a 2.5 hour time to reach 375K and 2.0 watts to maintain that temperature. The frequency of this calibration will determine the significance to the average power requirement.

3.2.2.2 In-Flight Solar Calibration

To obtain a solar calibration of the four Earth-viewing channels, the detector assembly is rotated precisely to the proper solar viewing angle. Special apertures then have to be used to define the total angle ($2\delta_2$) and the unobscurred angle ($2\delta_1$). An unobscured angle of 5° ($2\delta_1 = 10°$) and a total angle of 9.6° ($2\delta_2 = 19.2°$) have been selected to meet the design guidelines.

There are five design guidelines or restrictions which affect the solar aperture design:

- A minimum two-minute sampling period with the unobscured field is desired.
- The total angle should not include the earth limb to a tangent height of 450 kilometers.
- The total angle should not include any of the spacecraft.
- The spacecraft attitude control error of 1.4° (RSS) must be included.
- Design identicalness between the TIROS and AEM is desired.

Viewing Time. For a worst case AEM orbital sunrate of travel of 3.71° per minute, $2\delta_1$ equals two minutes x 3.71° per minute + 1.4° or 8.82°. Therefore, the smallest $2\delta_1$ unobscured angle is nine or ten degrees.

Earth Limb Interface. The Earth limb at a 450 kilometer target height restricts the view angle from the spacecraft horizontal to 20.2° for TIROS and 15.9° for AEM. Including the spacecraft attitude error, these become 18.8° for TIROS and 13.5° for AEM.

Spacecraft Interference. The angle above the spacecraft horizontal is a function of the placement of the instrument on the spacecraft mounting platform. The elevation of the rotational axis for the sensor assembly and the distance to the edge of the spacecraft are the critical areas. These cannot be identified at this time so assumptions regarding placement on the spacecraft will have to be made.

Spacecraft Attitude Control. The 1.4° RSS attitude control error is included in the calculations so that the Earth limb will not impact the calibration accuracy.

Design Identicalness. It appears that the aperture size can be made identical for both spacecraft, but the tilt angle and rotational position will vary by about five degrees.

Figure 3-10 illustrates the solar calibration aperture configuration and its angle of tilt with the spacecraft interface plane.

If we set the total unobscured angle ($2\delta_1$) to ten degrees to be consistent with the view angle of the solar parameter channel, $2\delta_2$ equals 19.2° if the distance from the detector to the aperture is 77.5 mm. Since TIROS can accommodate 18.8° from the horizontal, a view angle of 0.4° above the horizontal and a tilt of 9.2° is required. For AEM, the instrument will have to be close to the edge to accommodate a view angle of 5.7° above the horizontal and the tilt angle will be 3.9° to the horizontal. The aperture radius in both cases will be about 10 mm.

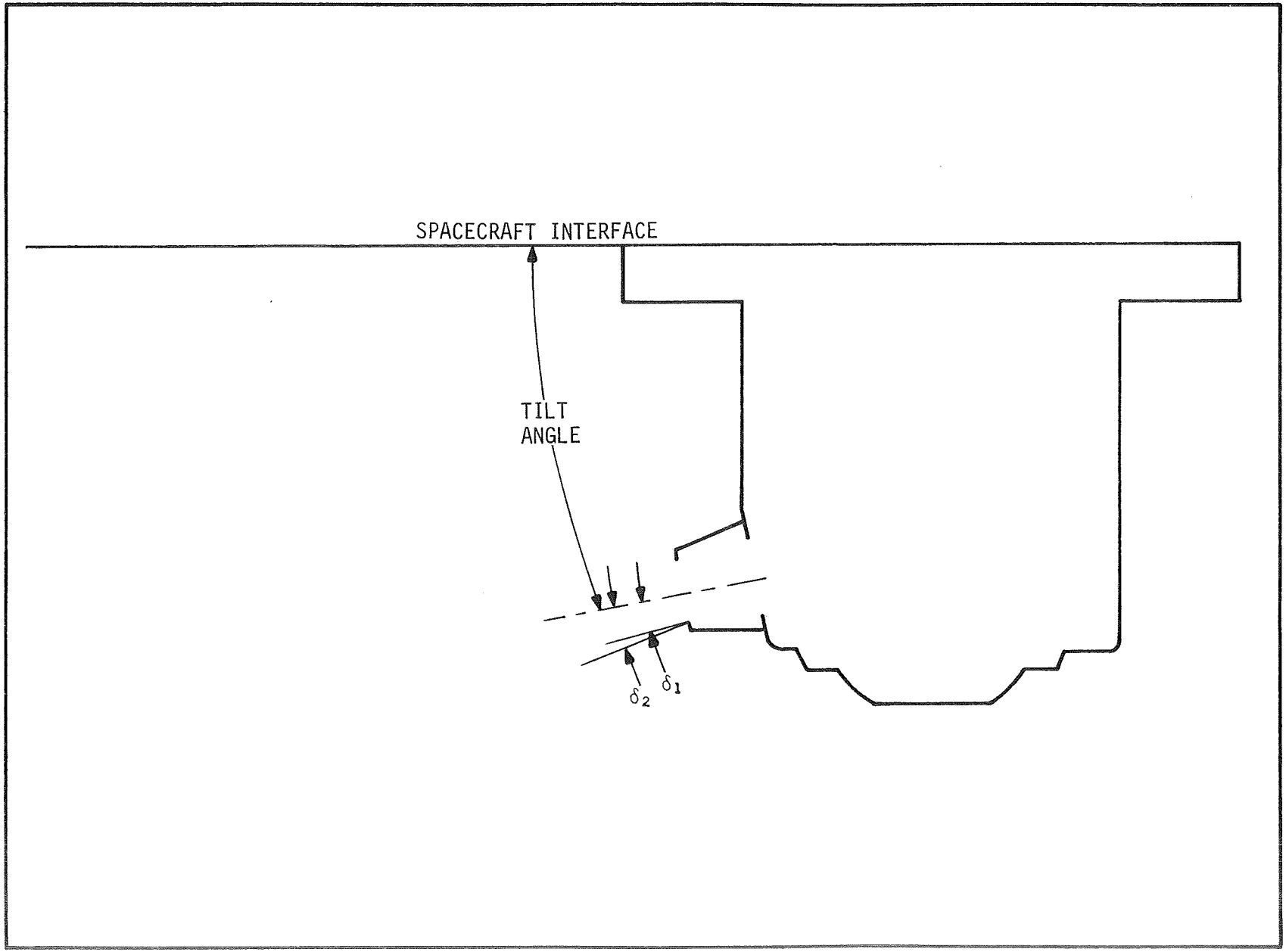

FIGURE 3-10 SOLAR CALIBRATION APERTURE CONFIGURATION

It may be that the instrument could be made identical and the mounting interface tilted. Viewing of the solar or space scene by the solar parameter channel provides a calibration reference for the solar calibration of the medium and wide field of view channels.

3.2.2.3 In-Flight Calibration Mechanism

The rotation mechanism for the blackbody or solar calibration sequences needs to provide accurate and repeatible positioning, particularly in the solar viewing positions. Data generated by the TIROS spacecraft provide knowledge of the spacecraft orientation within the error band of the altitude control system with an accuracy of 0.14°. It is expected that the AEM spacecraft or other instruments included in the payload will provide the same accuracy. Since the channels have a cosine response over the unobscured total angle field of view, an uncertainty of 0.14° at the extreme of the ±5° field has a potential error of 0.022 percent. Other potential sources of error include the aperture areas, fields of view, and field of view direction measurements. The field of view and its direction can be affected by the position of the detector with respect to the aperture. A repeatibility of position to 0.14° over an expected range of 180° requires an accuracy to one part in 1,300; certainly an achievable figure. The 11 or 12-bit accuracy required can be provided directly by the 12-bit system ADC or by a digital encoder attached to the mechanism. A rotational time of between ten seconds and one minute would probably not cause an unacceptable loss of data. A stepping system with 0.12° per step operating at 40 steps per second allows a 180° rotation in 37.5 seconds.

Complementing the elevation gimballing of the sensor subsystem is the azimuth gimbal. It will be capable of ±35° of travel as a minimum and should operate similarly to the calibration gimbal. Its purpose is to provide increased frequency of solar viewing both for solar constant measurements and channel calibration. While positioning to the accuracy of the calibration gimbal is not necessary, knowledge of its position is required to that accuracy. A position readout similar to that used for the calibration gimbal could be utilized. There are not enough commands available to position the azimuth gimbal to all the

desired positions. Three commands could be used; rotate forward, rotate aft, and stop rotation. The latter would be a timed command set to stop the rotation at the position computed from initial position and rotational speed information.

3.2.3 Solar Constant Radiometer

A prime mission goal is the measurement of the solar constant with an accuracy of ±0.1 percent and a precision of ±0.01 percent. Radiometric standards necessary to verify performance of those levels do not exist. Parallel development of various cavity radiometers has progressed in recent years to the point where it is possible to analytically determine that an accuracy of ±0.1 percent with a precision of ±0.02 percent is attainable. A cavity radiometer has been tentatively selected for Channel 5 of ERBSS. Several candidate radiometers are listed below.

(1) Eclectic Satellite Pycheliometer (ESP) developed by J. Hickey of Eppley Labs.
(2) Active Cavity Radiometer (ACR-IV) developed by R. Willson of JPL.
(3) Primary Absolute Cavity Radiometer (PACRAD) developed by J. Kendall of JPL.
(4) PMO developed by Fröhlich and Brusa of Physikalisch--Meteorologisches Observatorium (PMO), Davos, Switzerland.
(5) CROM developed by Crommelynch of Institut Royal Météorologigue de Belgique, Brussels.
(6) A High Speed Active Cavity Radiometer (HSACR) approach was studied by the University of Wisconsin.

The ESP will be flown in August, 1978 on the Nimbus-7 spacecraft as a channel of the ERB instrument. The ACR-IV is scheduled for use on the Solar Maximum Mission (SMM) and Spacelab 1 while CROM is the contribution of the European Space Agency to Spacelab 1.

Hickey, Willson, and Suomi,* have all suggested simultaneous solar measurements be made by the various radiometers. As ERBSS will have three concurrent flights, simultaneous solar measurements by three radiometers operating as Channel 5 or the same radiometers operating in different modes of operation would be possible. In June of 1976, the ESP, two ACR-IV's and the PACRAD were flown on a sounding rocket to measure the solar constant.** The measurements show a spread of only 0.37 percent overall with only a 0.07 percent difference between the ESP and the ACR-IV.

The ESP, as the name suggests, is capable of operation in a number of modes either actively or passively. It is shown schematically in Figure 3-11. Its unencumbered field of view, as shown, is 1.8°, i.e., the full 0.5 cm^2 collecting area is unobscured over 1.8°. The central angle is 5°; the same as the ACR-IV. For ERBSS, the unencumbered or unobscured field of view will be 10° and the total field of view will be 19.2°, making the central angle 14.6°. This allows a much shorter (about 10 cm) view limiter reducing the overall package length. The temperature difference between the two inverted cones is measured by a differential, toroidal thermopile identical in concept to those recommended for Channels 1 through 4. In the "active Angstom mode" (Eppley reference), the secondary cavity is servo controlled to heat up that cavity so a null is proportional to the radiant power incident on the primary cavity. In a passive Augstom mode, the power on the secondary cavity is preset and the temperature difference between the two cavities is measured by the thermopile. The measured irradiance is then a function of the preset power and the temperature difference.

The ACR-IV, shown schematically in Figure 3-12, is the latest in a series of cavity radiometers developed by JPL, including the PACRAD. The two conical cavities are made and mounted as identically as possible with the secondary cavity seeing only the housing. The primary cavity sees the view limiter and the scene when the shutter is opened. In operation, with the shutter closed power of a magnitude equal to or slightly greater than a solar constant is applied to the primary cavity with an active servo maintaining the temperature difference

*Private communications.

**Duncan, et.al., Rocket Calibration of the NIMBUS-6 Solar Constant Measurements, GSFC, March, 1977. Also, Duncan, et.al., Applied Optics, 16, p. 2690, 1977.

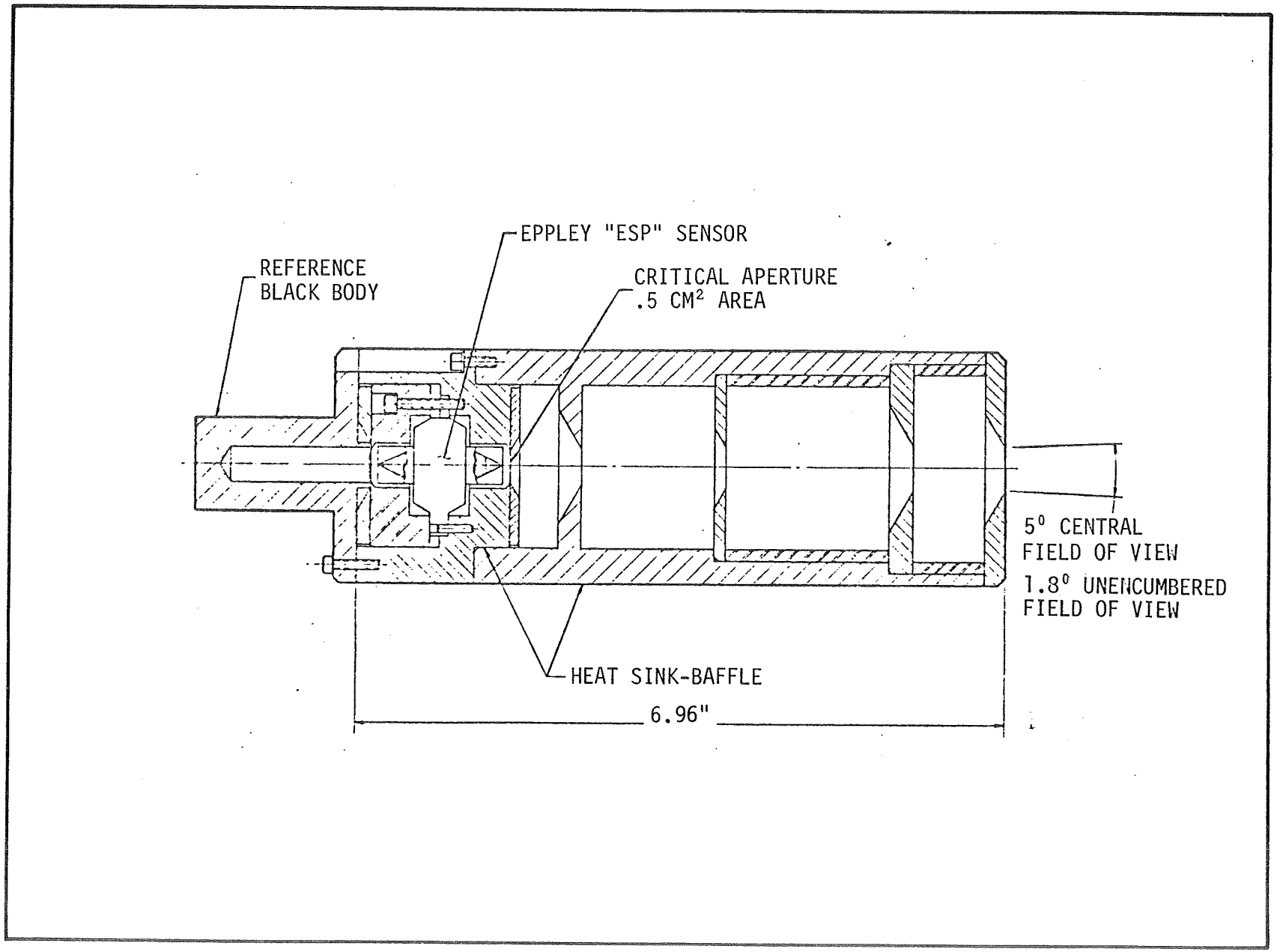

Figure 3-11 Schematic Drawing of Eppley-Gulton ESP

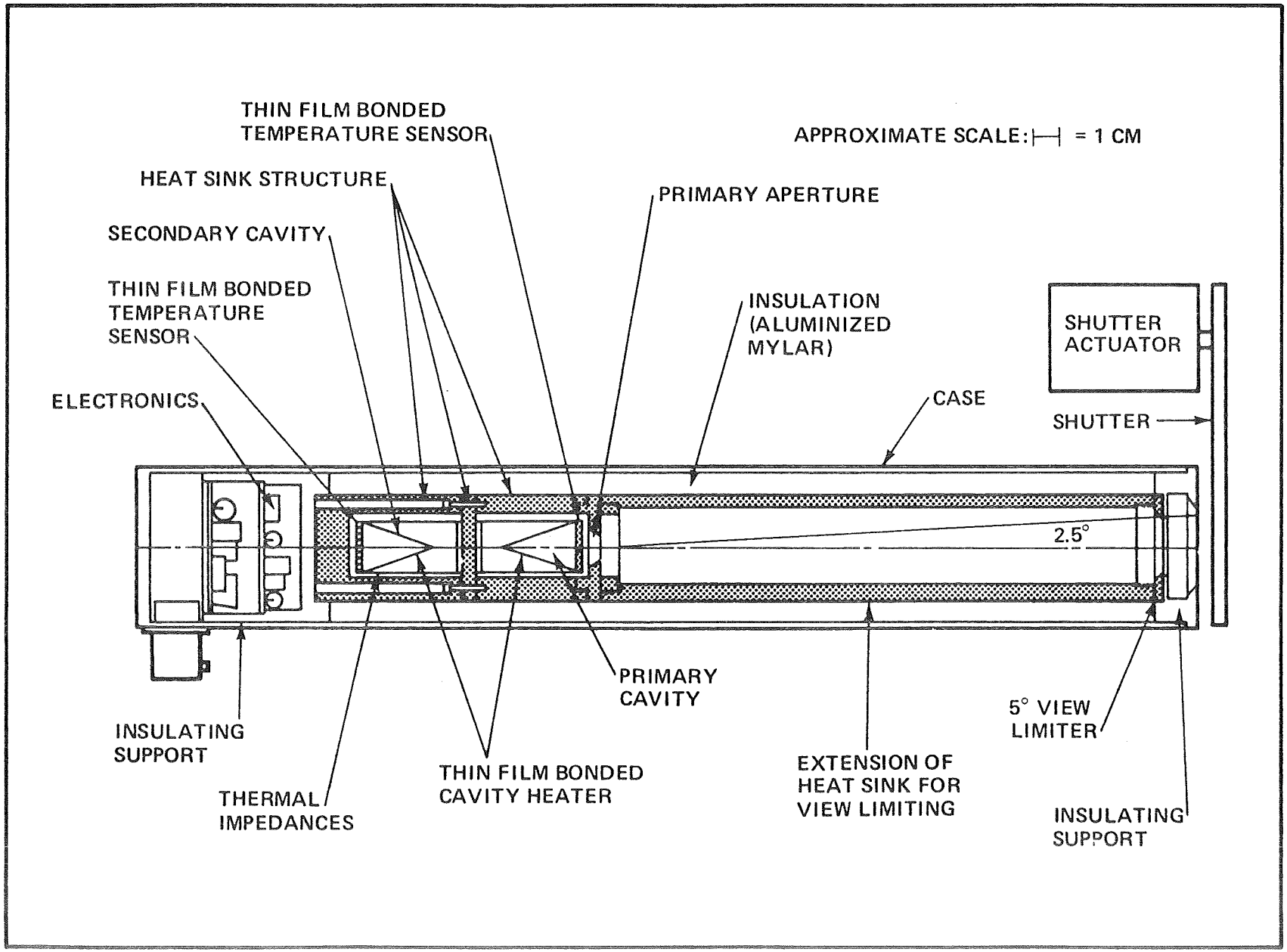

Figure 3-12 Schematic Drawing of JPL-TRW ACR IV

between the two cavities. Nickel resistance probes are used as temperature sensors. When the shutter opens for solar viewing, the servo adjusts the primary cavity power to maintain the temperature difference between the primary and secondary cavity. The measured irradiance is proportional to the difference in power between the shuttered and open states plus a small bias term. The length of the view limiter can be reduced to approximately 10 cm for the 10° unobscured field of view necessary for the ERBSS mission.

As a task within a "Wide Field of View Earth Radiosity Study" for the NASA Langley Research Center (Contract NAS 1-13204), conducted by the University of Wisconsin in 1974, a high speed ACR was among candidate detectors for Earth viewing. A design approach was formulated and various operational analyses were performed but no hardware was produced or tested as part of this contract. It was concluded that detector time constants on the order of twenty milliseconds were achievable with active, closed-loop servo control. Since this detector has not been developed or tested in final form, it is not, at present, being considered for ERBSS use. Future development, however, may demonstrate the potential of this detector for both solar and Earth irradiance measurements.

There are detailed accurate data available for weight and power requirements for PMO or CROM. The PACRAD has a long time constant requiring a large heat sink mass to minimize the effects of thermal drifts in measurements. Although exact data are not available, its weight appears to be much greater than the weight required for ESP or ACR-IV. Information obtained from Gulton Industries places the ESP weight at three pounds and its operational power at 0.5 watts. Recent discussions with Dr. Willson at JPL regarding a dual ACR-IV sets its weight at approximately 6.5 pounds and the power at five watts. It is supposed that both numbers could be halved for a single unit and that the five watts includes power for circuitry not needed in the ERBSS application. At any rate, monthly solar measurements result in a duty cycle which makes the average power requirement for either the ESP or the ACR-IV negligible.

Whichever cavity radiometer is chosen for flight with the ERBSS, it is recommended that thermal/optical/electrical modelling be performed to identify error terms and to minimize those errors through design or data processing techniques.

3.2.4 System Electronics

The functional block diagram of Figure 3-13 provides a capsule view of the entire system electronics. As discussed in Section 3.2.1.3, the DC signals from the thermopile detectors are amplified by a chopper stabilized amplifier, demodulated, integrated, and sampled and held for multiplexing to the A to D converter. The five channels and at least 13 telemetry channels needed for data reduction or interpretation are digitized to 12-bit resolution (4,095 levels).

Three, eight-bit time slots are allotted to the non-scanning assembly, or 24 bits every 0.1 second. The major frame period is 32 seconds allowing 20 data cycles every major frame. Two 12-bit words can be converted every 0.1 second providing a maximum data rate of 240 bits per second. This allows 27 housekeeping conversions plus the five data channel conversions every 1.6 seconds. Two 12-bit conversions will be made every 0.1 second and the data stored or baffled for readout into the TIROS Information Processor as three, eight-bit words.

Drive systems are included for the three mechanisms, i.e., the calibration gimbal, the azimuth gimbal and the solar constant radiometer shutter. The gimbal drives will require only simple drive systems such as a geared-down stepper. The calibration gimbal drive (see Section 3.2.2.3) requires good accuracy and a larger gear ratio. A geared-down stepper or a torquer device would be used for the solar constant radiometer shutter. The system control logic and circuitry will generate the necessary drive clocks and reference levels while the power supply will generate the necessary motor drive voltages which are derived from the 28-volt pulse load powerline.

System command requirements are summarized in Table 3-4. Twenty-three commands have been identified for 16 command functions. The addition of five spares brings the total to 28. The main instrument ON/OFF turns on the +28 volt main power and the +28 volt pulse load power buses to the instrument. Power is

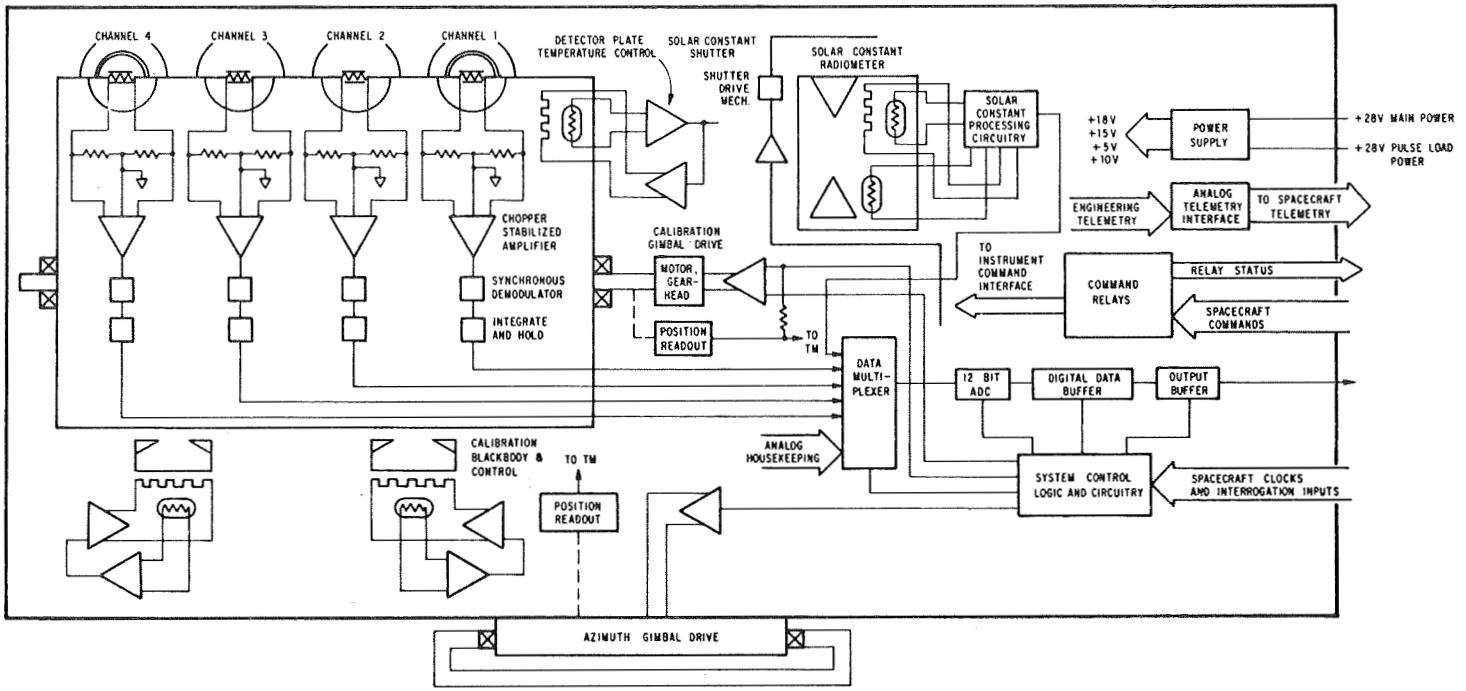

Figure 3-13 Non-Scanning Assembly Functional Block Diagram

Table 3-4

PULSE DISCRETE COMMANDS

Function	Number of Commands
Main Instrument Power ON/OFF	2
Channels 1 through 4 ON/OFF	2
Channel 5 ON/OFF	2
Detector Plate Temperature Control ON/OFF	2
Standby Heater Power ON/OFF	2
Blackbody No. 1 HIGH	1
Blackbody No. 1 LOW	1
Blackbody No. 1 OFF	1
Blackbody No. 2 HIGH	1
Blackbody No. 2 LOW	1
Blackbody No. 2 OFF	1
Channel 5 Shutter Open/Close	2
Calibration Gimbal Forward/Reverse	2
Azimuth Gimbal Forward	1
Azimuth Gimbal Reverse	1
Azimuth Gimbal Stop	1
Spares	5
	28

supplied to Channels 1 through 4 by the second command function while Channel 5 ON/OFF allows independent control of the solar monitor. Power for the detector plate heater and control system can be turned on or off by the fourth command function. Standby heater power ON/OFF bypasses the main instrument power to turn on instrument heaters during an instrument off mode. This allows the instrument to reach equilibrium after turn-on more quickly. The blackbody command, when high, sets the blackbody to its highest control temperature, probably about 375K. The blackbody low command sets the blackbody at an intermediate temperature whereas OFF allows the blackbodies to go to an equilibrium temperature close to the instrument temperature. The Channel 5 shutter is opened for solar monitoring or space reference and remains closed for internal calibration.

A calibration gimbal forward command automatically sequences the detectors to the next position in that direction. To go from the Earth position to the blackbody position, for example, two commands are necessary. The second command is given after the intermediate or solar calibration position is reached. A reverse command follows the same sequence and automatic turn-off is implemented if the wrong command is given and the gimbal goes by a stop position. The azimuth gimbal position is controlled by three commands; forward, reverse, and stop. The latter command is a timed command, following the forward or reverse command by a calculated time period, to allow stopping at a predetermined position. The position is verified by the readout and readjusted if necessary. The state of each command is verified by a voltage level to the Digital B telemetry system.

A total of 37 analog telemetry points have been identified. Twenty-three, and possibly more of these, will be multiplexed and digitized for inclusion with the sensor data on the TIP. Table 3-5 lists the analog telemetry functions to be monitored. The 14 points not multiplexed are monitored by the spacecraft analog telemetry system.

Five voltage buses are available from the spacecraft; +28 Volt Main, +28 Volt Analog Telemetry, +28 Volt Pulse Load, +10 Volt, and +5 Volt. The latter two

Table 3-5

ANALOG TELEMETRY

1	Channel 1 Aperture Temperature*
2	Channel 2 Aperture Temperature*
3	Channel 3 Aperture Temperature*
4	Channel 4 Aperture Temperature*
5	Channel 5 Housing Temperature*
6	Channel 5 Aperture Temperature*
7	Blackbody Number 1 Wall Temperature
8	Blackbody Number 1 Baffle Temperature
9	Blackbody Number 1 Base Temperature*
10	Blackbody Number 2 Wall Temperature
11	Blackbody Number 2 Baffle Temperature
12	Blackbody Number 2 Base Temperature*
13	Instrument Housing Temperature Number 1
14	Instrument Housing Temperature Number 2
15	Main Electronics Temperature
16	+15 volts
17	-15 volts
18	+10 volts
19	+5 volts
20	+18 volts
21	-18 volts
22	Reference Voltage Number 1*
23	Reference Voltage Number 2*
24	Calibration Gimbal Position
25	Azimuth Gimbal Position*
26	Shutter Temperature*
27-30	Solar Aperture Temperatures, Channels 1-4*
31-35	Detector Reference Junction Temperatures, Channels 1-5*
36-37	Filter Dome Temperatures*

*Included as housekeeping telemetry in Digital A format.

are for interface logic circuitry and will be used as needed for the data output buffer. The +28 volt pulse load bus will be used for the motor drives and the heaters. Photon isolators or other techniques will be used to maintain ground integrity. As suggested by the name, the +28 volt analog telemetry bus is used for selected analog telemetry circuits for functions not monitored by the Digital A system or functions required for proper instrument performance. The +28 volt main powers the instrument converters to generate the various amplifier or logic circuitry voltages.

Proportional controllers are envisioned for the blackbodies. Pulse width modulated control is a good possibility for power saving. The same type of system will be implemented for the detector plate temperature control.

3.2.5 Thermal Requirements

Thermal isolation from the spacecraft means that electrical power dissipated within the instrument needs to be radiated away to achieve a reasonable operating temperature. Since a wide range of solar angles and solar exposure times are possible, the instrument must be designed to operate under these conditions. The gimbal bearing provides the required low conduction to the spacecraft.

There are three areas of electrical dissipation to consider; the rotating sensor assembly, the main electronics, and the solar constant radiometer. The sensor assembly has poor conduction to the rest of the instrument as it is isolated by bearings and the flex cable provides but a small path. As several watts are expected to be needed in this area, radiative couplings will have to be employed to hold the detectors and analog signal processing electronics to a reasonable temperature. High emissivity surfaces with an area of at least 0.5 square foot are needed. However, that portion of the cylinder exposed when rotated to any calibration position should be of low emittance. Shutters for the solar viewing ports are preferable as nearly three watts of intermittant heating can be introduced to the sensor assembly.

The flatplate thermopile detectors are differential devices indicating the temperature difference between equal absorbing areas exposed on one side to the scene and on the other side to a reference. Intermediate or reference junctions are connected to the detector plate. If the temperature difference between the reference and measurement junction exceeds several degrees, responsivity and thereby calibration accuracies are affected. To avoid significant temperature variations in the detector plate (which is also the temperature of the reference scene for the back side of the detector), heaters are used to control the plate temperature to ±0.5°C. Analyses indicate that less than two watts are adequate to accomplish control over the full range of orbital conditions.

Approximately 11 watts are dissipated in the main electronics module. A package temperature of approximately 27°C can be achieved using available area (at least 60 square inches) for radiation to Earth and space.

The field of view apertures can introduce significant errors if they differ widely in temperature from the detectors. Either a negative or positive heat flow from the detectors to the apertures causes a calibration error. In the shortwave channels there is a similar result caused by coupling of the Suprasil-W filters to the apertures and the scene. The effects due to the scene can be minimized by imaginative processing of the data by computer (see Section 4). To minimize heat transfer from the aperture and baseplate to the detector, low emittance surfaces are recommended. Preliminary analyses indicate that a 27°C temperature difference between the detector and aperture can occur before the 4 W/M^2 system error budget is exceeded. As the temperature difference is reduced, the error is rapidly reduced. A decision based on a more extensive analysis needs to be made to determine whether the apertures should be directly attached to the housing or be decoupled and possibly heater controlled. Analyses made to date are based on the worst case medium field of view apertures as the wide field of view channels have a smaller view factor and therefore are less sensitive.

3.2.6 Power and Weight Summary

System power and weight estimates have been made for the non-scanning assembly. Power usage can be broken down into seven major areas; signal conditioning electronics, main electronics, solar constant radiometer, power supply, heaters, calibration blackbodies and motors. Operation of the latter two, i.e., blackbodies and motors, has been assumed to be on a very low duty cycle. Motor operation is estimated to be required no more than 15 to 20 minutes per month while the blackbodies require warmup, stabilization and operating true of about six hours per month. The solar constant radiometer could also be operated on a low duty cycle basis if necessary. Our independent estimate of the power required for the solar constant radiometer lies between the power figures received from Gulton for the ESP and JPL for the ACR-IV. All other power figures shown in Table 3-6 have been independently estimated.

Table 3-6
ERBSS NON-SCANNING ASSEMBLY POWER BUDGET

Signal Conditioning Electronics	2.0 Watts
Main Electronics	2.8 Watts
Solar Constant Radiometer	1.3 Watts
Power Supply (60% Efficiency)	4.0 Watts
Heaters	3.0 Watts
Calibration Blackbodies	0.1 Watts
Motors	0.0 Watts
Sub-Total	13.2 Watts
Unforeseen	1.8 Watts
Total	15.0 Watts

The signal conditioning electronics are the analog circuits within the rotating assembly (see Figure 3-9) for amplification and conditioning of the thermopile signal. The main electronics include telemetry, clocks, analog to digital conversion and interface electronics. The power supply includes power supply losses and any preregulation losses. The detector heat sink or mounting interface temperature is controlled by the heaters at a constant temperature. The three watts figure is a worst case based on a cold orbit.

The weight budget for the non-scanning assembly was estimated including the azimuth gimbal and is detailed by Table 3-7. Notice that the solar constant radiometer weight has been estimated at seven pounds as opposed to the three pounds estimated for the ESP and the 3.5 pounds estimated for the ACR-IV. This was included to assure sufficient thermal mass and also includes the electronics.

Table 3-7
ERBSS NON-SCANNING ASSEMBLY WEIGHT BUDGET

Subassembly	Pounds	KG
Mounting Base and Bearing	3.0	1.4
Baseplate	3.6	1.6
Cover	3.5	1.1
Rotating Cylinder	4.0	1.8
Cylinder Housing	8.5	3.9
Blackbodies	4.0	1.8
Motors/Position Readouts	2.6	1.2
Solar Constant Radiometer	7.0	3.2
Electronics	7.5	3.4
Cables, Connectors, etc.	3.0	1.4
Contingency	9.3	4.2
Total	55.0	25.0

3.3 SCANNING ASSEMBLY

The important characteristics of the scanning assembly are sumarized by Table 3-8 and Figures 1-2 and 3-2. Scanning is achieved with a rotating drum as shown. This allows the entire scene to be chopped without contamination by optical elements and minimization of polarization sensitivity. This is in keeping with a general design philosophy intended to minimize error inputs which could affect long-term channel calibration. Figure 3-14 is a simplified block diagram of the scanning assemblies channel. The chopped scene energy is converted to an electrical signal by the detector, amplified, demodulated,

Table 3-8

ERBSS SCANNING ASSEMBLY CHARACTERISTICS

Field of View:		3°C Circular in Channels 6, 7, and 8
Spectral Response	Channel 6	0.2 to 5 μm
	Channel 7	5 to 50+ μm
	Channel 8	1.589 to 1.689 μm
Baseline Detector	Channel 6	LiTa O^3 Pyroelectric
	Channel 7	LiTa O_3 Pyroelectric
	Channel 8	PbS Photoconductor
Measurement Frequency:		0.053 Second (All Channels)
Scan Line Period:		6.4 Seconds (TIROS)
Solar Calibration Channels 6 and 8:		Monthly; Every 53 Milliseconds for 90 Seconds or More
Orbital Altitude:		600 KM (AEM), 833 KM (TIROS)
Data Rate: (Maximum Required)		750 Bits Per Second
Commands:		21
Weight:		20 KG (44 Pounds)
Power:		30 Watts (Orbital Average)

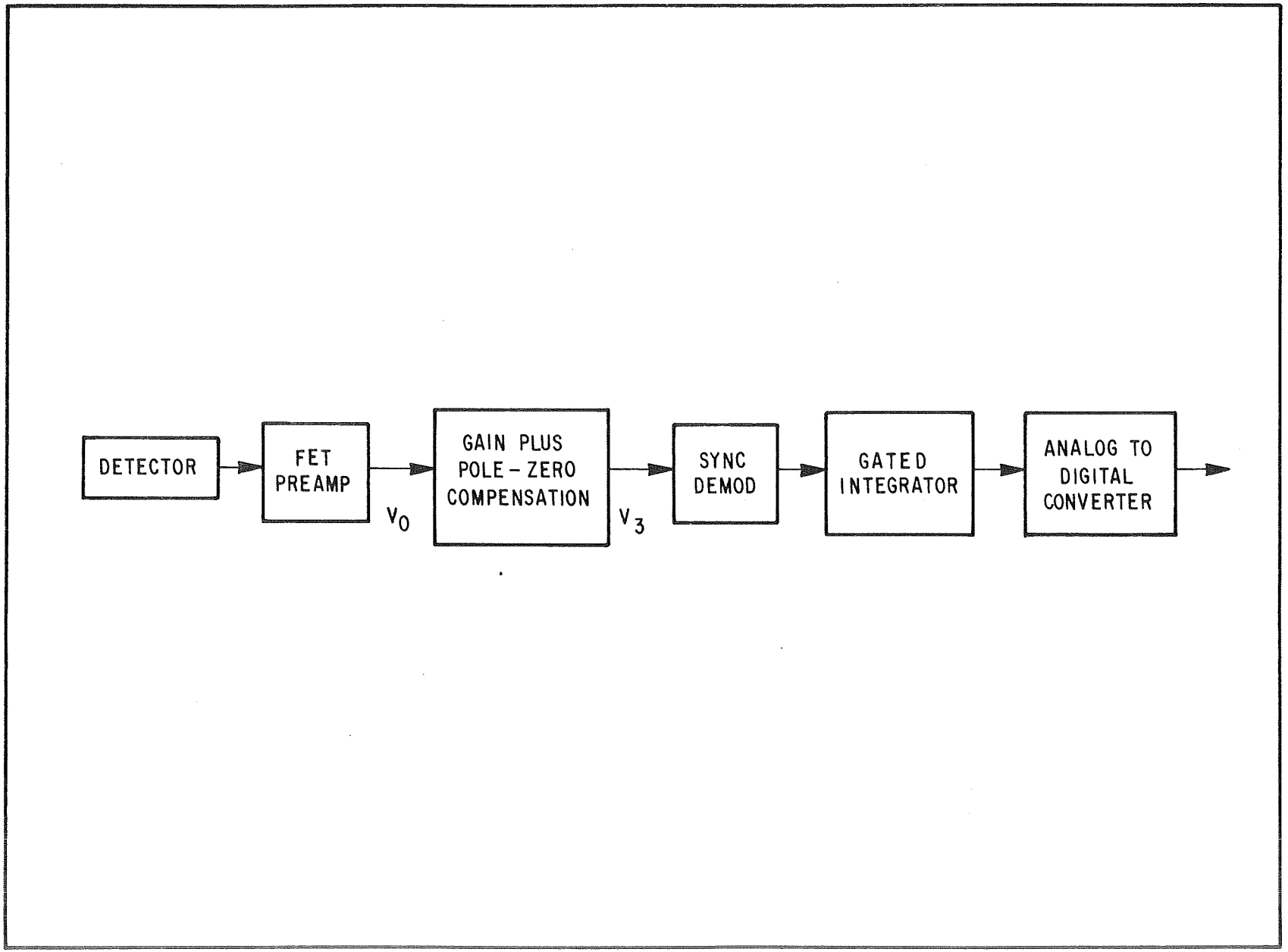

Figure 3-14 Elements of the Signal Processing Electronics

filtered, and held by the electronics. Since the system only responds to chopped radiation, unchopped background such as the optics, etc., are not a part of the signal. Therefore, variances in the temperatures of the optics, housings, stops, etc., which are unchopped do not affect the detector response and need not be included in the error analyses.

3.3.1 Optical Design Requirements

The very simple optical system recommended for the scanner is shown in Figure 3-15 and is identical, except for the filter, on all channels. A collecting diameter of 1 cm has been baselined and is set by Mirror M-2. The field stop sets the field of view to three degrees. To eliminate difference in signal due to radiance variations within the field of view and to detector nonuniformities, relay Mirror M-1 is used to form an image of the objective mirror on the detector. It is sized so that the image of the objective will fall within the detector sensitive area. To reduce polarization sensitivity of the optical configuration to a polarized scene, the relay Mirror M-1 is mounted orthogonally with respect to the objective Mirror M-2 in such a manner that the polarization components at M-1 are reversed at M-2; effectively cancelling if the mirrors have identical coatings. The configuration also allows for equal average angles of incidence at the two mirrors further reducing polarization sensitivity.

The chopper is a low-emittance specular surface on the optics side. It reflects the reference blackbody to the optics during closure and is referred to as M-3. Due to its low emittance, temperature variances are not highly significant as error sources. The reference blackbody is controlled very accurately at a radiance level which allows a single polarity signal. That is, in Channel 7, for example, the radiance of the reference blackbody is greater than the scene radiance. In Channels 6 and 8, the reference will be a black level.

The filter for Channel 6 is the same material used for the shortwave channels in the non-scanning assembly. The bandpass is set spectrally (0.2 to 5 μm) by the absorption of the material. The recommended substrate for the Channel 7 filter is Type II diamond. The shortwave cut-on can be set by an interference

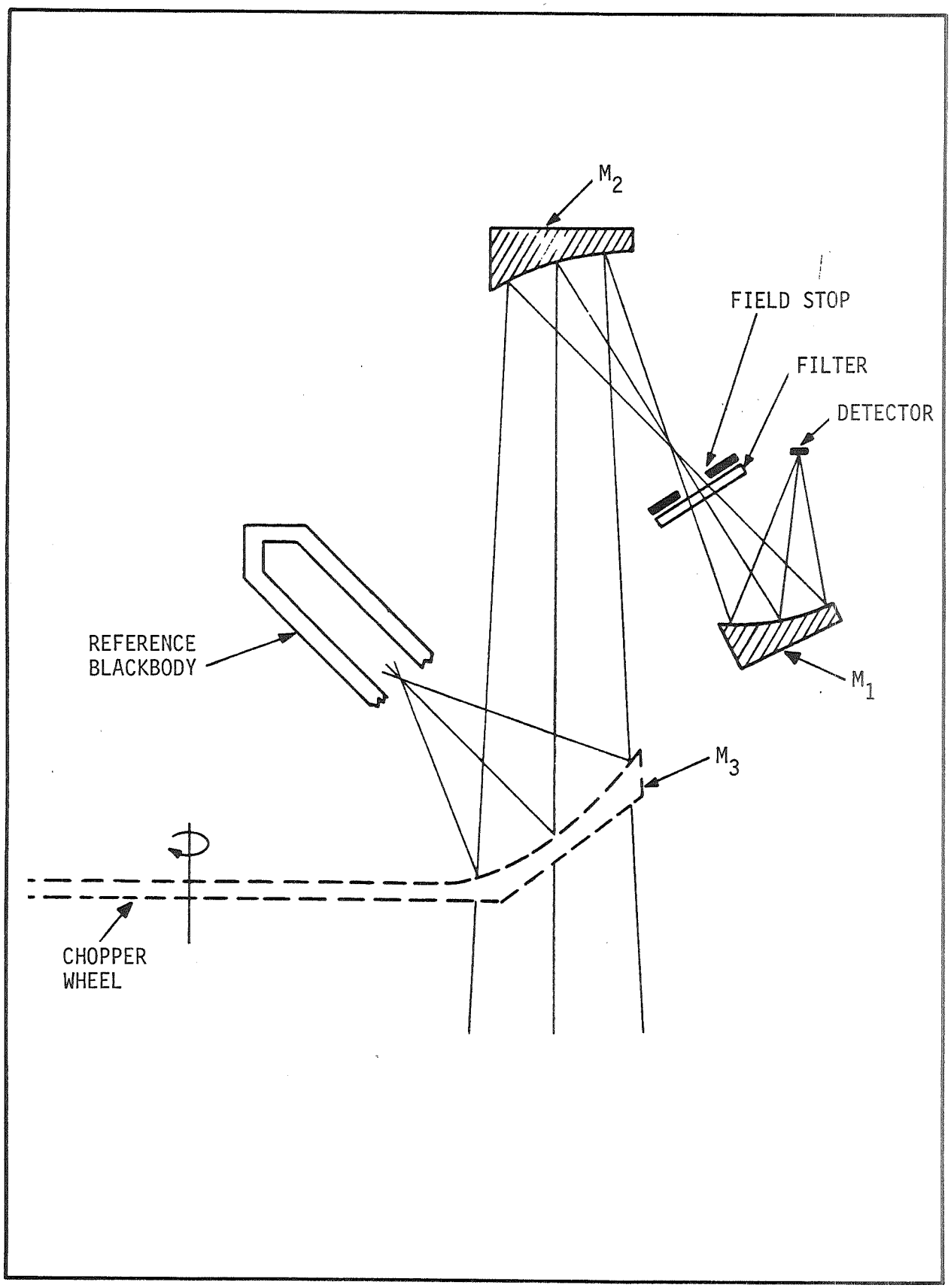

Figure 3-15 ERBSS Scanner Optical Schematic

or an absorption coating while the longwave cutoff is a function of the detector coating. A narrow bandpass interference filter with a quartz or glass substrate is recommended for Channel 8.

To reduce the number of optical components and increase sensitivity, the filter can be used as the detector window. Aluminum enhanced for ultraviolet reflectance is recommended for the Channel 6 mirrors. It is quite possible that the same coating can be used for Channels 7 and 8 also, but there is little information available at this time on the infrared reflectance of the ultraviolet enhanced aluminum. Due to this uncertainty, we recommend the use of gold as the mirror coating in Channels 7 and 8.

3.3.2 Scanning Channel Detectors

Noise equivalent radiances (NEN's) of $1.1 \times 10^{-5} w \cdot cm^{-2} SR^{-1}$ and $1.3 \times 10^{-5} w \cdot cm^{-2} SR^{-1}$ are required for Channels 6 and 7 respectively. A signal to noise ratio of 300 is required in Channel 8 for a cloud reflectance of 0.1, a solar zenith angle of 45°, and a spectral bandwidth of 0.1 μm. As shown by the analyses of Section 4, the NEN requirements of Channels 6 and 7 can be met with Triglycine Sulphate (TGS) or Lithium Tantalate ($LiTa\ O_3$) pyroelectric detectors. Because of its relatively low Curie point temperature of approximately 45°C, problems have been encountered with depoling of TGS. The $LiTa\ O_3$ detector has a Curie temperature in excess of 100°C and no depoling problems. Based on this and its availability from several United States and United Kingdom suppliers, $LiTa\ O_3$ has been tentatively selected for Channels 6 and 7.

The analyses of Section 4 indicates the futility of using pyroelectric detectors for Channel 8. Various detectors have been considered on the basis of their room temperature performance including Lead Selenide (PbSe), Lead Sulphide (PbS), and Mercury Cadmium Telluride (HG Cd Te). Of these, PbS has the best sensitivity and has been tentatively selected for use in Channel 8. For a three-degree field of view and 1 cm diameter collecting optic, the detector size is approximately 0.18 cm diameter for all scanning channels.

As stated in the previous section, the cutoff wavelength of Channel 7 is set by the detector response. Contrary to popular belief, the responses of pyroelectric detectors are not flat out to several hundred micrometers, but are a function of the black coatings used in the detector. Typical of these is the response of a detector used on the Large Infrared Radiometer for the Venus Pioneer probe shown in Figure 3-16. The response is not flat and is probably less than 50 percent at 50 micrometers. While thicker, more absorbent coatings are possible, these lead to excessive thermal resistance and slower time constants. The nonflatness of the response in Channel 7 leads to greater dependence on accurate radiance response calibration of the channel. Accurate measurements of the spectral response are also imperative. Wedge detectors, i.e., two detectors forming a V-shaped collector have been used with more specular black coatings. A typical response is shown in Figure 3-17. This improved response is gained at the expense of reduced sensitivity produced by the more than doubling of the detector area. It is recommended that the detector response requirements be considered further and that the detector configuration be held open until such time as the requirements can be firmly stated.

Another problem with the pyroelectric detectors is their microphonically induced noise. The mechanical mounting of the detector in its package and the electrical configuration contribute to the detectors sensitivity to microphonic noise. Structural resonances will have to be kept well above the chopping frequency (55 Hz) and detector mounting techniques optimized for this application.

3.3.3 Signal Processing Electronics

As illustrated by Figure 3-18, the detector output is amplified by a field effect transistor (FET) preamplifier, amplified and filtered by a post-amplifier, synchronously demodulated, filtered by an integrator, and converted to digital form. The FET preamplifier is located in the detector capsule for the pyroelectric detectors to minimize microphonics and provide low-noise amplification. A FET preamplifier is used with the PbS detector for low noise but also for its high impedance characteristics.

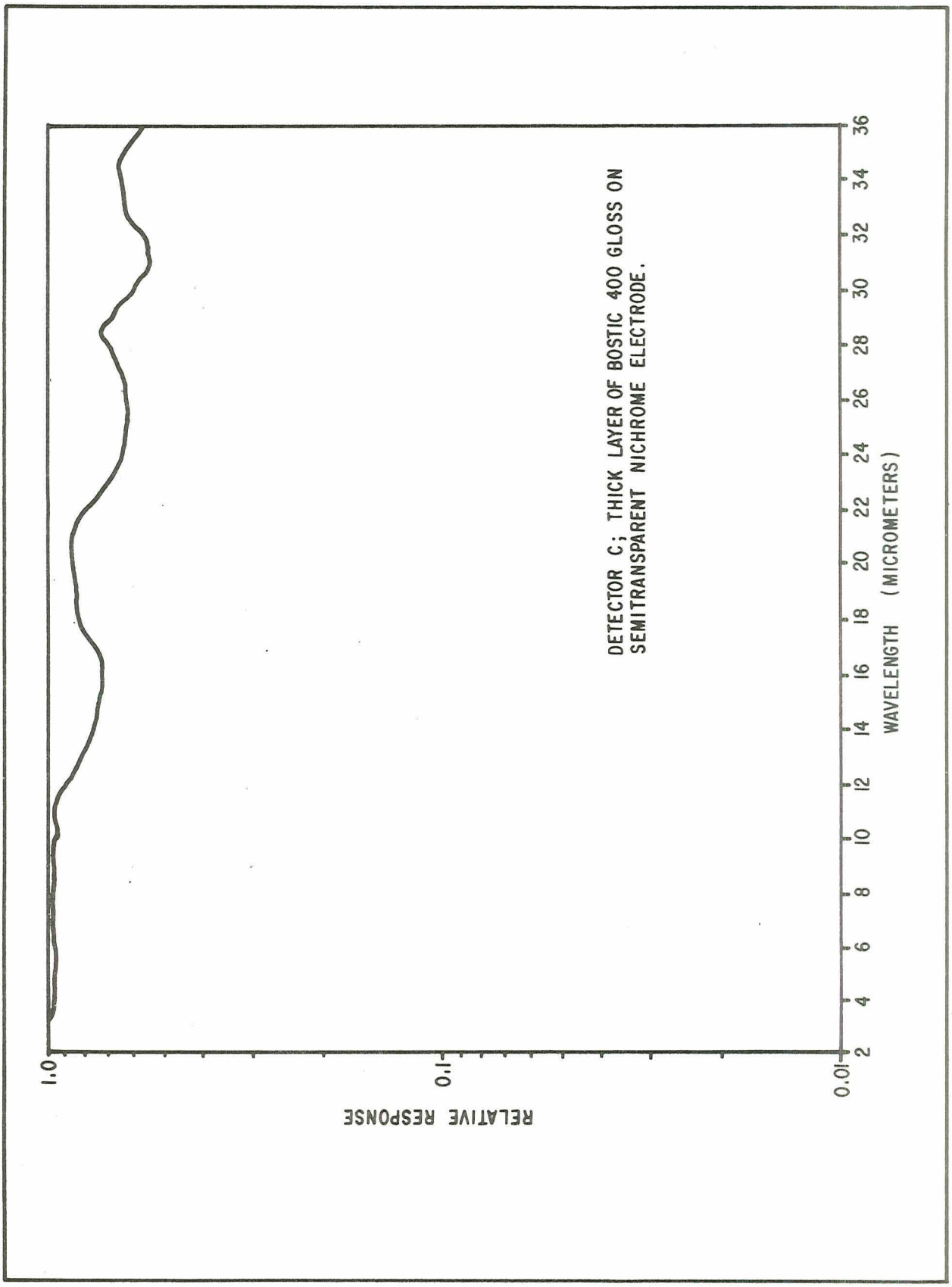

Figure 3-16 LIR Detector Response

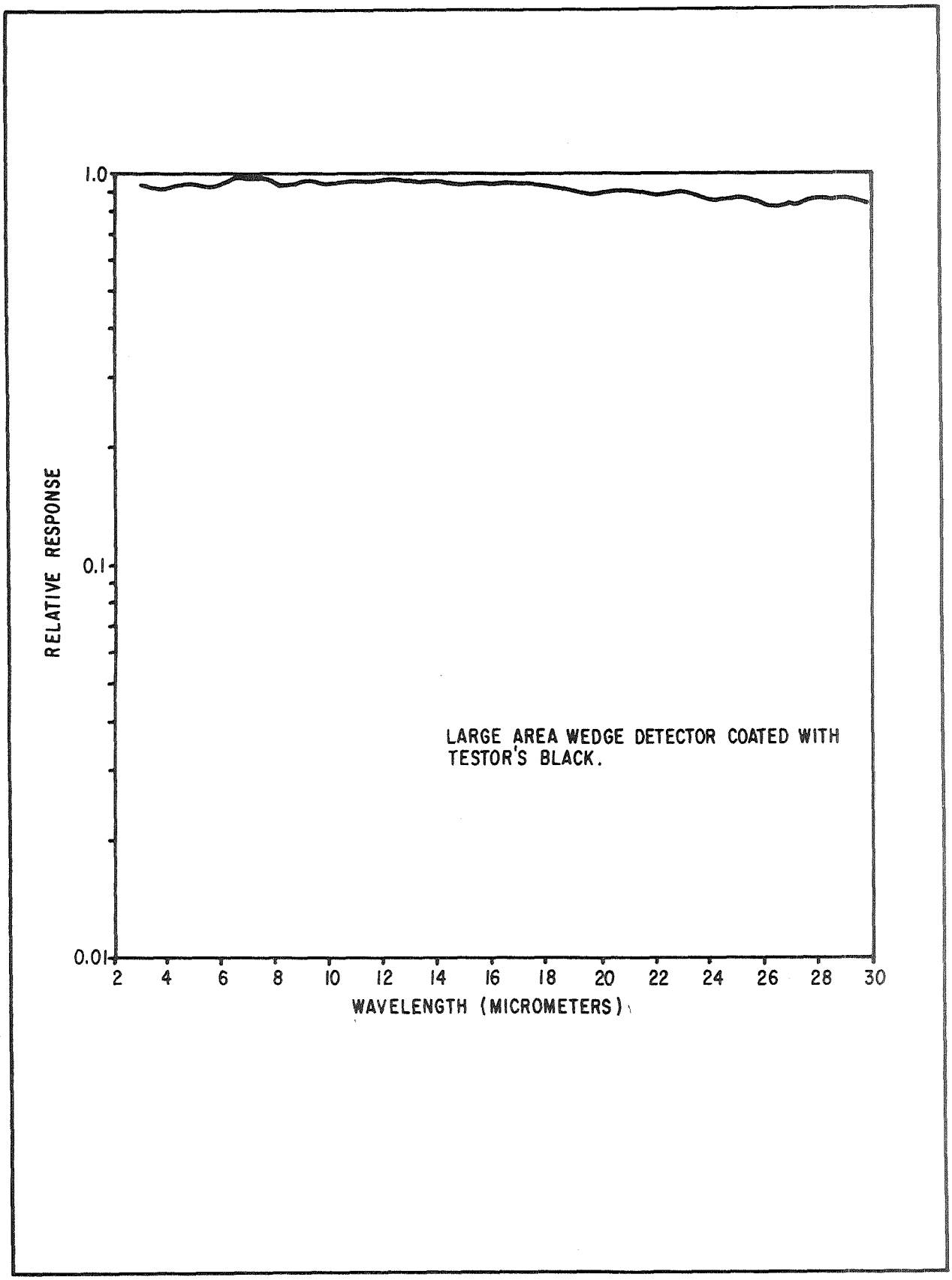

Figure 3-17 Wedge Detector Response

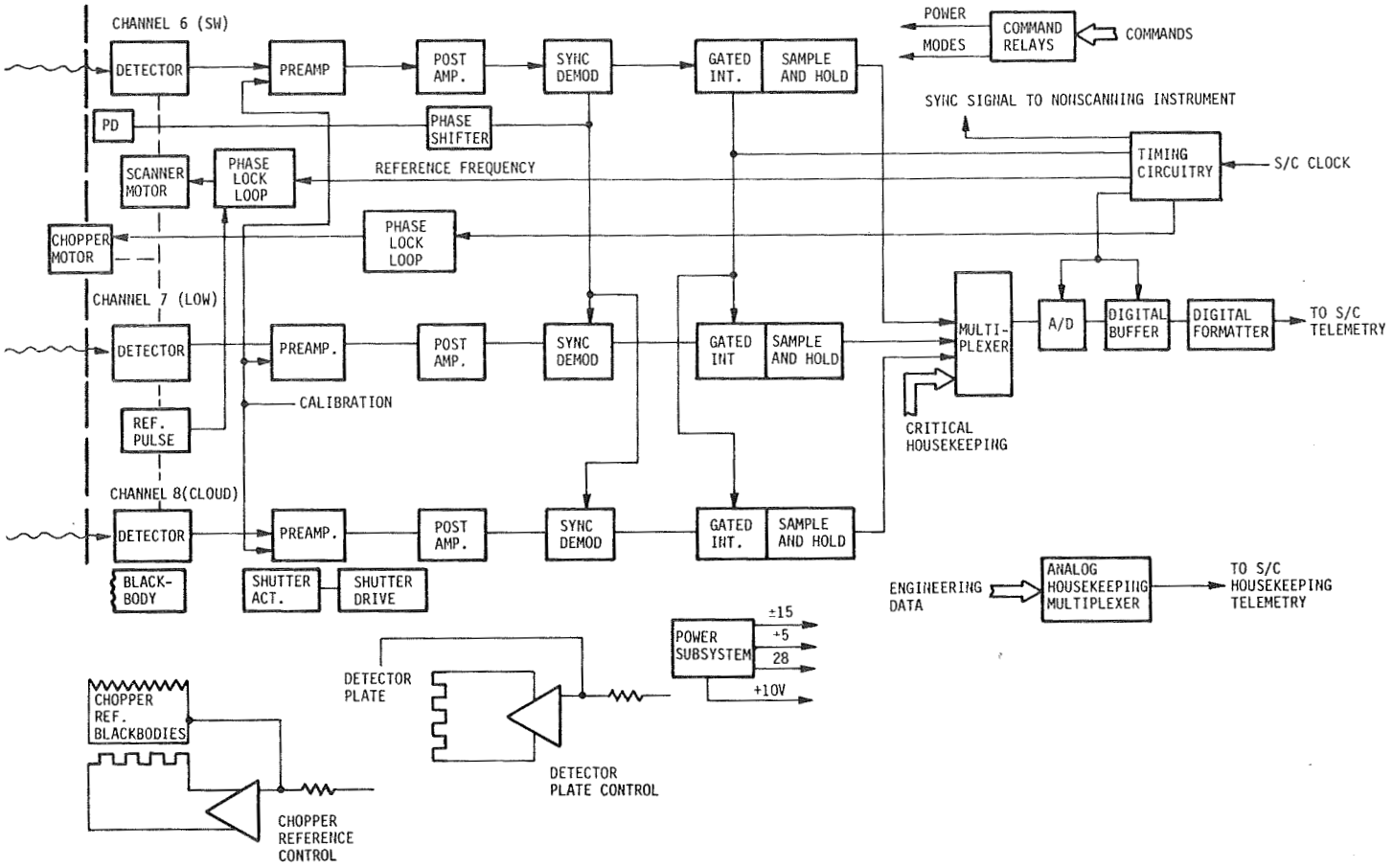

Figure 3-18 ERBSS Scanner Electronic Block Diagram

The FET noise has an important contribution to the detector/preamplifier noise as shown in Figure 3-19. Being essentially a capacitor, the detector signal and noise decrease as a function of frequency; the noise dropping-off beginning at the electrical time constant (T_E) and the signal at the thermal time constant (T_{TH}). The signal to noise is optimum over the range of frequencies from the thermal time constant to the point where the detector and FET noise are equal. The lower the FET noise the larger the range becomes. The 55 Hz chopping frequency is consistent with the present state of technology for the available detectors and FET's. The preamplifier contribution to the total system noise should not be significant in Channel 8.

Because of the thermal lag or time constant in pyroelectric detectors, a signal from a scene may be contaminated by the heating due to a previous scene. This is called the "memory" effect in pyroelectrics and other thermal detectors. The so-called memory effect can be compensated electrically by selection of the proper electrical poles and zeros in the post-amplifier, a technique demonstrated during previous programs. The post-amplifier also provides amplification and sets the predemodulation upper cutoff frequency. The synchronous demodulator is controlled by a signal derived from the chopper keeping the effects of small rotational velocity changes to a minimum. As with the demodulator used on the chopper stabilized amplifiers for the non-scanning channels, the crossover points are suppressed to eliminate switching spikes and maximize response linearity.

The gated integrator is also controlled by the chopper so that three chopping periods are integrated. This sets the integration period to approximately 53 milliseconds. A very small portion of this time is used to sample and hold the integration output and then to discharge the integrator. No error is associated with this operation as it is performed during a suppressed crossover point on the demodulated waveform. The sampled signal is then multiplexed to the analog to digital converter for quantizing (see Figure 3-14). Data rates and data interfaces are discussed in Section 3.3.7.

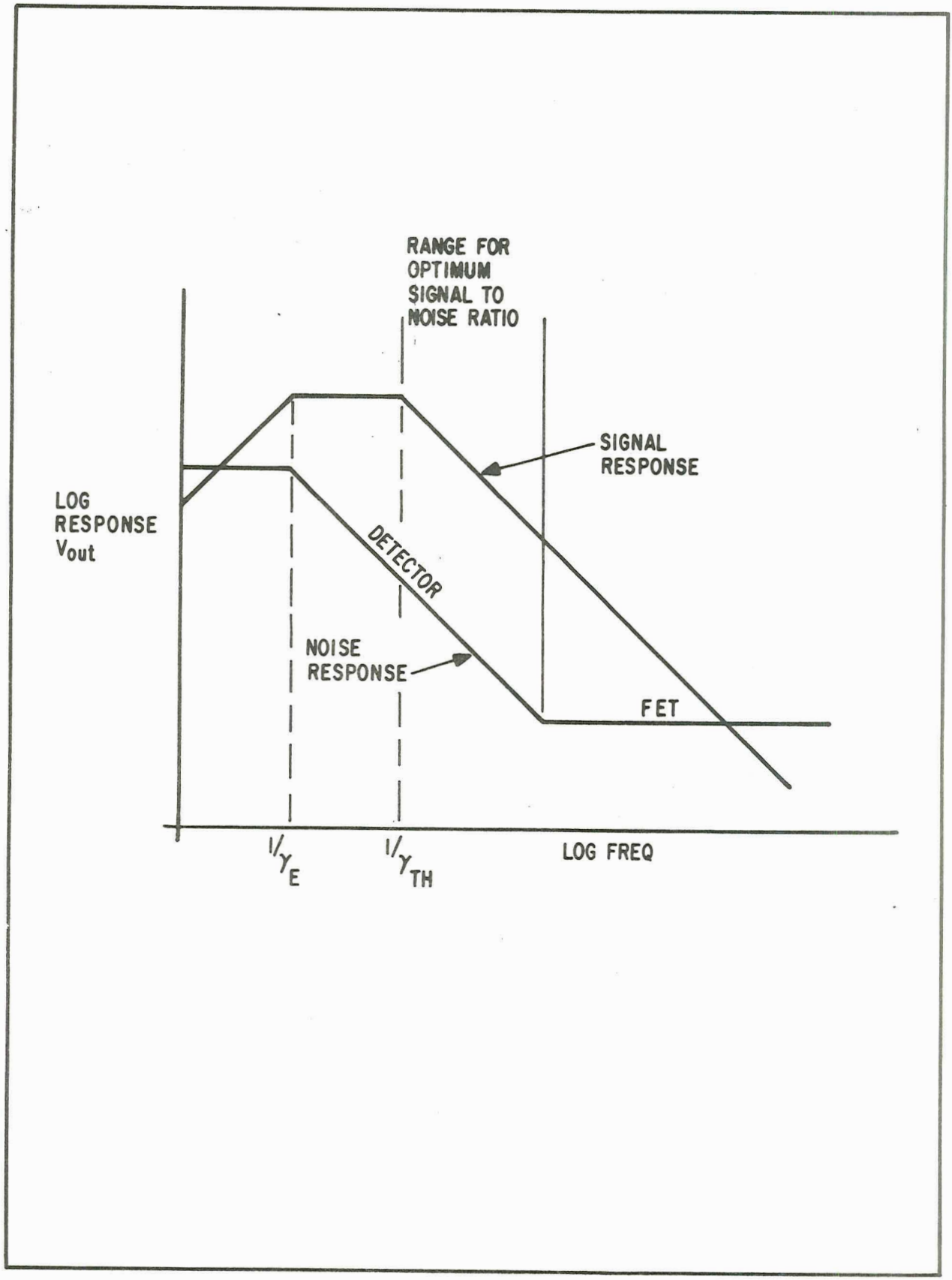

Figure 3-19 Pyroelectric Detector/Preamplifier Signal and Noise

3.3.4 Chopper Drive

The drive system for the three bladed chopper in the scanner has to be designed with the following requirements in mind:

a. The chopping frequency has to be in the range for optimum detector/preamplifier signal to noise ratio.
b. The period for the gated integrator will be three chopping periods so that any variation to response due to differences between the chopper teeth is averaged out.
c. The integration period is synchronized to the spacecraft clock and the scan period is synchronized to the major frame period of 32 seconds. Therefore, the chopper speed has to be synchronized to the spacecraft clock.
d. Variations in the chopper speed must be less than one part in 1,500 to avoid demodulation noise contributions.
e. The designs for TIROS and AEM shall be as identical as possible.
f. The chopper momentum must be compensated to 0.02-in-lb-sec.

It has been determined that a 6.4 second scan period provides nearly perfect subsatellite contiguity to adjacent lines at the Earth's surface. This allows five scans per major frame. A three-degree field of view then requires 53 1/3 milliseconds out of the 6.4 second period and a sampling frequency of 18.75 Hz. This sets the chopping frequency (three chops per sample) to 56.25 Hz and the rotational speed of the chopper drive to 1,125 rpm. Based on recent detector and preamplifier information (see Section 3.2.2), the 56 Hz chopping frequency is in the right range for optimum signal to noise. Therefore, the criteria of a, b, and c (above) can be met. To implement the requirements of c and d, a direct drive with a phase lock loop control is recommended. An encoder/tachometer generating a velocity clock is compared to a reference clock generated by the spacecraft in the phase lock loop control loop. The error signal thus derived is used to control the chopper speed so that the encoder frequency and the reference frequency are exactly the same.

This system lends itself to synchronization with the spacecraft clock and phasing to the TIP major frame. Since a counter is used to derive the reference clock from the spacecraft clock, a different division factor can be readily accomodated if the AEM and the TIROS clocks are not identical.

Initial calculations based on a conceptual drive system including the chopper, shaft, motor, and encoder show a potential momentum of 0.13 in-lb-sec and the necessity for momentum compensation of the chopper. To meet the uncompensated momentum requirement then, compensation to ±15 percent of the chopper drive momentum is required; a fairly easy requirement to meet.

3.3.5 Scan Drum Drive

Some of the scan drum drive requirements are tied in with the chopper and sampling requirements. However, the drum drive has several unique requirements included in the following overall requirements list:

a. The scan drive shall be synchronized with the major frame and the spacecraft clock. It is preferable that the start of a line of scan data is coincident with the beginning of the major frame.
b. There is no firm requirement on scan velocity control so a 0.1 field of view (0.3°) requirement has been arbitrarily imposed.
c. The designs for TIROS and AEM shall be as identical as possible.
d. There shall be periodic calibration of Channels 6 and 8 by the solar diffuser and Channel 7 by the internal blackbody.
e. The scan drive momentum must be compensated to 0.02 in-lb-sec.
f. There is no firm requirement on contiguity of adjacent scan lines at nadir.

The real problem with the scan drum concept is making electrical connections, i.e., power, grounds, clocks, data, etc., going into and out of the drum. There are two choices; the first being complete drum rotation with slipring interface and the second, partial drum rotation with a flex cable interface. There are advantages and disadvantages to both and, we have found, proponents and opponents

for both. The completely rotating drum has the advantages of a simple electrical drive system and automatic calibration if there is sun every scan. The major disadvantages in the slipring interface with its potential noise and wear are failure problems. The slipring contacts also add to the total torque load of the drive system.

The partially rotating system would probably have a controlled velocity scan from horizon to space and a faster but uncontrolled reversal back to the starting position. It would have to rotate on command to calibration positions consistent with one, two, or all of the channels. The advantage, of course, is the elimination of the sliprings and use of a flex cable with possibly better reliability. However, take-up reels for flex cables require space and weight allocations. The drive system would be electrically far more complex with its bi-directional control requirements. Assuming a 6.4 second period, continuous use, and two-year life, the slipring will undergo nearly ten million rotations and the flex cable an equal number of flexes. Life test data are available showing the ability of the sliprings to survive as many as 36 million rotations. Life testing has also been performed on flex cable assemblies with 34 million and 39 million cycles or flexes accumulated without a failure. It is recommended that life testing of the drive system selected commence early in a hardware program.

Perhaps it would be useful to state clearly the reasons a scan mirror system has not been recommended. The basic problem with a scan mirror is that radiance emanating from it is chopped and becomes a part of the signal. Therefore, surface or contamination-induced scatter provides a scene-dependent error source which cannot usually be calibrated out. Because the mirror has a finite emittance and absorptance, radiance errors dependent on emittance (which can change due to contamination) and the temperature of the mirror can be induced. A third problem with a 45° scan mirror is that it provides a surface sensitive to the state of polarization of the scene (see Section 4).

Because of the difference in altitudes between TIROS and AEM, the ground footprint or image of the field of view for identical systems will not be identical.

It is, in fact, proportional to the altitude, being 43.6 kilometers for the TIROS and 31.4 kilometers for the AEM. The subsatellite velocities for the two spacecraft are nearly equal, causing a movement along the ground track in a 6.4 second period of 42.1 kilometers for TIROS and 44.2 kilometers for AEM. This shows that there is a slight overlap in the subsatellite footprints for adjacent line for TIROS and a large overlap for AEM. Contiguity is achieved at a scan angle of approximately four degrees for AEM with this scan rate and field of view. A faster scan rate, i.e., a period of 4.6 seconds, would provide contiguity at nadir but would require a faster sampling rate and higher chopping frequency. The latter would not be compatible with the detector and preamplifier optimum signal to noise. Another possibility would be to modify the optical system for AEM, making field of view approximately four degrees but keeping the sampling rate unchanged. But a faster scan rate and the larger field of view violate the design identical requirement. It is our recommendation that we live with nadir underlap from the AEM orbit, keeping the instruments for both spacecraft identical.

3.3.6 In-Flight Calibration

Channels 1 through 4 are referenced to the solar constant radiometer during solar calibration for traceability to an absolute standard. To that end, we have looked at solar calibration of the scanning channel by 1) direct solar viewing and 2) via diffusers. It is felt that reflective diffusers are potentially the best answer for calibrating Channels 6 and 8 if true diffusers, i.e., with specular reflectance components, can be made. This better simulates the Earth scene and provides signal levels within the dynamic ranges of those channels. A blackbody target is the best choice for Channel 7, the longwave channel.

A direct solar view saturates Channels 6 and 8 and does not fill the fields of view for those channels causing incomplete detector illumination. Uniformity of response of the detectors is probably not better than five percent over the full detector area leaving a significant uncertainty related to which portion of the detector is illuminated.

For a diffuse reflector, the radiance at the optical system is:

$$H_{in} = \frac{H_s R \cos\theta}{\pi},$$

where H_s is the incoming solar irradiance, R is the diffuse reflectance of the diffusing surface, and θ is the angle of incidence of the incoming solar irradiance with respect to the normal to the surface. The critical parameters are the measurement of the solar irradiance by Channel 5, the reflectance of the surface and the accurate knowledge of the incidence angle. For an incidence angle of 45°, and an aluminized diffuser ($R \cong 0.9$), the radiance at the telescope is approximately 280 W/M^2SR with a solar spectral distribution.

A similar system was used for the ERB mission with marginal success. The diffuser concept used was borrowed from a Backscatter Ultraviolet experiment using an aluminum substrate with aluminized overcoat. A residual specular component, the inability to make two diffusers alike, and nonuniform surfaces caused problems. Nevertheless, very constant responses to these calibration targets were obtained with the ERB instrument for Nimbus-6. Since these diffusers were illuminated by the sun at the dawn terminator, the solar incidence angle was nearly a constant and no incidence angle reflectance sensitivity was apparent. For the ERBSS mission, there is a potentially wide variance in the solar incidence angle which can cause a variability in the specular component. The use of scatter plate technology, as used in scatter plate interferometry, is suggested for this application to minimize the specular component of reflectance over the wavelengths of interest. A test program to demonstrate the viability of the various possibilities for the calibration target for Channels 6 and 8 is recommended. Lambertian reflectance, a known incidence angle and coating or reflectance stability are the keys to a successful calibration which can be referenced to Channel 5. To remove the angular and coating uncertainties, it may be advisable to have a cavity radiometer mounted in a way to measure the reflected energy at the same time the scan drum is rotated to the calibration position. This, of course, will add to the weight, power and volume requirements and is not presently included in those budgets.

Since the solar diffuser will provide little reflected energy beyond five micrometers, a small, narrow field blackbody target is indicated for calibration of Channel 7. The emittance of this target should be known and constant and the temperature readout accuracy should be on the order of ±0.05°C to keep the uncertainty at the NEN level. The blackbody target is operated at a controlled level, above the ambient, on command, or can be allowed to drift with the instrument with control power off. In a study performed by Eppley Labs for Barnes Engineering Company on the VTPR program, blackbody targets using hexagonal honeycomb cavity were analyzed. Emittance variations of 0.01 percent over target temperatures from 290K to 310K were calculated for a 4:1 depth to diameter ratio of the honeycomb and a wall emittance of 0.95. The honeycomb array should be large enough to overfill the 3° Channel 7 field of view but should also be baffled to avoid coupling with emissive elements within its acceptance field.

3.3.7 System Electronics

The requirements for the signal processing, scan drive, and chopper drive electronics have been discussed previously. This section is devoted to the data interface, commands, and telemetry requirements for the ERBSS scanner. The system electronics block diagram was shown previously as Figure 3-18 and reference will be made to it.

3.3.7.1 Data Interface

The ERBSS scanner generates three, 12-bit data words every 53 1/3 milliseconds for a maximum data rate of 675 bits per second. Several of the critical telemetry points are also converted during backscan dead time but do not affect the overall data rate. Also, several levels of an electronic staircase level inserted in the data stream during the backscan are also converted in scanner dead time.

Either nine or ten, eight-bit time slots every 0.1 second have been alloted to ERBSS. For a scan period of 6.4 seconds this means that 4,608 bits (576, eight-

bit words), or 5,120 bits (640, eight-bit words) can be accomodated. The scanning assembly can generate 360, 12-bit words, or 4,320 bits every scan.

As the scanner converts three, 12-bit words (36 bits) every 53 1/3 milliseconds, it is not in synchronism with the TIP which shifts 72 or 80 bits into time slots every 0.1 second. If ten time slots are allocated to the ERBSS scanner, data can be shifted into the TIP in real time, although all ten time slots will not be used every minor frame. Provision in the instrument for 144 bits of buffered storage along with insertion of zeros every 3.2 seconds would allow the use of only nine time slots. The data would be formatted as follows:

24 bits:	Sync code
120 bits:	Zeros
2,160 bits:	Earth and space data
144 bits:	Zeros
864 bits:	Electronic calibration
648 bits:	Critical housekeeping telemetry
576 bits:	In-flight calibration data
72 bits:	Zeros
4,608 bits	

3.3.7.2 Commands

A preliminary list of command requirements is provided in Table 3-9.

Table 3-9
ERBSS COMMAND REQUIREMENTS

Function	Number of Commands
Power ON/OFF	2
Scan Motor ON/OFF	2
Chopper Motor ON/OFF	2
Scan to Nadir	1
Scan to Stow	1
Scan to Calibration	1
Gimbal Forward	1
Gimbal Reverse	1
Gimbal Stop	1
Blackbody ON/OFF	2
Calibration Shutter Open/Close	2
Spares	3
Total	19

A total of 19 discrete commands can now be identified. The power ON/OFF command switches on the 28 volt bus to the instrument providing power to all elements. The scan motor and chopper motor ON/OFF commands are intermediate commands for independently turning on and off the scan and chopper drives.

The scan to nadir, scan to stow, and scan to calibration commands tell the scan drive to go to those positions and stop. The nadir command is used if the telemetry shows a failure about to occur in the scan drive and allows data to be taken in the nadir position only. The stow command is intended to use during launch, particularly to the high contamination AEM shuttle launch. The scan to calibration is an alternative allowing the scanner to stop at the calibration position rather than scanning across the target and may not be used.

The gimbal is operated in the same way as the non-scanning assembly gimbal. Timed commands along with preknowledge of the gimbal position will allow rotation to the desired position. At the present time there is no definite plan

to control the backbody target. If this proves to be desirable, the blackbody ON/OFF command provides that capability. The calibration shutter is opened by command to allow solar energy into the diffuser cavity. The closed command puts the shutter into the normal operating position when solar calibrations are not being made.

3.3.7.3 Scanner Telemetry

Twenty-one analog telemetry points have been tentatively identified as shown by Table 3-10. Of these, 16 to 18 will be included as Digital A points. It is possible that there will be two other voltages to be monitored.

3.3.8 Thermal Requirements

A preliminary thermal analysis has been made of the ERBSS scanning assembly. The scan drum and the remainder of the instrument have been treated as nearly isolated bodies, each radiating to Earth, space, and the spacecraft. The design is intended to keep temperatures to 25°C or less. If the spacecraft finish in the immediate area of the assembly has a low emmitance, i.e., approximately 0.05, the radiating efficiency is greatly improved. The following finishes are recommended:

Scan Drum: Interior Surfaces, Black
Exterior Surface by Motor, Black
Other Exterior Surfaces, Second Surface
Silvered Teflon

Instrument Housing: Earth Facing Surface, Gold
Drum Interface, Gold
All Other Exterior Surfaces, Second Surface
Silvered Teflon

Table 3-10

ERBSS SCANNER ANALOG TELEMETRY

Function
Detector Temperature, Channel 6
Detector Temperature, Channel 7
Detector Temperature, Channel 8
Calibration Blackbody Temperature No. 1
Calibration Blackbody Temperature No. 2
Calibration Blackbody Temperature No. 3
Chopper Reference Temperature, Channel 6
Chopper Reference Temperature, Channel 7
Chopper Reference Temperature, Channel 8
Scan Drum Temperature
Main Electronics Temperature
Bias Current, Channel 8 Detector
Azimuth Gimbal Position
Scan Motor Current
Chopper Motor Current
+15 Volts
-15 Volts
+10 Volts
+5 Volts
Reference Voltage No. 1
Reference Voltage No. 2

The detector mounting surface and the chopper reference targets are actively controlled. The control temperatures will have to be determined after more detail of the design interfaces and power dissipations are identified. Control of the Channel 8 detector is the most critical and a secondary fine control may be necessary.* The desired operating temperature has not yet been identified for the blackbody target. The shutter for the solar calibration assembly should remain closed when calibration is not being made.

3.3.9 Power and Weight Summary

Estimates have been made for the power and weight of the scanning assembly and these are summarized in Tables 3-11 and 3-12.

*i.e., it may be necessary to establish a secondary temperature control interface between the temperature controlled detector mounting surface and the detector to provide fine control to $<<0.05^{\circ}C$.

Table 3-11

SCANNING ASSEMBLY POWER BUDGET

	Watts
Scan Drum Electronics	4.8
Chopper Drive Transistors	3.5
Chopper Motor	2.3
Main Electronics	5.4
Power Supply (60 percent efficiency)	6.8
Scan Drive Transistors	3.5
Scan Motor	2.3
Total	28.6

Table 3-12

SCANNING ASSEMBLY WEIGHT BUDGET

Subassembly	Pounds	KG
Housing/Structure	6.0	2.7
Drum Structure	2.6	1.2
Chopper and Drive	3.1	1.4
Scan Drum Drive	4.5	2.0
Diffusers, Mirrors, etc.	1.3	0.6
Telescopes and Detectors	1.5	0.7
Electronics	9.0	4.1
Gimbal	3.0	1.4
Miscellaneous	4.5	2.0
Contingency	8.5	3.9
Total	44.0	20.0

Section 4
INSTRUMENT ANALYSES

A number of analyses have been performed during the contract to attain an appreciation for the magnitudes of various error terms. In addition, LTV, a contractor for the Langley Research Center, has examined computer programming techniques for interactively reducing some of those errors with existing data. Most of the analyses are related to the non-scanning, Earth-looking, medium and wide field of view channels. A tabulation of the errors related to those channels is found in Section 4.1. A summary of the iterative technique for reducing shortwave channel error due to dome heating is presented in Section 4.2. Section 4.3 contains the error analysis for the scanning channels while Section 4.4 has the results of residual momentum calculations for the scanner components. An analyses was performed earlier in the program to ascertain maximum dimensions for the non-scanning assembly. The results are found in Section 4.5.

4.1 MEDIUM/WIDE FIELD OF VIEW CHANNELS ERROR ANALYSIS

The medium/wide field of view channels are subject to error inputs related to heat transfer, optical, and electrical uncertainties. These have been categorized in Table 4-1 as Extraneous Irradiance, Angular Response, Polarization, Channel Noise, Quantization Noise, and System Linearity.

4.1.1 Channel Response

All of the medium and wide field of view channels use thermopile detectors in the direct current mode. The response expression can be written:

$$\Delta W = W - W_o = \frac{\Delta CF}{S_o GS(T) V_a}$$

where:

Table 4-1

SUMMARY OF MEDIUM/WIDE FIELD OF VIEW IRRADIANCE UNCERTAINTIES

Uncertainty Term	Shortwave Channel W/M^2	Total Channel W/M^2
Extraneous Irradiance		
• Solar View	±0.22	±0.35
• Earth View	±0.22	±0.35
Angular Response		
• Solar View	±0.31	±0.31
• Earth View	0.13 ± 0.12	0.05 ± 0.12
Polarization (Earth View Only)	±0.485	Negligible
Channel Noise	±0.03	±0.028
Quantization Noise	±0.1	±0.1
Time Constant		
• Solar View	±0.033	±0.033
• Earth View	±0.066	±0.033
RSS'd Total		
• Solar View	±0.80	±0.85
• Earth View	0.13 ± 0.9	0.05 ± 0.8

- W is the irradiance at the channel aperture in an assigned spectral interval (0.2 to 5 micrometers, SW; or 0.2 to 50+ micrometers, T) in W/M^2,
- W_o is the apparent target irradiance caused by emissions of the thermopile and other optical components,
- ΔC is the digitized channel output signal in counts. (It is the difference in counts with the source exposed and with the aperture covered with a black plate at the detector temperature.)
- S_o is the thermopile sensitivity in air at 25°C ($\sim V/WM^{-2}$),
- G is the channel electronic "gain" in bits per volt (at the thermopile),
- S(T) is the ratio of the thermopile sensitivity at the pertinent temperature to its sensitivity at 25°C,
- V_a is the vacuum to air ratio (the ratio of the thermopile sensitivity in vacuum to its sensitivity in air),
- F is the filter factor and is the ratio of the total irradiance of the source in the assigned spectral interval for each channel to the actual irradiance reading the detector.

$$F = \int_{\lambda_1}^{\lambda_2} H(\lambda)d\lambda \Big/ \int_{\lambda_1}^{\lambda_2} H(\lambda)\tau(\lambda)d\lambda$$

where:

$H(\lambda)$ is the source spectral irradiance, $\tau(\lambda)$, is the spectral sensitivity function of the channel (primarily the transmission of the Suprasil-W hemisphere) and λ is the wavelength in micrometers. (The thermopiles are assumed here to be spectrally nonselective.)

Note that the ERBSS thermopile channels with Suprasil-W filters will be calibrated in terms of irradiance in the assigned spectral intervals, not in terms of the filtered irradiance at the thermopile receivers.

F for the filtered channels should, in theory, be different for various sources (solar simulator, sunlight at the ground, and extraterrestrial sunlight), but Suprasil-W is so transparent that in practice, no spectral corrections need be applied for the various sources. F = 1 for the unfiltered (0.2 to 50+) measurements.

Thermopiles are "thermal detectors" and respond to thermperature changes of their receiver surface. The receiver is warmed by incident radiation and cooled by its own emission. Thermal detector signals, therefore, depend upon the net irradiance at the receiver surface.

The thermopile signals are generated by temperature differences between thermocouple junctions in intimate contact with the primary receiver and corresponding referenced junctions. The reference junctions in the case of the Eppley circular wire-wound thermopiles are in intimate contact with a reference receiver identical to the primary receiver, but facing in the opposite direction. The reference receiver will view a relatively massive low emittance aperture so that its field of view will be filled by its reflection and reflections of its surroundings. All sources seen by the reference receiver will be nearly at the same temperature as the thermopile body. Terms to represent temperature changes of the reference receiver are not included in the formulae given here. The time constants of the primary and reference receivers are matched, so that thermopile body temperature changes will not generate false signals. However, to keep the thermopile response nearly constant and linear, the mounting surface for the thermopile is controlled to a nearly constant temperature. The thermopiles are in a heat transfer situation with the mounting interface, the field of view limiting aperture, the scene, and in the case of the shortwave channel, the Suprasil-W domes. The wide field of view channels as part of their "scene" see an annular view of space or the Earth limb around the Earth. During solar calibration, the field of view is more limited but as the sun subtends only one-half degree, there is also a heat transfer to space. The term W_o in the response equation then includes unwanted or extraneous heat transfer with the aperture, mounting surface, dome (SW only), and space.

In addition to the thermal error inputs, there are optically related inputs to $W_{\bar{0}}$ such as scattered light and angular response uncertainties. Both effects are amplified in the shortwave channel due to the hemispheric dome. Scene polarization also has a strong effect in the shortwave channels, again because of the dome. The electrical effects include the detector time constant, thermally-induced noise, quantization noise, and linearity associated with the detector and electronics. While these terms are identifiable, they represent random errors which cannot readily be eliminated and reduced in magnitude. Electrical offsets can, of course, be calibrated out. The term ΔC in the response equation indicates a relative change in the system output rather than an absolute value.

4.1.2 Extraneous Irradiance Magnitudes

Preliminary thermal analyses have been performed on the medium and wide field of view truncated hemispheric apertures without the Suprasil-W domes, and on the solar viewing apertures.

As indicated earlier, LTV has developed an iterative technique for the reduction of data in the wide field of view shortwave channel which reduces the magnitude of errors associated with heating of the Suprasil-W dome by the scene irradiance. In determining the magnitudes of errors associated with any particular error source we have taken into consideration whether such an error may be reduced by iteration with additional data or by calibration. Extraneous irradiance during the Earth-looking mode has two contributors; coupling with the aperture and mounting surface, and heating of the dome by scene irradiance. We have found that the worst case for the first is the medium field of view total channel. The worst case for the latter is the wide field of view shortwave channel.

The thermal analysis of the two truncated hemispheric apertures and of the solar viewing apertures was performed with a Monte Carlo thermal view factor program which accounts for specular reflections and which can exactly model curvilinear surfaces, rather than approximating them by a series of flats.

Earth Viewing Position. In this position each detector looks out directly into its hemispherical aperture shield. There are two sizes of this shield; one for the medium field of view and one for the wide field of view. These shields are identical except for dimensions, so the radiation models were also similar (Figure 4-1). The nodal breakdown is:

Node	Description
1	Space or Earth
2	Hemispherical aperture shield
3	Stationary floor (2 is mounted to this)
4	Detector
5	Rotating floor (4 is mounted to this)

A Monte Carlo program determined the radiation interchange factors with these surface properties:

Node	Finish	ε	ρ Diffuse	ρ Specular
1	--------	1	0	0
2	Gold	0.03	0	0.97
3	Gold	0.03	0	0.97
4	Detector	1	0	0
5	Gold	0.03	0	0.97

Errors are introduced into the detector's signal because of radiative heat transfer between the detector and the surroundings which are not part of the scene. Thus we need to examine the heat transfer between Node 4 (detector) and Nodes 2, 3, and 5.

Node 4 is well-mounted to Node 5 so that there is no temperature differential between them; thus there is no heat transfer between them. The thermal design of the instrument required that there be a gradient between the rotating portion (Nodes 4 and 5) and the stationary portion (Nodes 2 and 3), and with the rotating portion of 298°K and the stationary portion at 284°K under normal operating conditions.

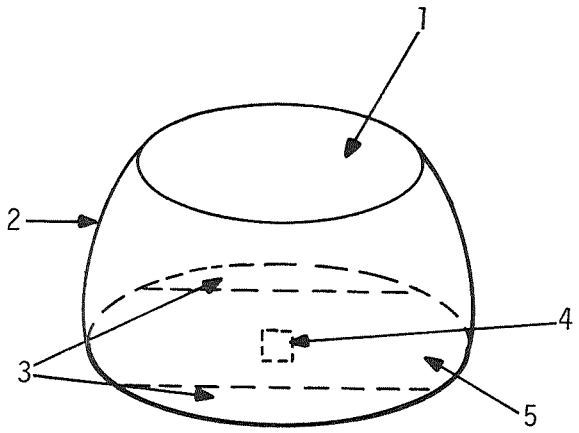

Figure 4-1 Earth Viewing Aperture Nodal Breakdown

The error term is thus $Q = \sigma(B_{2+3-4})\ (T_4^4 - T_{2+3}^4)$ where σ = Stefan-Boltzman constant = 5.66961×10^{-8} watts/m^2 - $^oK^4$.

B_{2+3} = radiative interchange factor
= 9.097×10^{-7} m^2 for the medium field of view aperture
= 3.389×10^{-7} m^2 for the wide field of view aperture

For a detector area of 3.167×10^{-5} m^2

Q/A = 2.25 w/m^2 for the medium field of view aperture
Q/A = 0.84 w/m^2 for the wide field of view aperture

The exact coupling for each channel can be determined by thermal testing and calibration. Temperatures of the apertures and thermopiles are included in the data stream. Relatively simple correction factors can then be applied to the data, reducing the magnitude of the error term. Assuming an uncertainty in the temperature readouts and emittance and view factors equivalent to 2°C, the uncertainty in the total medium field of view channel can be estimated at ±0.35 w/m^2.

When the detectors are rotated to the sun-viewing position, they look into a large cavity (which is a portion of a cylinder) before they view the actual solar aperture enclosure (Figure 4-2). This cavity has been modeled as in Figure 4-3, using these surface finishes.

Node	Finish	ε	ρ Diffuse	ρ Specular
Apertures (A-D)	Hole	1	0	0
Detectors (F-G)	----	1	0	0
Cylinder Ends	----	1	0	0
Cylinder Curve	Gold	0.03	0	0.97
Floor	Gold	0.03	0	0.97

Notice that in this preliminary analysis, the actual solar aperture enclosure has not been modeled except as an entrance hole with $\varepsilon = 1$. This is probably

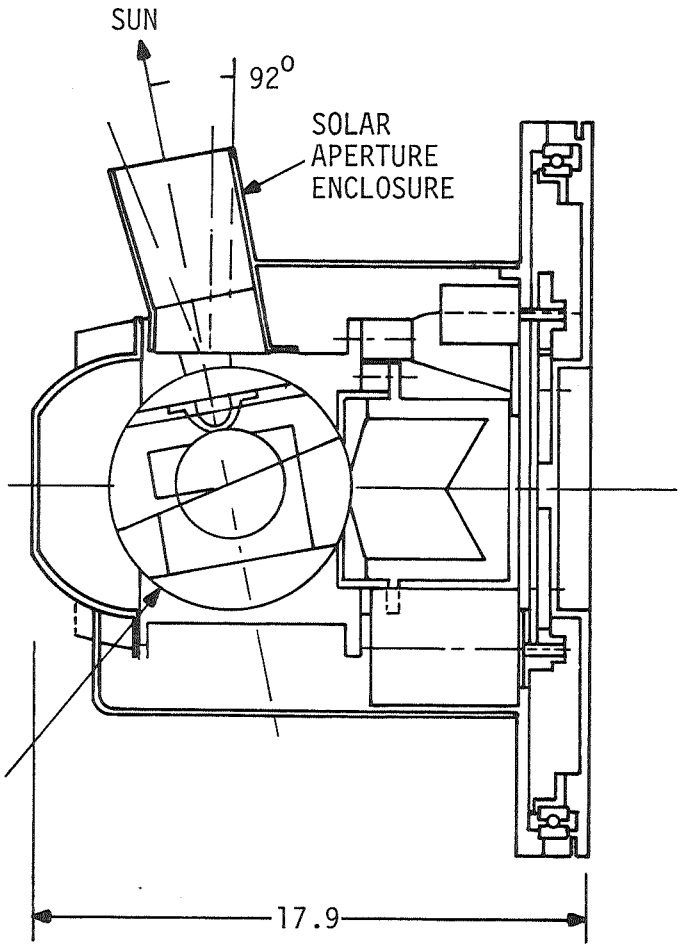

Figure 4-2 Cross-Section with Detectors in Sun-Viewing Position

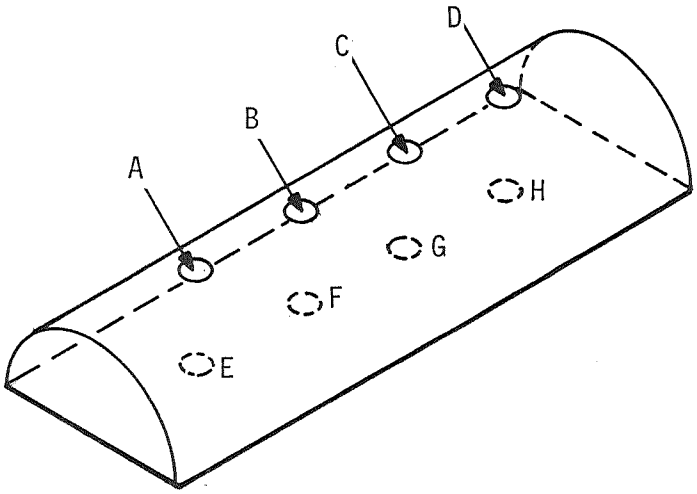

Figure 4-3 Nodal Breakdown of Cylindrical Cavity

close to correct because energy leaving the detector will not reflect back to the detector. Using 298°K for the floor and detector and 284°K for the rest of the enclosure we get, for detector F or G,

Interchange	B, m^2	Q/A, w/m^2
Detector - cylinder, curve plus ends	9.760×10^{-6}	24.1
Detector - hole	16.736×10^{-6}	41.4

These effects are much larger than the desired 4 w/m^2. The temperature differential cannot be reduced because of the need to dump electrical power being dissipated in the rotating part, so these potentially large effects will have to be calibrated out using in-flight temperature measurements (see Section 5.0).

In the shortwave channel, the Suprasil-W filter absorbs most of the longwave radiation. Scene irradiance causes cooling of the filter causing heat transfer from the thermopile and an error. As shown in Section 4.2, the error can be reduced to 0.2 w/m^2 using an iterative computer programming technique. Another source of error associated with the filter is the longwave leak shown by Figure 4-4.

If we assume an emittance of 1.0 for the Earth and a transmittance for the quartz filter of 0.9 at wavelengths greater than 1,000 μm, the longwave leak for a temperature of 300K is 8.75 w/m^2. Because of the flat-plate nature of the thermopiles, absorption drops off rapidly at larger wavelengths, considerably reducing this term. Assuming that the total and shortwave channels are identical except for the filter, the longwave leak can be removed using measurements from the total channel. The response of the total channel is composed of shortwave and longwave components and can be expressed as:

$$R_T = W_{SW} + W_{LW}$$

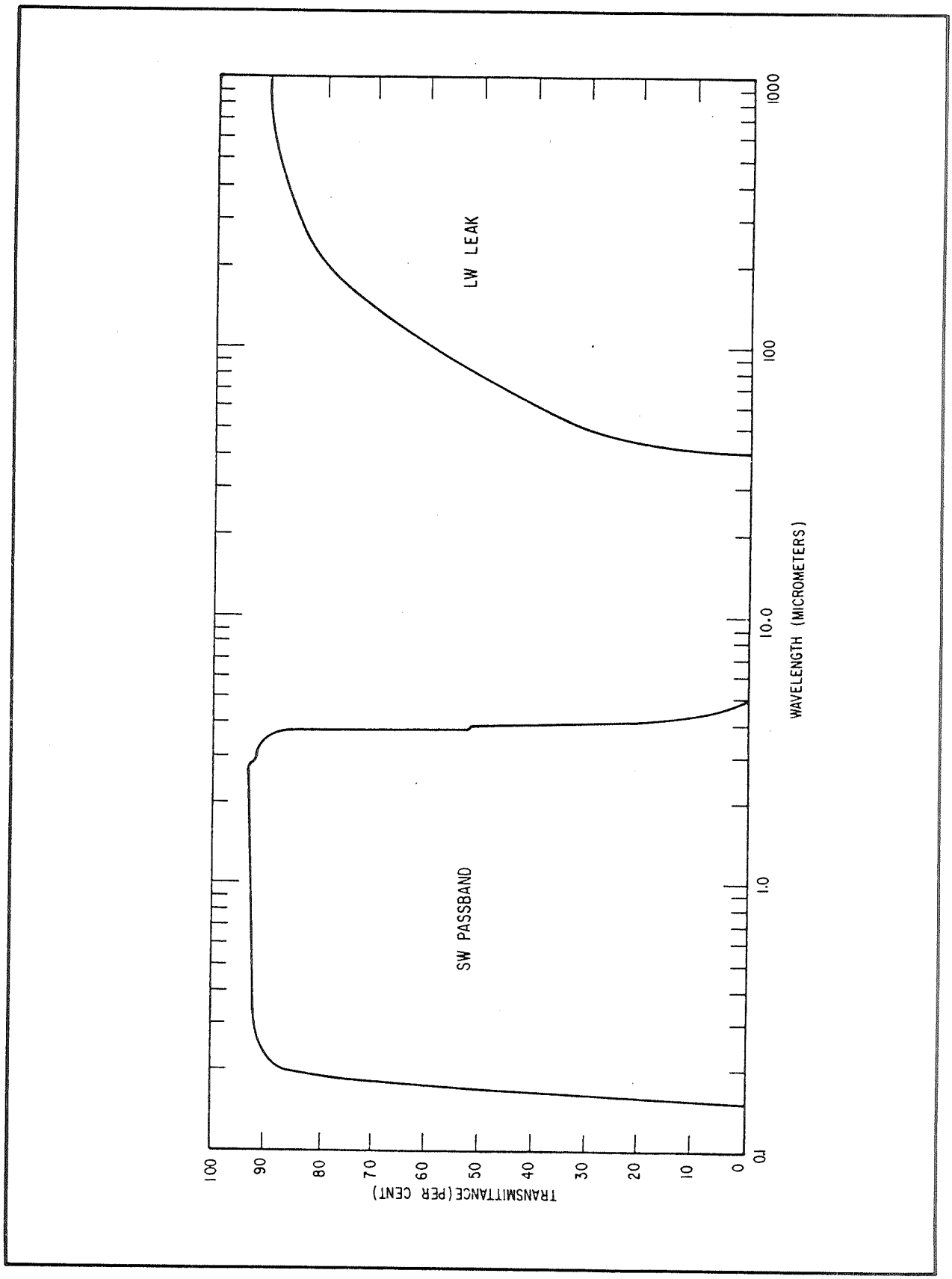

Figure 4-4 Transmittance of Fused Quartz (1mm)

The shortwave channel response is comprised of the shortwave solar reflected radiator and the leak term as follows:

$$R_{SW} = W_{SW} + L$$

The difference between the readings in the two channels is then $W_{LW} - L$. At a 300K Earth temperature, the leak is less than two percent of the longwave total. Knowledge of the spectral responses of the channels at the longer wavelengths reduces the uncertainty of this term to less than ± 0.1 W/M^2.

Shortwave channel errors due to extraneous irradiance can be RSS'd to ± 0.22 W/M^2 while the total channel is ± 0.35 W/M^2.

4.1.3 Angular Response

The angular response error terms include response errors due to the Suprasil-W dome in the Earth-looking mode, scattering for the Earth-looking mode, and pointing inaccuracies identifiable with the solar viewing. The Suprasil-W dome provides a small focusing effect causing a departure from a cosine response. This is more pronounced at the higher angles (from the normal) and is negligible at the smaller angles. Therefore, it can be stated that there is no effect for solar viewing. With the detector radius equal to 0.58 times the filter dome radius, the solid angle field of view is increased from 2.5613 SR to 2.5665 SR in the WFOV channel. This represents an increase of 0.2 percent and a response increase of 0.002×400 W/M^2 = 0.8 W/M^2. Much of this error can be removed by calibration with a wide field of view target and measurements of the solid angle channel response. The uncertainty associated with the error term is estimated to be 0.12 W/M^2.

As indicated above, the error is a percentage of the highest expected shortwave irradiance in the wide field of view. This is calculated for an average scene albedo of 0.37, an average zenith angle of 13.0° and a solar constant of 1368 W/M^2 and is approximately 400 W/M^2. The worst case total irradiance for a wide field of view channel is based on a scene with 50 percent cloud cover,

an albedo of 0.43, an average ground temperature of 300K, and an average cloud temperature of 240K resulting in a total scene irradiance of 500 W/M^2.

Energy scattered into the field of view or scattered away from the field of view also affects the channel response. A scattering analysis was performed on the shortwave and total wide field of view channels to get a worst case. For low emittance surfaces on the field of view apertures and on the detector mounting plane, the total channel energy is increased by 0.01 percent and the shortwave by 0.033 percent. Based on the worst case scenes discussed above, the total channel error is 0.05 W/M^2 and the shortwave 0.13 W/M^2. These are bias errors difficult to calculate out. The shortwave scattering is highly dependent on dome polish and cleanliness. The angular response uncertainties are then 0.13 $W/M^2 \pm 0.12$ W/M^2 in the shortwave channel and 0.05 $W/M^2 \pm$ 0.12 W/M^2 in the total channel. No attempt was made to determine the deviation from true cosine response due to the angular and spectral dependence of the thermopile flat plate receiver absorptance.

The solar calibration field of view is ±5°. The uncertainty in the direction vectors of the spacecraft axes with respect to the solar vector is expected to be ±0.14°. The uncertainties in the angular readouts of the azimuth and calibration gimbals are approximately ±0.05°. In any one direction, the root sum squared uncertainty then is approximately ±0.15°. At one extreme of the solar field of view the response is proportional to the cosine of 5°. The response uncertainty due to an uncertainty of direction of 0.15° is then cos 4.85° - cos 5° or 0.0225 percent. For a full scale reading of 1370 W/M^2, the uncertainty is ±0.31 W/M^2.

4.1.4 Hemispherical Filter Polarization Analysis

One of the most important tasks of the instrument definition study was to conduct studies to optimize the design of the Suprasil-W hemispherical dome filters, consider polarization sensitivity, thermal emission, contamination sensitivity, and angular response. In the following paragraphs, the results of the polarization analysis are presented.

Two worst case polarization fields due to Rayleigh scattering were considered: a fully symmetrical field (satellite solar zenith angle, Z = 0°), and a highly unsymmetrical field (solar zenith angle, Z = 57.58°). In each case, the signal on the detector from the polarized field was compared with that from a field of the same intensity distribution but unpolarized. The results are as follows:

Z	Difference in Signal Between Polarized and Unpolarized Field (percent)
0° (Symmetrical)	0.349
57.58 (Asymmetrical)	0.003

The symmetrical case is the worst by far. The more asymmetrical the polarization field, the more nearly the dome transmission approaches that for unpolarized light.

4.1.4.1 State of Problem

Determine the difference in signal of a hemispherical fused silica dome for unpolarized Earth radiation and for polarized radiation due to a normal Rayleigh scattering polarization field. Consider two cases, both of which involve a fully illuminated Earth disc.

1. A worst case symmetrical polarization field about the satellite nadir (subsatellite solar zenith angle, Z + 0°).
2. A worst case asymmetrical polarization field with the maximum solar zenith angle which still permits full illumination of the visible Earth disc (subsatellite solar zenith angle, Z = 57.58°).

The worst case, or maximum polarized field, involves picking a low optical thickness τ and low surface albedo A, low values of τ and A reduce the depolarizing effects of multiple scattering.

4.1.4.2 Method of Solution

The transmittance of the dome will vary with angle of incidence on the dome surface, with the degree of polarization of the incident light, and with the orientation of the plane of the polarized component relative to the plane of incidence. In order to reduce the problem to manageable proportions, it was subdivided into a number of discrete steps.

Determination of Polarization Field. The characterisitcs of the polarization field were determined with the aid of the Coulson, Dave, and Sekera tables for a plane parallel Rayleigh scattering atmosphere (U.C. Press, 1960). The tables give the Stokes polarization parameters I, Q, and U for light scattered by the atmosphere, for various optical thicknesses, τ, surface albedo A, solar zenith angles, μo, and scattered ray zenith and azimuth angles, μ and ϕ. A worst case polarization field was assumed:

$\tau = 0.15$ ($\lambda = 0.5$ μm) and
A = 0 (no reflection from the surface)

A Fortran program (SATPOL, courtesy L.L. Stowe of NOAA), was used to convert table data from target coordinate system to nadir and azimuth angles in the satellite coordinate system. Inputs to the program are the satellite altitude (600Km), and the subsatellite solar zenith angle (two cases: 0° and 57.58°). The output includes the target solar zenith angle (the interpolation variable μo), target zenith and azimuth angles (μ and ϕ, from target to satellite), and satellite nadir and azimuth angles (η, α). The latter two angles define a spacific target position as seen from the satellite.

For a 600Km orbit, the angle from the nadir to the horizon is given by:

$$\theta = \sin^{-1} [6378.39/(6378.39 + 600)]$$
$$\theta = 66.067°$$

Thus, the total field of view of the Earth disc from the satellite is 132.134°.

The visible disc was divided into four concentric zones of equal area when projected onto a plane perpendicular to the satellite nadir. The satellite nadir angle for the centroid of each area was then determined.

The coordinate conversion program generates data only at 16 discrete nadir angles, so it was necessary to use nadir angles different from the desired values, and make corresponding corrections in the weighting factor for each zone.

Desired Nadir Angles	Values Used	Weighting Factor
38.54	39.37	0.265
54.07	51.33	0.205
60.69	59.99	0.265
64.62	64.45	0.255

The target solar zenith angles generated by the program are in between the Uo values in the CDS tables, and interpolation was required to obtain the corresponding values of I, Q, and U. For the first case (Z = 0), there is no variation of polarization characteristics with azimuth angle, so only four data points were required. For the second case (Z = 57.58°0, there is no symmetry about satellite nadir, so four data points were generated for each of seven azimuth angles from 0° to 180°. In this case, there is left-right symmetry about the sun line plane.

Two FORTRAN programs were written: INTOR for Z = 0°, and INTOR2 for Z = 57.58°. These programs obtained interpolated values for I, Q, and U (where I = total intensity and Q and U are the Stokes parameters), and calculated the following quantities for each of the 32 data points:

Iv (vertical intensity component): $Iv = 0.5\ (I - Q)$

Ih (horizontal intensity component): $Ih = 0.5\ (I + Q)$

P (degree of polarization): $P = Q^2 + U^2)^{\frac{1}{2}}/I$

X (orientation of plane of polarization relative to vertical plane in appropriate azimuth): $X = 0.5 \tan^{-1}(-U/Q)$

All subsequent calculations were made using Iv and Ih only, with P and X being used to check correlation with the CDS tables. The P values correlated closely with the tabulated values, but major discrepancies were found between the calculated and the tabulated values of X. Since X was not required for the present study, no attempt was made to resolve the discrepancy.

Dome Characteristics. The following characteristics were assumed for the dome:

- Fused silica index of refraction, 1.4623 (0.5 μm)
- 5.974 mm, outer radius
- 1.0 mm, thick
- 4.974 mm, inner radius
- 4.974 mm, inner surface to detector
- 6.35 mm, detector diameter
- $\frac{\text{Detector Radius}}{\text{Mean Dome Radium}} = \frac{3.475}{5.474} = 0.580$

The dome is concentric about the center of the detector; thus, any ray aimed at the center of the detector, from any angle, will be normal to the dome and will not be deviated.

The dome was simulated on the optical analysis program ACCOS-V, and a pattern of rays was traced around the rim of the detector for each of the four nadir angles, with the dome axis assumed vertical. This accurately established the dimensions and shape of the effective aperture of the dome for each nadir angle. Another set of rays was then traced from the center to the edge of the aperture, thus establishing the angle of incidence on the dome as a function of radial distance from the beam center.

A large-scale drawing was made of the effective aperture for each of the four nadir angles, and the area for equal radial increments within the ellipse was determined. Data for a nadir angle of zero (circular aperture) is given in Table 4-2 to illustrate the procedure. For nonzero nadir angles, the outer area increments were adjusted to stay within the ellipse. In all cases, the areas used where the projected areas onto a plane perpendicular to the chief ray, rather than the actual area along the curved surface.

Table 4-2

RELATIVE APERTURE EFFECTS, NADIR ANGLE ZERO

Relative Aperture	Radius of Actual Aperture (mm)	Angle of Incidence (degrees)	Cumulative Area (mm^2)	Incremental Area (mm^2)
0.1	0.317	3.05	0.316	0.316
0.2	0.634	6.10	1.263	0.947
0.3	0.951	9.17	2.843	1.579
0.4	1.268	12.27	5.053	2.211
0.5	1.585	15.41	7.896	2.843
0.6	1.902	18.59	11.370	3.474
0.7	2.219	21.83	15.476	4.106
0.8	2.537	25.14	20.213	4.738
0.9	2.854	28.55	25.583	5.369
1.0	3.1707	32.06	31.583	6.001

Transmittance of Dome. A FORTRAN program, POLAR, was written to generate tables of dome transmittances as a function of incidence angle for three conditions: unpolarized, polarized in the plane of incidence, and polarized perpendicular to the plane of incidence.

Summation Over the Dome. Because of the variation of aperture area and shape with nadir angle, the summation procedure was slightly different for each of the four nadir angles. For a given nadir angle, however, the summation was identical for all azimuth points. For each of the 32 data points, two summations on the dome were done: one for the polarized field, and one for an unpolarized field but with the same intensity distribution, thereby providing a means of normalizing. Four FORTRAN programs were written: SUMI for the first nadir angle 39.37°, SUM2 for the second nadir angle, etc. The input for each data point was Iv, the vertical intensity component, and Ih, the horizontal intensity component. For the unpolarized case, the summation was as follows:

$$A(1)\ (Iv + Ih)TA(1) + A(2)\ (Iv + Ih)TA(2) + \ldots$$
$$+ A(n)\ (Iv) + Ih)TA(n)$$

where

A(1) = first area increment
TA(1) = transmittance of the dome for unpolarized light at the angle of incidence corresponding to the first area increment.

For the polarized case, a more complex summation was performed. The summation was done in three parts as follows:

1. For the circle inscribed within the ellipse, the summation was done exactly as in the unpolarized case since by symmetry arguments there is no net effect due to polarized field.

$$A(1)\ (Iv + Ih)TA(1) + \ldots$$

2. For the next two or three area increments, each increment was divided into three approximately equal areas, and the angle of rotation about the incident chief ray to the center of one of the outer areas was determined from the large scale drawing. Symmetry about the major axis of the ellipse was assumed.

One-third of the area increment was computed as follows:

$$SUMA(I) = A(I) \pm Ih \times Tv(I)1 + \pm Iv + Th(I)1$$

where

A1(I) = One-third of area A(I)
Tv(I) = Transmittance of the dome for light polarized in the plane of incidence, at the angle of incidence corresponding to area increment A(I)
Th(I) = The same for light polarized perpendicular to the plane of incidence.

For the other two-thirds of the area, new values of Iv and Ih were calculated as follows:

$$IvC = Iv \times \cos^2\theta + Ih \times \sin^2\theta$$
$$IhC = Iv \times \sin^2\theta + Ih \times \cos^2\theta$$

The area calculation was then done as before:

$$SUMB(I) = A2(I) \pm IhC \times Tv(I)1 + \pm IvC \times Th(I)1$$

where

A2(I) is two-thirds of area increment A(I)
Tv(I) and Th(I) as described above
θ is the angle of rotation in the aperture as described above.

The total sum for the area increment consisted of:

$$SUM(I) = SUMA(I) + SUMB(I).$$

3. Outer Area Increments in the Ellipse. For these outer area increments, the ellipse had narrowed sufficiently that the rotation of the dome normal around the segment did not introduce a significant error. For these segments, the summation formula used was:

$$SUM(I) = A(I) \pm Th \times Tv(I)1 + \pm Iv \times Th(I)1.$$

The output for each of these summing operations was two numbers, one proportional to the polarized radiation signals and the second proportional to the unpolarized radiation signals. The ratio of these numbers is a measure of the sensitivity of the dome to variations in polarization of light received form the Earth.

Summations Over the Earth. The results of the summation analysis are given in Tables 4-3 through 4-8.

Table 4-3

SUMMATION ANALYSIS, SYMMETRICAL CASE (z = 0°)

Nadir Angle (η)	Weight	Polarized	Unpolarized	Difference
39.37°	0.265	1.43580	1.43385	0.00195
51.33°	0.205	1.36668	1.36233	0.00435
59.99°	0.265	1.49869	1.49233	0.00636
64.45°	0.255	2.01903	2.00964	0.00939

Mean weight value, polarized: 0.265 x 1.43580 + 0.205 x 1.36668...= 1.57266.

Mean weighted value, unpolarized: 0.265 x 1.43385 + 0.205 x 1.36233...= 2.56717.

Differences of mean weighted values: 1.57266 - 1.56717 = 0.00549

0.00549/1.57266 = 0.00349 x 100 = 0.349 percent.

Table 4-4

SUMMATION ANALYSIS

Asymmetrical Case (Z = 57.58°) Nadir Angle (η) = 39.35°

Azimuth	Polarized	Unpolarized	Difference
0	0.91666	0.91235	0.00431
30	0.90828	0.90538	0.00290
60	0.92067	0.92089	-0.00022
90	1.02510	1.02771	-0.00261
120	1.24417	1.24675	-0.00258
150	1.48561	1.48647	-0.00086
180	1.59254	1.59239	0.00015

Mean value, polarized = 1.15615.

Mean value, unpolarized = 1.15599.

Table 4-5

SUMMATION ANALYSIS

Asymmetrical Case (Z = 57.58°) Nadir Angle (η) = 59.99°

Azimuth (α)	Polarized	Unpolarized	Difference
0	1.08617	1.08026	0.00591
30	1.04953	1.04545	0.00048
60	0.99749	0.99759	-0.00010
90	1.05950	1.06304	-0.00354
120	1.30844	1.24675	-0.00258
150	1.48561	1.48647	-0.00086
180	1.59254	1.59239	0.00015

Mean value, polarized = 1.27413.

Mean value, unpolarized = 1.27410.

Table 4-6

SUMMATION ANALYSIS

Asymmetrical Case (Z = 57.58°) Nadir Angle (η) = 59.99°

Azimuth (α)	Polarized	Unpolarized	Difference
0	1.43966	1.43352	0.00614
30	1.37316	1.36878	0.00438
60	1.24206	1.24204	0.00002
90	1.23459	1.23859	-0.00400
120	1.50378	1.50841	-0.00463
150	1.91379	1.91615	-0.00236
180	2.08337	2.08416	-0.00079

Mean value, polarized - 1.54149.

Mean value, unpolarized = 1.54166.

Table 4-7

SUMMATION ANALYSIS

Asymmetrical Case (Z - 57.58°) Nadir Angle (η) = 64.45°

Azimuth (α)	Polarized	Unpolarized	Difference
0	2.13760	2.12975	0.00785
30	2.04246	2.03661	0.00585
60	1.82217	1.82160	0.00057
90	1.72421	1.72920	-0.00499
120	2.04691	2.05321	-0.00630
150	2.54211	2.54504	-0.00293
180	2.77600	2.77691	-0.00091

Mean value, polarized = 2.15592.

Mean value, unpolarized = 2.15605.

Table 4-8

SUMMATION ANALYSIS

Asymmetrical Case (Z = 57.58°) Summation of Nadir Values

Nadir Angle (η)	Weight	Polarized	Unpolarized	Difference
39.37°	0.265	1.15615	1.15599	0.00016
51.33°	0.205	1.27413	1.27410	0.00003
59.99°	0.265	1.54149	1.54166	-0.00017
64.45°	0.255	2.15592	2.15605	-0.00013

Mean weighted value, polarized = 1.52583.

Mean weighted value, unpolarized = 1.52578.

Difference of mean weighted values: 1.52583 - 1.52578 = 0.00005

0.00005/1.52583 = 0.00003 x 100 = 0.003 percent.

4.1.4.3 Summary of Results and Recommendations

As noted at the beginning of Paragraph 4.1, two polarization fields due to Rayleigh scattering were considered: a fully-symmetrical field (satellite solar zenith angle, Z = 0°), and a highly unsymmetrical field (solar zenith angle, Z = 57.58°0). In each case, the signal on the detector from the polarized fields was compared with that from a field of the same intensity distribution but unpolarized. The results are as follows:

Z	Difference in Signal Between Polarized and Unpolarized Field (percent)
0° (Symmetrical)	0.349
57.58° (Asymmetrical)	0.003

The symmetrical case is the worst by far. The more assymetrical the polarization field, the more nearly the dome transmission approaches that for unpolarized light.

Using the ACCOS-V optical analysis program, the area of the dome used when viewing the sun and when viewing the Earth was determined for two dome sizes, and the common area* determined for each as follows:

RT/RD	Common Area	Mean Dome Rad (mm)
0.50	14.9 percent	6.350
0.58	19.2 percent	5.474

RT = Radius of detector = 3.175 mm

RD = Mean Dome Radius

If the dome radius is plotted against the maximum angle of incidence on the dome, the slope is changing rapidly in the region of 5 to 7 mm dome radius.

*As discussed in the report, "An experiment Definition Study for a Radiation Climate Radiometer", NASA CR-132407, November 1975, keeping as much common area for the shortwave Earth and solar views reduces the sensitivity of their ratio, or Earth albedo, to errors brought about due to changes in the transmission of the dome after launch.

Thus, a relatively small increase in dome radius has a more significant effect in reducing the maximum angles of incidence on the dome, which in turn will reduce the transmission variations due to polarization, than in reducing common area. It is, therefore, recommended that an RT/RD ratio close to 0.50 be used. This should reduce the polarization error by 30 percent, making the difference about 0.24 percent. This results in a worst case bias of 0.97 W/M^2 or an average uncertainty of ± 0.485 W/M^2.

4.1.5 Channel Noise

Experience with the ERB channels shows that the channel noise is largely due to the electronics. We can still, however, express the noise in terms of its equivalent incoming irradiance or NEI (noise equivalent irradiance). This is given by the expression:

$$NEI = \frac{(NEP)(\Delta f)^{\frac{1}{2}} Ke}{A\varepsilon_o Km}$$

where NEP is the detector noise equivalent power in watts $Hz^{-\frac{1}{2}}$, Δf is the noise equivalent bandwidth in $Hz^{\frac{1}{2}}$, Ke is the electronics degradation factor (ERB experience indicates that Ke is approximately 50), ε_o is the optical efficiency (equals unity for the total channels and 0.93 for the shortwave channels), A is the detector area and K_m is the electronics chopping factor estimated to be 0.4.

The thermopile NEP is that associated with the thermopile resistance or Johnson noise and is expressed by the equation:

$$NEP = \frac{A(4kTR)^{\frac{1}{2}}}{S}$$

where

k = Boltzmann constant = 1.38042×10^{-23} watt sec k^{-1}

R = Thermopile resistance = 1,000 ohms

T = Temperature = 298K

A = Thermopile collecting area = $3.17 \times 10^{-5} m^2$

S = Thermopile sensitivity = 2×10^{-5} volts $watt^{-1} m^2$

Evaluating, NEP = $1.29 \times 10^{-8} W\ Hz^{-\frac{1}{2}}$

For a sampling time of 1.6 seconds (t_s),

$$\Delta f = \frac{1}{2t_s} = 0.3125 \text{ Hz and } (\Delta f)^{\frac{1}{2}} = 0.559\ Hz^{\frac{1}{2}}$$

The NEI can now be calculated and is:

$2.84 \times 10^{-2} W/M^{-2}$ for the total channel, and

$3.06 \times 10^{-2} W/M^{-2}$ for the shortwave channel

4.1.6 Quantization Noise

The analog to digital converter in the system adds a random noise to the channel noise which is proportional to the quantizing level. For the ERBSS, the quantization level referred to the front end is the total dynamic range divided by 4,096, the number of quantizing levels (for a 12-bit system). Assuming that the dynamic range will be set for the solar calibration, the full range is 1,370 W/M^2 and a quantizing interval is 0.334 W/M^2. The RMS quantization noise for any converter is the quantizing level divided by $\sqrt{12}$ and is slightly less than $\pm 0.1\ W/M^2$.

4.1.7 System Linearity

The linearity of the system electronics is calibratable except for uncertainties in the analog to digital conversion of approximately ±0.012%. Recent linearity measurements made on a toroidal thermopile indicate excellent linearity over a

range of approximately 1000 to 1 with the upper level at about 1.2 solar constants. No departure from a linear response was seen and a linearity uncertainty of ±0.05% is estimated. The total system linearity uncertainty is then ±0.0514%. At full scale equal to 1370 W/M^2, the linearity uncertainty becomes ±0.7 W/M^2.

4.1.8 System Time Constant

The error caused in the system response due to the detector time constant was investigated. The worst case appears to be the shortwave, medium field of view channel. At the Earth's surface, the medium field of view has a footprint 1111 KM in diameter. During a 1.6 second integration time, the footprint moves by 10.5 KM along the satellite track. This causes a worst case signal response change of 0.6 percent limiting the effect of a slow detector response. For a completely cloudy scene, an albedo of 0.85 and a solar constant of 1368 W/M^2, the scene radiance is approximately 275 W/M^2. In the worst case, a detector time constant (TC) of one second causes a response error of 0.33 W/M^2. If TC is 0.5 seconds, the error is only 0.067 W/M^2; while if 2.0 seconds, the error is 0.74 W/M^2. The time constant can be electrically corrected, but uncertainties associated with vacuum-to-air changes and aging will exist. If the time constant can be corrected with an uncertainty of ±20 percent, the uncertainty for a one second time constant detector is ±0.066 W/M^2 in the shortwave channel. The total channel uncertainty is estimated to be about half of that or ±0.033 W/M^2. The time constant effect in the wide field of view channels is expected to be negligible.

During solar calibration, the sun moves across the field at a maximum rate of 3.71° per minute. In 1.6 seconds it moves 0.099° causing a worst case scene variation of (cos 4.901° - cos 5°) x 1370 W/M^2 = 0.2043 W/M^2. If the time constant is one second and is corrected to ±20%, the scene uncertainty is ±0.033 W/M^2 for either shortwave or total channels.

4.1.9 Calibration Uncertainties

In the ERBSS non-scanning assembly, all channels are calibrated in orbit against the sun with Channel 5 the reference for the other four. On the ground, solar simulators and other types of targets such as integrating spheres can be used for the shortwave channels while the same targets plus blackbodies can be used for the total and solar constant channels. Until the details of the targets and the interfaces with the instrument in the calibration mode are known, analyses related to calibration uncertainties would have greater uncertainties due to the present unknowns than would finally be realized. Because of this we have not included any calibration uncertainties in the analysis. It can be stated, however, that far greater errors are expected with ground targets for the shortwave irradiance spectra than for the longwave spectra. Serious considerations of actual preflight solar calibration using high-flying aircraft or other means such as Shuttle should be explored.

4.2 SHORTWAVE CHANNEL THERMAL ERROR REDUCTION

The shortwave channel filter for the ERBSS non-scanning assembly is a hemisphere of Suprasil-W fused quartz. Use is made of the natural absorption characteristics of that material to limit the spectra of radiation incident upon the shortwave thermopile to approximately 0.2 to 5.0 μm. It has been noted, however, that normal variations in the terrestrial longwave radiation incident to the dome causes intraorbit variations in the dome temperature distribution in spite of the fact that the dome is connected to the same heat sink as the detector. Therefore, the contribution to the thermopile signal of radiant energy from the dome is not constant for all operational conditions. Attempts to interpret thermopile response assuming a constant dome temperature distribution would result in a significant measurement uncertainty.

In a memorandum dated 7 January 1977, entitled, "ERBSS Wide Field of View Shortwave Channel Data Reduction", written to Mr. C.V. Woerner of LaRC and written by Mr. M.R. Luther of Vought Hampton, an interactive technique for data reduction which virtually eliminates this error is presented. A relationship

between the longwave radiation incident upon the dome and the average dome temperature was established and found to be nearly linear. From wide field of view total and shortwave data, and initial assumptions about the average filter temperature, the longwave irradiance is computed and used to establish a true filter temperature as shown by Figure 4-5. This is a flow chart of the overall data reduction scheme. Results obtained indicated that one iteration per calculation for the shortwave irradiance is sufficient. Typically, the longwave and shortwave irradiance appears as shown by Figure 4-6; the filter temperature varying with the longwave irradiance. These data were generated using a modified version of the Colorado State University (CSU) Earth radiation budget simulation program. Actual data and reduced data, using the technique of Figure 4-5, was compared with the errors shown in Figure 4-7. The measurement uncertainty has been computed to be ± 0.18 W/M^2 which we have rounded off to ± 0.2 W/M^2.

4.3 SCANNER CHANNELS ERROR ANALYSES

The uncertainties in Channels 6, 7 and 8 are as extraneous irradiance, channel noise, quantization noise, detector thermal drifts, and system linearity. They are summarized by Table 4-9.

Table 4-9

UNCERTAINTY ANALYSES SUMMARY FOR SCANNING ASSEMBLY CHANNELS

Parameter	SW Channel (W/M^2-SR)	LW Channel (W/M^2-SR)	Cloud Channel (W/M^2-SR)
Extraneous Radiance	$\pm 3.0 \times 10^{-3}$	± 0.059	Negligible
Channel Noise	± 0.058	± 0.07	$\pm 5.4 \times 10^{-4}$
Quantization Noise	± 0.026	± 0.013	$\pm 4.2 \times 10^{-4}$
Detector Thermal Drifts	± 0.037	± 0.019	$\pm 1.5 \times 10^{-2}$
System Linearity	± 0.086	± 0.044	$\pm 1.4 \times 10^{-3}$
RSS'd Total	± 0.113	± 0.104	± 0.0151

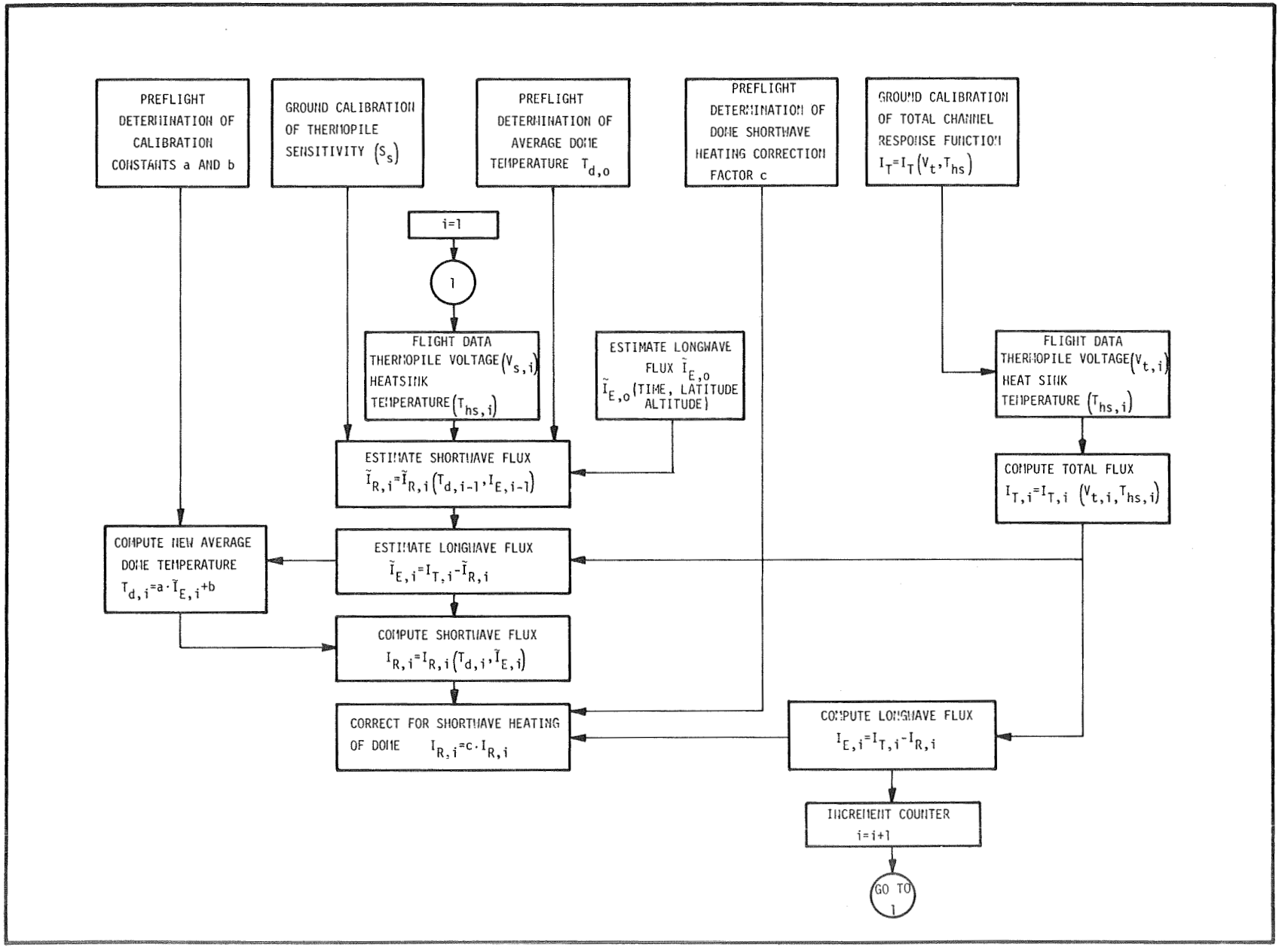

Figure 4-5 Flowchart of ERBSS Wide Field of View Instrument Data Reduction Procedure

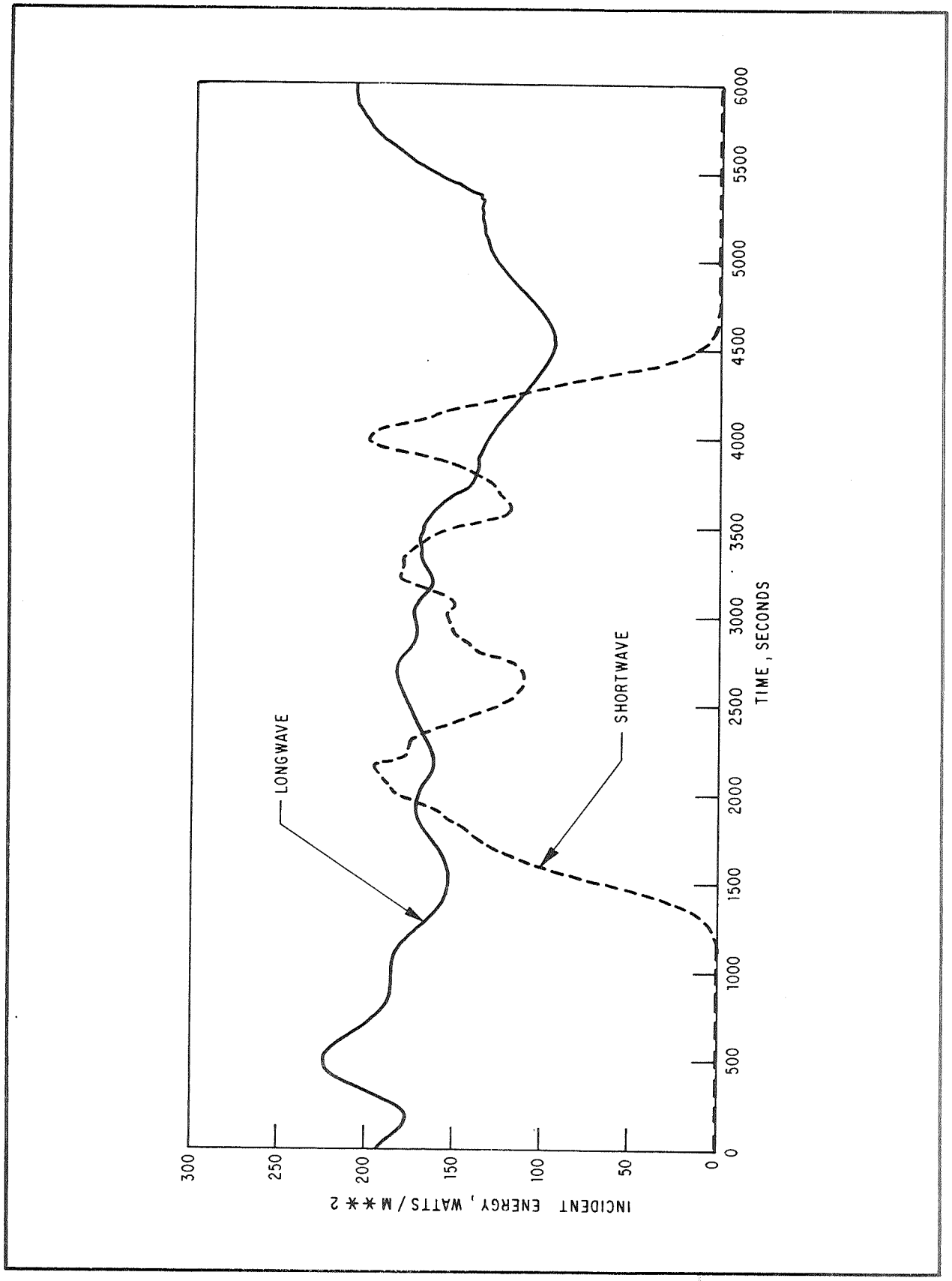

Figure 4-6 Shortwave and Longwave Radiation Incident to the Spacecraft at 833 KM (September)

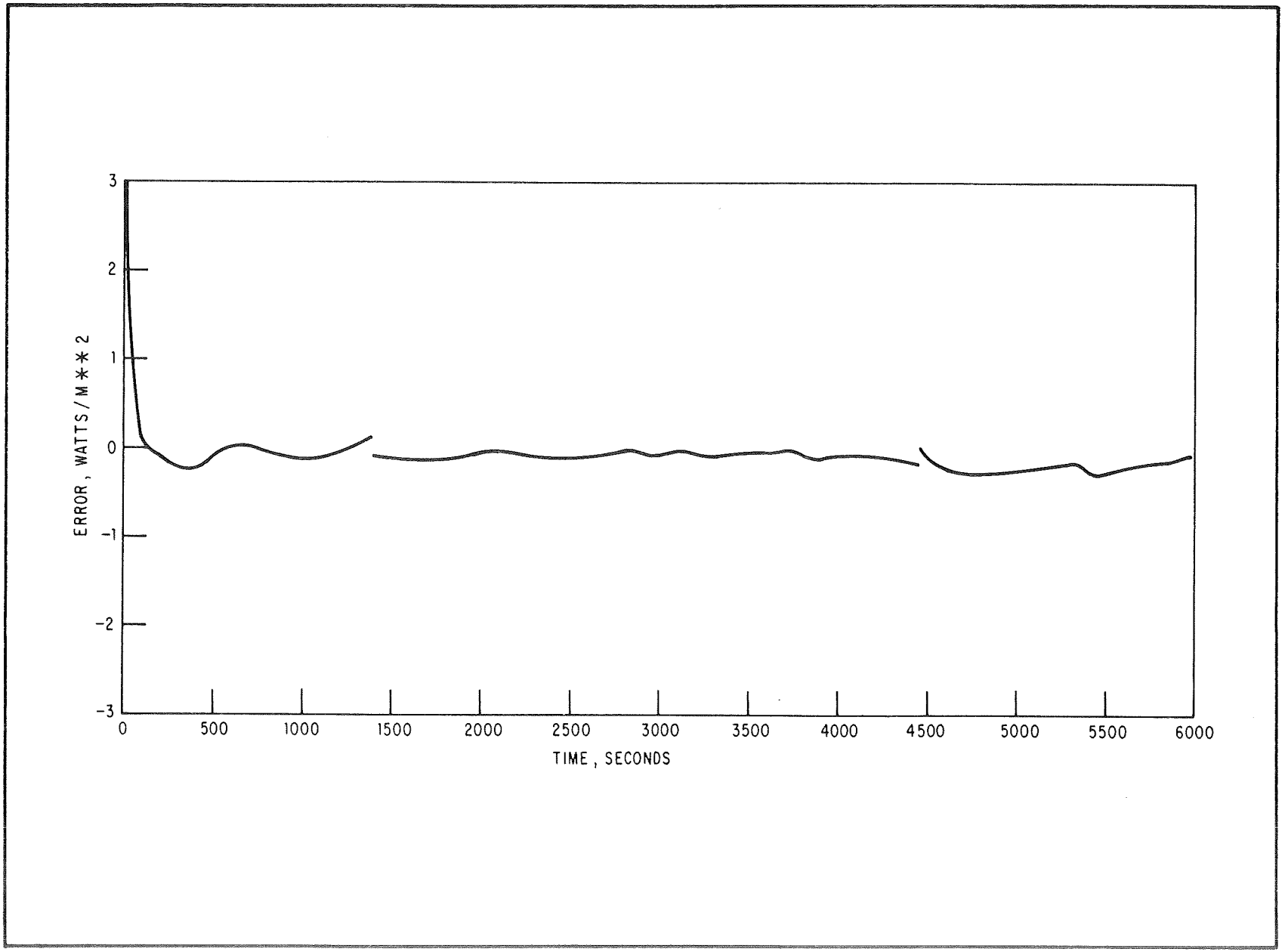

Figure 4-7 Error in Determination of Incident Shortwave Radiation From Simulated Flight Data

4.3.1 Extraneous Irradiance

Because of the simplicity of the optical design and the fact that none of the optics radiance is chopped, extraneous irradiance has its only source at the chopper. When the chopper is open, the power incident on the detector emanates entirely from the scene (ignoring a small amount of scattering). During chopper closure, the power incident on the detector comes from the chopper and the chopper reflected reference target. The peak to peak signal from the detector is proportional to the difference between the scene and the chopper caused radiances. This difference in power at the detector may be expressed

$$\Delta P = Ao\Omega\varepsilon_o (Ns-Nc)$$

where

Ao = collecting area
Ω = solid angle field of view
ε_o = optical efficiency of elements up to the detector
Ns = scene radiance
Nc = chopper radiance.

Once per scan, space is observed, Ns becomes essentially zero, and the chopper radiance factor is known. The chopper is a high reflectance, specular mirror during closure. However, it has a finite temperature and a finite emittance and therefore has a finite radiance. The chopper reference target is a controlled, or at least an accurately monitored source having a high emittance. The uncertainties associated with the chopper and chopper reference target come from component temperature changes between space views and temperature sensor readout uncertainties. Calculations have been made of the magnitudes of these uncertainties using the following assumed parameters:

- The reflectances of all mirrors and the chopper are 0.97
- The emittance of the reference blackbody is 0.99
- The emittance of the chopper is 0.03

- The reference blackbody temperature and the chopper temperature are both 308K
- The reference blackbody temperature uncertainty is ±0.05°C
- The chopper temperature uncertainty is ±0.2°C.

The magnitudes of these effects were well below the noise level in Channel 8 (cloud) and are considered insignificant. The shortwave channel (6) uncertainty is $\pm 3.0 \times 10^{-3} W/M^2\text{-SR}$ while the Channel 7 uncertainty is ±0.059 $W/M^2\text{-SR}$. It can be concluded that the only channel affected by these sources is Channel 7, the longwave channel.

4.3.2 Channel Noise

Noise equivalent radiances (NEN's) and/or signal to noise ratios have been calculated for Channels 6, 7, and 8. For Channels 6 and 7, LiTaO pyroelectric detector characteristics were assumed while signal to noise calculations have been made for both Lead Sulphide (PbS) and pyroelectric detectors in Channel 8. In all cases, a one-centimeter diameter collecting optics and a circular three-degree field of view were assumed. The NEN for a channel can be expressed by the equation

$$NEN = \frac{(NEP)(\Delta F)^{\frac{1}{2}} Ke}{Ao\Omega\varepsilon_o Km}$$

where:

- NEP is the detector's noise equivalent power
- Δf is the noise equivalent bandwidth and is equal to 1/2Ts, where Ts is the integration time. For Ts = 53 1/3 milliseconds, Δf = 9.375 Hz and $(\Delta f)^{\frac{1}{2}} = 3.06\ Hz^{\frac{1}{2}}$
- Ke is an electronics noise factor, we will use Ke = 1.2
- Ao is the collecting area and is 0.7854 cm^2
- Ω is the solid angle field of view; for a three-degree circular field, $\Omega = 2.15 \times 10^{-3} SR$

- ε_0 is the effective optical efficiency for each channel
- Km is chopping factor for conversion from a peak to peak to rms signal and is 0.4.

Detector NEP. In Channels 6 and 7 a detector of 0.18 cm diameter can be accommodated. Literature and conversations with detector manufacturers indicate that $LiTaO_3$ detectors with NEP's of 7.5×10^{-10} watts $Hz^{-\frac{1}{2}}$ are available with selection and the proper FET. PbS detectors are readily available with NEP's of 3.5×10^{-12} watts $Hz^{-\frac{1}{2}}$.

Optical Efficiency. In Channel 6, the mirrors are assumed to be aluminum with an average reflectance of 0.91 over the spectral band. The detector window and filter are identical with a transmittance of 0.92. If necessary, the filter can be the detector window. The overall efficiency is 0.7.

The filter in Channel 7 should definitely be the detector window to enhance to optical efficiency. A transmittance of 0.6 is assumed for this element. The two mirrors each have a reflectance of 0.98 and the overall efficiency is 0.576.

A very narrowband filter is required in Channel 8 with a transmittance of 0.4 assumed. The two mirrors each have a reflectance of 0.97 and the detector window transmittance is 0.92. The overall efficiency is 0.346.

With the calculated NEP and optical efficiency parameters and other values above, the channel NEN's have been calculated. The shortwave channel has a NEN of 0.058 W/M^2-SR while the longwave channel has a NEN of 0.07 W/M^2-SR. (During the Radiation Climate Radiometer study, NEN's of 0.11 and 0.13 W/M^2-SR were desired for the SW and LW channels respectively.) The NEN calculated for Channel 8 is 5.4×10^{-4}-SR with the PbS detector and 0.12 W/M^2-SR for the $LiTaO_3$ detector.

The cloud channel is to have a signal to noise ratio of at least 300 when viewing a cloud with a surface reflectance of 0.1 and a solar zenith angle of 45°.

The scene radiance under these conditions and a bandwidth of 0.1 micrometers is 0.513 W/M^2-SR. The signal to noise ratio is 950 with the PbS detector and 4.3 with the $LiTaO_3$ detector. It is obvious that a pyroelectric detector cannot meet the requirements of Channel 8.

None of these channel noise calculations have included the effects of microphonics with the pyroelectric detectors in Channels 6 and 7. The magnitude of noise generated by microphonics in typical pyroelectric detectors is 10 to 50 μvolts per g of vibration. Since the exact mounting configuration is not known and a final detector/FET design has not been made, the magnitude of the microphonic effect on the ERBSS design cannot be quantified.

4.3.3 Quantization Noise

The full scale radiance for the SW, LW, and cloud channels are assumed to be respectively, 370, 190, and 6 watts/M^2-SR. The noise in each channel due to quantization is the quantizing level divided by $\sqrt{12}$. The quantizing level is the full scale radiance divided by 4,096 since we plan to employ a 12-bit converter. The quantizing noises for each channel are then ±0.026 W/M^2-SR in the shortwave channel, ±0.013 W/M^2-SR in the longwave channel, and $\pm 4.2 \times 10^{-4}$ W/M-SR in the cloud channel.

4.3.4 Detector Thermal Drifts

The $LiTaO_3$ pyroelectric detectors have a responsivity/temperature coefficient of approximately 0.2 percent/°C. Controlling the detector temperature to ±0.05°C should be possible with active control of the detector mountin interface.

Based on the full scale radiance, the uncertainties due to temperature drift of the detectors in Channels 6 and 7 are ±0.037 W/M^2-SR and ±0.019 W/M^2-SR respectively. The PbS detector has a much greater coefficient, approximately four to five percent/°C. With the same control, i.e., ±0.05°C, the uncertainty in Channel 8 is $\pm 1.5 \times 10^{-2} W/M^2$-SR. This may be too great for this channel and improved control may be the answer.

4.3.5 Linearity

The chopped scanning system is similar to the MFOV/WFOV channels in that detector response linearity is the major contributer to uncertainties while the analog to digital converter also contributes a small amount. Other electrical nonuniformities such as those observed in amplifiers and the synchronous demodulator can be calibrated. Pyroelectric detectors are not, by nature, linear due to heating as the source radiation increases. These nonlinearities, however, can be characterized by calibration to an uncertainty of ±0.02%. The analog to digital converter contributes an amount equal to ±1/2 of the least significant bit or ±0.012% for a 12-bit converter. Other electrical effects are negligible and the linearity uncertainty is ±0.0233% of full scale radiance.

Maximum shortwave radiance is based on a solar zenith angle of zero, and an albedo of 0.85 which calculates to be 370 W/M^2-SR. The worst case radiance in the longwave channel is based on a scene temperature of 320K and was calculated to be approximately 190 W/M^2-SR. The maximum radiance in Channel 8 is approximately 6 W/M^2-SR. The linearity uncertainties associated with Channels 6, 7, and 8 are respectively; ±0.086 W/M^2-SR, ±0.044 W/M^2-SR and ±0.0014 W/M^2-SR.

4.4 RESIDUAL MOMENTUM CALCULATIONS

There is a TIROS requirement that all rotating components have momentum less than 0.02 in-lb-sec or be compensated to that amount. Both the chopper drive and the scan drum and its drive produce momentum greater than 0.02 in-lb-sec. The chopper will rotate at 1,125 rpm or 117.8 radans per second. The design rotational speed for the scan drum is 0.98 radians per second with a period of 6.4 seconds if operated continuously in one direction.

Assuming a chopper thickness of 0.188-inch, the chopper drive moment of inertia breaks down as follows:

Chopper and blades:	4.55×10^{-4} in-lb-sec^2
Shaft:	0.0034×10^{-4} in-lb-sec^2
Motor rotor and hub:	6.05×10^{-4} in-lb-sec^2
Total inertia	1.06×10^{-3} in-lb-sec^2

At a rotational velocity of 117.8 radians per second, the chopper momentun is approximately 0.125 in-lb-sec, or 6.25 times the allowed amount.

The drum is fairly massive with a moment of inertia of approximately 0.1 in-lb-sec^2. At the rotational velocity of 0.98 radians per second, the momentum is approximately 0.1 in-lb-sec or five times the allowable.

The moment of inertia of the rotating cylinder with the detectors, etc., in the non-scanning assembly is 8.2×10^{-3} in-lb-sec^2. At the planned rotational velocity, the allowed momentum will not be exceeded. It is obvious that some form of momentum compensation should be planned for the scan drum and the chopper drive. None is required for the non-scanning instrument.

4.5 MAXIMUM DIMENSION ANALYSIS

During the design study, an analysis was preferred to determine the impacts of the requirements of Section 2 on the dimensions of the non-scanning assembly. As shown by Figure 3-1, the field of view aperture has a large effect on the overall length and height of the assembly while the solar apertures have a significant effect on assembly width. Aperture dimensions and how they were determined and the pertinent requirements were discussed in Section 3.2.1.1.

The length of the rotating cylinder, not including mechanisms, etc., is a function of the spherical radii of the medium and wide field of view apertures. As shown by Tables 3-2 and 3-3, Rsp is 39.7 mm for the MFOV channels and 52.3 mm for the WFOV channels. The corresponding diameters are then 79.4 mm and 104.6 mm respectively. Since there are two medium and wide field of view apertures, and assuming a 2 mm thickness for each, the necessary cylinder length is:

$$2(79.4 + 4) + 2(104.6 + 4) = 384 \text{ mm} = 38.4 \text{ cm}.$$

The remainder of the package length includes 7.7 cm for the solar constant radiometer, 6 cm for the cylinder mechanism and 8.9 cm for the cylinder bearings, flex cable, and electronics space on the other end. The overall length of the total assembly is then:

$$7.7 + 6 + 38.4 + 8.9 = 61 \text{ cm}$$

These figures represent the instrument length for $2\delta_2 = 132°$, and $2\delta_1 = 126°$ in the wide field of view channels. If the 132° total angle ($2\delta_2$) can be relaxed and $2\delta_1$ remains fixed at 126°, instrument length can be reduced as shown by Table 4-10.

Table 4-10
LENGTH REDUCTION AS A FUNCTION OF $2\delta_2$

$2\delta_2$	Length Reduction
132°	None
133°	3.2 cm (1.25 inch)
134°	5.5 cm (2.2 inch)
135°	7.4 cm (2.9 inch)
136°	8.9 cm (3.5 inch)

A significant decrease in overall package length can also be achieved through a reduction in the unobscured angle $2\delta_1$. Changing $2\delta_1$ from 126° to 124° provides nearly 5 cm of package shortening as the spherical radius is reduced by 12.4 mm.

The worst case aperture height (L) is found in the medium field of view apertures for the TIROS mission (see Tables 3-2 and 3-3). The requirement that 75 percent or more of the signal be due to the unobscured ($2\delta_1$) view angle makes $2\delta_1$ 50° for a $2\delta_2$ of 66°. Since L varies with these angles as:

$$L = \frac{2Rd}{\tan 2\delta_2 - \tan\delta 2_1},$$

As δ_2 and δ_1 became closer in value, L increases. The aperture height for the TIROS mission will be nearly 0.5 cm greater than the aperture for AEM. The medium field of view aperture height is about 1.2 cm greater than the wide field of view aperture. Reduction of the 75 percent requirement or of the detector diameter would also be effective in reducing aperture height.

The same rules used to size the Earth view field of view apertures are used to size the solar field of view apertures, i.e.,

$$R_A + R_D = L \tan \delta_2$$

$$RA - RD = L \tan \delta_1$$

To keep δ_2 close to δ_1, L, the aperture height, must be as long as possible. For the present dimensions, L is 7.75 cm, R_A is 10 mm, $2\delta_1$ is ten degrees, and $2\delta_2$ is 19.2°. The major problems with the solar viewing are the 450 KM Earth limb avoidance and lack of knowledge as to where the instrument will be mounted on the spacecraft. On TIROS, the angle from the horizontal to the 450 KM limb height is 20.2° while on AEM it is 14.9°. If the spacecraft instability of 1.4° is subtracted, the two angles are 18.8° and 13.5°. Therefore, the $2\delta_2$ values picked require a 0.4° unobscured view above the horizontal on TIROS and 5.7° on AEM. The tilt of the aperture from the horizontal is 9.2° on TIROS and 3.9° on AEM. These are summarized by Table 4-11.

Table 4-11
SOLAR APERTURE PARAMETERS FOR TIROS AND AEM

	$2\delta_1$	$2\delta_2$	L	R_A	Aperture Tilt	View Above Horizontal
TIROS	10°	19.2°	7.75 cm	1 cm	9.2°	0.4°
AEM	10°	19.2°	7.75 cm	1 cm	3.9°	5.7°

To keep from having different tilts and yet keep $2\delta_1 = 10°$, the aperture would have to be sized for the AEM case, i.e., $2\delta_2 = 13.5°$. Under these conditions the aperture height becomes 20.55 cm, an increase in aperture height and package width of 12.4 cm or about five inches. This increase can be reduced to 8.25 cm if $2\delta_1$ is set to nine degrees.

Section 5
ERBSS TEST PROGRAM

ERBSS testing at the component, subassembly, assembly, subsystem and system levels needs to be well planned, well thoughtout, well coordinated and well executed to meet the system accuracy goals. Final system level testing and calibration with the Ground Checkout Equipment (GCE) should prove the ability of the instruments to meet specified performance requirements when in orbit. As illustrated by Figure 5-1, component, subassembly, assembly, subsystem and even system level tests provide vital information for software development and organization, and the ultimate data processing and reduction for performance verification at the system level. Stability and repeatibility requirements dictate repetition of certain system tests and calibrations during that period of time between instrument integration, i.e., final assembly, and satellite launch. While the instrument design stresses simplicity, the test program must stress the thoroughness and attention to detail leading to a well characterized instrument and understanding of the instrument data. As indicated previously in this report, calibration standards of the accuracies needed have not been developed.

An important part of the test and calibration program, then, will be the design and development of the sources, targets, standards, and transfer standards necessary to assure the needed accuracy levels.

The testing recommended and described in the following sections for the different levels is not inclusive of all testing which should be done on the ERBSS instruments. Rather, those tests peculiar to and necessary for the instruments described by Section 3.0 are discussed.

5.1 COMPONENT, SUBASSEMBLY AND ASSEMBLY TESTS

The important elements in this category are the detectors, optics, i.e., mirrors, filters, etc,; field of view apertures, signal processing electronics, analog to digital converters and gimbal position readouts. Any of these elements can adversely affect system accuracy if not properly characterized.

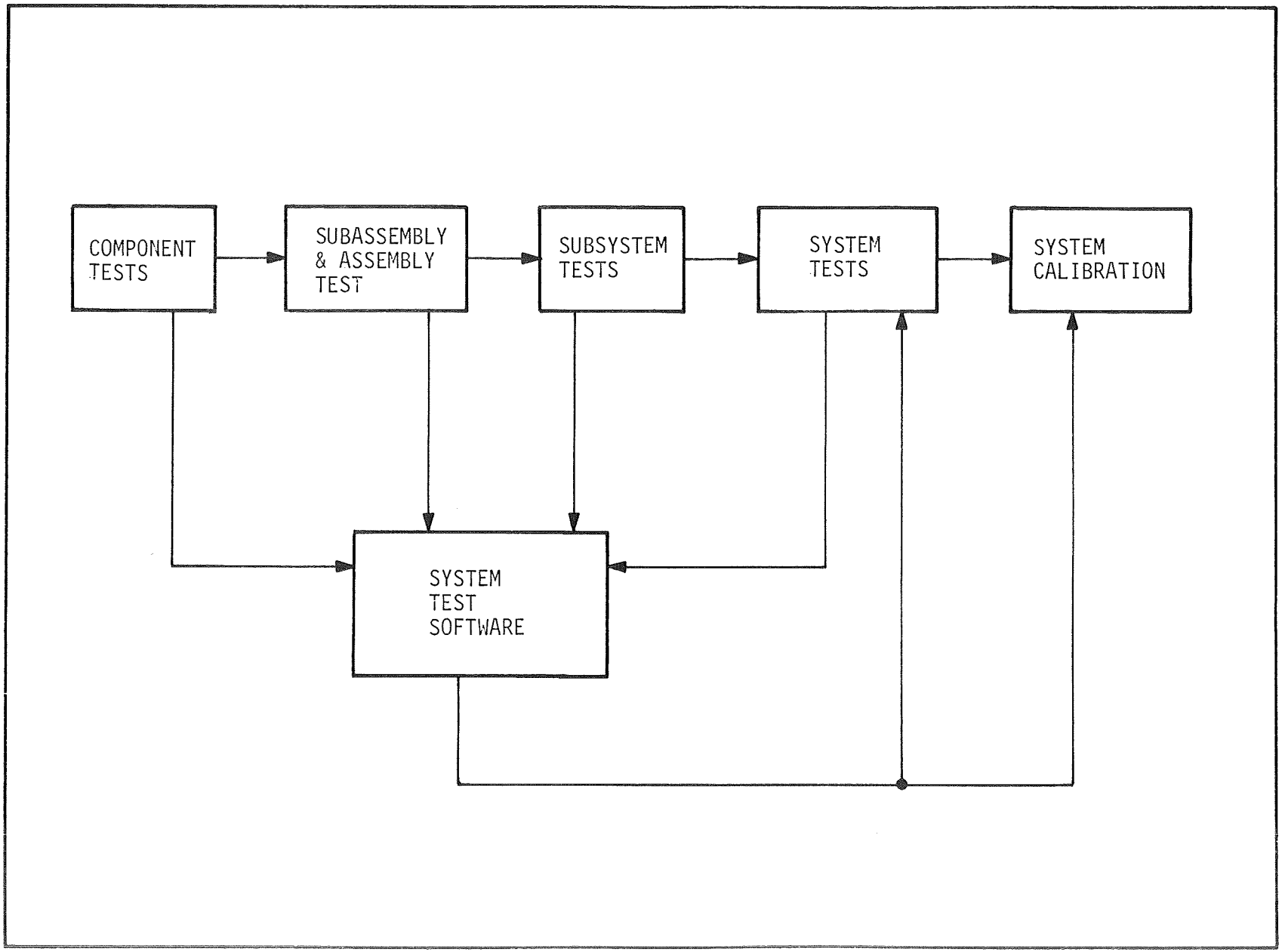

Figure 5-1 ERBSS Test Flow

5.1.1 Detectors

The thermopile detectors for channels 1 through 4, the cavity radiometer for channel 5, the pyroelectric detectors for channels 6 and 7 and the lead sulphide detector for channel 8 are all included in this category. The following tests should be performed on each detector.

(1) Radiance response calibration, i.e., responsivity
(2) Linearity of response
(3) Noise Equivalent Radiance or Irradiance as applicable
(4) Sensitivity of response to temperature and vacuum
(5) Responsive time constant; for the cavity radiometers both active and passive modes
(6) Spectral response at normal incidence for all detectors and over applicable incidence angles for the medium and wide FOV thermopiles
(7) Solid angular response over the appropriate incidence angles and at every 45° of rotation to obtain a complete, three dimensional response map
(8) Uniformity of response across the detector area.

5.1.2 Optics

Included as optics are the hemispheric, Suprasil-W dome filters for the shortwave mode and medium field of view channels, and the chopper, mirrors, and filters for channels 6, 7, and 8. Important to high accuracy operation are the scattering and spectral transmission of the hemispheric dome, spectral reflectance and emittance of the mirrors and chopper and filter transmissions. The tests recommended for these elements are:

(1) Spectral transmission vs applicable temperatures for the domes
(2) Scattering by the dome (this may be done as a system test)
(3) Spectral reflectance and emittance of the chopper and mirrors
(4) Spectral transmission vs applicable temperature for the shortwave, longwave and cloud channels of the scanner.

5.1.3 Medium and Wide Field of View Apertures

The height, aperture diameter and spherical radius of each truncated hemisphere aperture should be carefully measured. These will be tested at the system level for field of view response. An even more important parameter is scattering of unwanted energy to the detector from the aperture opening of the interior surfaces. The quality of the interior surface polish and coating and the knife edge of the aperture opening need to be carefully checked. Scattering from out of field sources will be tested at the subsystem level.

5.1.4 Signal Processing Electronics

The amplifiers, synchronous demodulator, integrator, and sample and hold circuitry are included in the signal processing electronics. As shown in Section 4.0 non-linearity is the largest contribution to the uncertainties in both the scanning and non-scanning assemblies. Gain, offset and linearity should be checked from the noise level to maximum level over the range of temperatures indicated by thermal analysis.

5.1.5 Analog to Digital Converter

The linearity of an ADC should be within ±1/2 of the least significant bit. This, and the offset, should be measured as a function of applicable temperatures using precision voltage sources.

5.2 SUBSYSTEM TESTS

Each of the two instruments will be made up of a number of subsystems which, in general, are separable entities which can be tested semi-independently. Tests are normally performed on the separate subsystems to demonstrate that operational and interface requirements are met prior to integration of the subsystems. Three types of "subsystem" tests are recommended; inflight target calibrations, an aperture/detector breadboard for characterization of thermal and optical parameters, and life test models of the scan drive and chopper drive mechanisms.

5.2.1 Inflight Target Calibration

The blackbody targets for the medium and wide field of view total channels and the long wave scanner channel would best be calibrated by an electrically calibrated cavity radiometer with a suitable field of view. Combining the cavity measurements with highly accurate temperature measurements of the blackbody will provide radiance vs temperature calibration of the blackbodies and reasonable estimates of the targets' emittance. Similar measurements are suggested for the shortwave/cloud channel scanner diffuse targets. A collimated, high intensity shortwave source such as a solar simulator is directed at the diffuser over the range of a solar angles expected in orbit. A cavity radiometer of suitable field of view provides radiance measurement at each incidence angle. Prior to this calibration, the diffuser should be tested out to 5.0μm for any specular reflectance component.

5.2.2 Aperture/Detector Breadboard

At an early time in the program, an aperture/detector should be assembled to measure thermal coupling, out of field scattering, polarization and the solid angle field of view. Combinations should include as a minimum, a wide field, shortwave channel and a medium field, total channel. These tests should be designed for later adaptation to system levels tests. At this level the purpose is to characterize the sources of error, showing discrepancies with modelled results, and providing the basis for design improvements.

5.2.3 Life Test Models

Life tests of the continuously operated scanner and chopper drives are recommended to be implemented early in the program. The purpose of these tests are to demonstrate the design reliability and to provide a degree of confidence in the design. Testing of this type of mechanism generally leads to design refinements, both mechanical and electrical. A one year life test is suggested with subsequent disassembly and wear measurements.

5.3 SYSTEM TESTS

After the instruments are assembled, various system level tests are performed to characterize various instrument responses and to provide inputs to data reduction software. Three types of tests for these purposes have been classified as thermal, optical and calibration tests.

5.3.1 Thermal Tests

Two varieties of thermal tests are recommended for specific but different purposes. These are thermal balance tests of the instruments and thermal response characterizations of the channels.

Thermal Balance Test The purpose of the thermal balance test is the verification of the thermal design of the instruments. As such, it needs to be performed in vacuum on the Engineering Models only. With temperature sensors mounted in various strategic points on the instrument, orbital fluxes are simulated to determine operating temperatures, gradients, and rates of change. Aperture coupling effects are also determined by varying the aperture temperatures with respect to the detector temperatures. By proper instrumentation, the gradients across both the apertures and the shortwave dome filters are measured.

Thermal Response Characterization The total channels of the nonscanning instrument measure the total earth radiation, both reflected and emitted. Over 99.5% of the reflected solar energy is measured by the shortwave channel. However this channel also measures a portion of the emitted radiation in the 3 to 5 micrometer spectrum and the quartz longwave leak (see Section 4.0). Emitted radiation from the dome filter also affects the shortwave response. The radiation interchange between the shortwave detector and its field of view can be broken down into the components $R + E_{SW} + E_{LW} + E_D$ where R is the refected irradiance, E_{SW} the emitted irradiance from 3 to 5 micrometers, E_{LW} the irradiance in the longwave leak, and E_D the dome irradiance. When the shortwave channel measurement is subtracted from the total channel, the difference is

$E_T - (R + E_{SW} + E_{LW} + E_D)$, where E_T is the total irradiance. The response to an emissive target, i.e., a blackbody, is $E_{SW} + E_{LW} + E_D$ in the shortwave channel and $E_T - (E_{SW} + E_{LW} + E_D)$, a first estimate of E_D, and, thereby, $E_{SW} + E_{LW}$, is determined in a first approximation (see Section 4.0). In a second iteration, fairly accurate values for E_D and $E_{SW} + E_{LW}$ can be determined. The percentage of $E_{SW} + E_{LW}$ as a function of E_T can then be determined for the expected range of Earth temperatures. These percentages can then be used for future data reduction to determine the exact reflected and emitted components. To perform these tests, wide field blackbody targets are needed for each channel. The target radiance measurements should be made by a cavity radiometer with the applicable field of view. Finally, the GCE and its software determine the dome irradiance, the extraneous transmitted emitted irradiance and aperture coupling.

A similar problem exists for the scanning channels, i.e., Channels 6 and 7. Although filter radiance is not a factor here, the same emitted radiance leaks exist for the shortwave channel. The longwave channel responds mostly to emitted radiance but will have some small response to reflected solar radiance and will not respond to a small amount of emitted radiance in the 3 to 5 μm range. The channel 6 response is then proportional to $R + E_{SW} + E_{LW}$ and the longwave channel response is proportional to $E_T + E_{SW} + R_{SW}$. Taking the responses of the two channels to a blackbody and summing them provides a total of $E_T + E_{LW}$, assuming that E_{SW} is the same for both channels. In the longwave portion of the spectrum the radiance has a linear variation with scene temperature. The combined channel response then can be expressed by an equation such as $AT^4 + BT + C$. The constants can be determined by the combined channel responses to three target temperatures, setting up three equations. It should be noted that the two channels are normalized prior to the addition for radiance response.

If the radiances omitted from the longwave channel and included in the shortwave channel are not equal (and they probably will not be), a reasonably good estimate can be made by convolving the system spectral response with the spectral radiance of the target using Planck's equation. The summed responses of Channels 6 and 7 then provides $E_T - E_{SW7} + E_{SW6} + E_{LW6}$ and the uncertainty in

the difference term $E_{SW6} - E_{SW7}$ should be small. A lookup table of these terms for the range of temperatures to be used in the test would be useful in the elimination of the difference term prior to proceeding as discussed above. Enough samples should be taken at each temperature to provide a statistically accurate average response.

Determination of the response of the longwave channel to reflected solar radiation does not lend itself to solution by testing. It is recommended that the accurately measured response of the longwave channel in the region between 3 and 6 micrometers be convolved with the expected spectral radiance of the sun. On a first approximation this can be determined from Planck's equation for a 5800K blackbody. A more accurate value may be determined using the Thekaekara model of the solar spectrum*. The ratio of this value to the total solar radiation multiplied by the corrected value for the reflected component measured by Channel 6. It should be emphasized that in ground tests with a solar simulator, the spectral response of that simulator must be known to provide a unique correction factor for that source in channel 7. Characterization of the error in terms in the non-scanning channels prior to system level calibration will allow software error term adjustments and accurate system calibrations.

During solar calibration, the non-scanning total channels have significant thermal coupling with the cylinder housing and the solar aperture (see Section 4.0). Since the total irradiance is only about 50 W/M^2, the effect on the shortwave channels is expected to be slight. The exact magnitude of this irradiance can be determined as a function of a range of instrument temperatures when viewing a cold blackbody target through the solar ports. From temperature sensors on the apertures, the cylindrical housing, and the detectors, and the channel response, the coupling constant can be determined. This could also be done in-orbit by observing space through the solar apertures before and after a sun observation.

*Matthew P. Thekaekara, "Extraterrestrial Solar Spectrum, 3000 - 6100 Å at 1 Å Intervals", Applied Optics, Vol. 13, No. 3, March 1974.

5.3.2 Optical System Tests

Three optical tests are recommended, including spectral response, field of view mapping and out of field response (scattering). These tests should probably precede the other system level tests.

Spectral Response It would be preferable to measure the entire system spectral response on a channel by channel basis. However, as the spectral resolution is increased and the bandwidth decreased, the amount of energy incident on the detector for generating a response diminishes. Of particular interest are the 3 to 6 micrometer range in the shortwave channels and the longwave channel, and the 30 to 100 micrometer range in the total and shortwave channels. Accurate system spectral response measurements in these areas aid in data analysis and reduction (see Section 5.3.1). If possible, then, system level spectral response measurements should be made. If that is not possible, component spectral response measurements, i.e., measurements of detectors, mirrors, filters, etc., should be convolved to determine the overall system response.

Field of View Mapping The field of view of channels 1 through 5 are dependent on the exact detector size, aperture opening and height, and detector uniformity of response. To establish the exact three dimensional response, hemispheric response plots every 45° are recommended. That is, plots should be made along the 0° - 180°, 45° - 225°, 90° - 270° and 135° - 315° axes over the angles of interest in divisions of approximately 1/10 the planar field of view. Use of a laser or other collimated source is suggested. It is also suggested that these measurements be made at two different wavelengths in each channel. The fields of view of Channels 6, 7 and 8 are set by a field stop. Three dimensional plots such as those described above are again recommended. A collimated white light source could be used for Channels 6 and 8 while an IR source would be appropriate for Channel 7.

Out Of Field Response The percentage of energy scattered to the detector from outside the field of view has been predicted for the wide field of view channels (see Section 4.0). Measurement of the out-of-field irradiance scattered onto

the field of view can be done as an extension of the field of view mapping. That is, continuation of the mapping beyond the nominal field may show small wings or fillets modifying the linear response of the field as it approaches the zero response point. Because the total scattered input is from an annulus around the field, the effect may not be noticeable with a single source at one field position due to the channel sensitivity. The source irradiance, therefore, will probably have to be increased when mapping in this area in order to see any response. The field response in this area can then be normalized by the ratio of the irradiances used in or out of the field.

Knowledge of the exact field response characteristics provides the exact solid angle field of view for calibration and will aid in later data interpretations.

5.3.3 Calibration

With the optical and thermal tests completed and the GCE software updated accordingly, the ERBSS instruments will be ready for calibration. These calibrations should include the instrument channels and inflight calibration targets and be performed both in-air and in-vacuum. The in-vacuum calibrations should be performed over a range of instrument temperatures as predicted by thermal models for orbital conditions. With the GCE software programs, it is expected that instrument precision and reproducibility will exceed the reproducibility of practical standards. Shortwave targets such as solar simulators, in particular, have been demonstratably unstable during ERB calibrations. The use of several cavity radiometers, with variable fields of view, which are referenced to and calibrated against a standard cavity maintained by the project, are recommended as transfer standards for the program. Their use will be described in the following sections.

5.3.3.1 Calibration of the Non-Scanning Instrument

During considerations of calibration techniques for the MFOV and WFOV channels, it became apparent that the medium field of view channels should be adjacent on the instrument as should the wide field of view channels. This will facilitate

the use of a single wide or medium field of view target for simultaneous testing of the two channels and iterative data reduction using outputs from both channels. Standard targets for these fields of view do not exist and the design and fabrication of suitable targets will be among the program tasks. Producing targets with highly uniform radiance over the fields of view required is expected to be difficult, particularly in the shortwave spectrum. Because of field of view overlaps, consecutive calibrations of the medium and wide field of view channels will probably be a necessity. Blackbody targets designed for minimal gradients are envisioned for use on testing not only the total channels but also the shortwave channels. Integrating spheres, similar to or identical to those produced under the guidance of Dr. Warren Hovis of NOAA for various instruments including the Coastal Zone Color Scanner (CZCS) and ERB for Nimbus-G, are recommended for shortwave and total channel calibrations. The interiors of these spheres are painted white while multiple banks of quartz-iodide lamps are maintained at nearly constant radiance by current control. The spherical shells can be temperature controlled by fluids.

A mechanized approach is suggested here with the target irradiance measured first by two cavity radiometers with fields of view identical to those being calibrated. The targets (or the cavities and instrument) will then be moved to the channels to be measured. An adequate number of data samples should then be taken to provide the statistics necessary to determine the average responses and the standard deviations. The cavity radiometers should have intra-channel spacings and apertures identical to those on the instrument. Four cavity radiometers are recommended for this purpose although it is conceivable that two cavities mechanized for variable spacing and apertures could be used. The exact fields of view of the cavity/aperture assemblies should be measured prior to calibration using the approach discussed in Section 5.3.2. To obtain highly accurate calibrations with non-uniform targets, the fields of view of the reference cavities and the channels need to be nearly identical. After channel calibrations, the targets should again be actuated to the cavities for another check of irradiance. All data from the instrument or test equipment should be sent to the GCE for processing. That is, the GCE should be designed for analysis of data from test equipment also. The four channels should be

calibrated at various irradiance levels (perhaps 10) by both targets and at various instrument temperatures (in vacuum).

During the "Earth looking" calibration, the four channels should be frequently rotated to the inflight calibration position, i.e., solar and blackbody. A solar simulator, monitored by a cavity or other sensor for intensity variation is directed at the solar ports during the solar calibration. Simultaneous viewing by all 5 channels would be preferable but consecutive illumination of each channel may be necessary using alignment mechanisms. Data is taken by the solar monitor in synchronism with channel data for normalization of intensity variations by the GCE. The solar simulator should be replaced by a cold wall (simulating space) at the solar ports either prior to or after the solar calibration for determining of thermal loading of the channels by the solar apertures and instrument housing during the solar measurement. After the inflight blackbody targets have been on long enough for stabilization, the channels are rotated to the blackbodies for calibration of the total channels. In this operation, the instrument serves as a transfer standard allowing the inflight blackbodies to be calibrated against the wide field blackbodies with traceability to the standard cavity.

The sequence of a typical calibration might be:

(1) Measurement of the blackbody target by the two cavities with MFOV apertures
(2) Movement of the target to the MFOV channels and measurements in those channels.
(3) The target is moved back to the MFOV cavities for remeasurement
(4) Blackbody target measurement by WFOV cavities
(5) WFOV blackbody calibration
(6) Blackbody remeasurement by WFOV cavities
(7) Rotation to inflight blackbody for calibration
(8) Measurement of shortwave target by MFOV cavities (with lights on and off to measure the emitted radiance with the lights off).
(9) Shortwave calibration of MFOV channels
(10) Shortwave target remeasurement by MFOV cavities

(11) Measurement of shortwave target by WFOV cavities
(12) Shortwave calibration of WFOV channels
(13) Remeasurement of shortwave target by WFOV cavities
(14) Rotation of channels to solar ports for space measurements
(15) Calibration through solar ports with solar simulator

The entire sequence is then repeated at different target radiances although inflight calibrations need not be made at each radiance level. The initial calibration would probably be done in air followed by the vacuum calibration. The in-vacuum calibration (the entire sequence) should be repeated at various instrument temperatures. The initial in-air and in-vacuum tests provide the baseline instrument characterization for additional in-air calibrations.

5.3.3.2 Calibrations of the Scanning Instrument

The scanning instrument channels should be calibrated using techniques and sequences similar to or identical to those used for the non-scanning instrument. Calibration should be performed both in the scanning and stopped modes of operation at nadir and at the in-flight targets as applicable to the design. The Earth looking calibration is performed with blackbody and shortwave targets (possibly the same targets used for the MFOV and WFOV channels) using a cavity radiometer with approximately a 3° by 6° field of view to measure the target radiance at the proper scan position. A sufficient number of samples for statistical purposes are then taken in the scanning and stopped mode in each channel. During calibration with the blackbody, samples are taken at the in-flight blackbody target scan position for calibration transfer via Channel 7. Similarly, samples are taken at the diffuser target position during calibration with the shortwave target in Channels 6 and 8.

The diffuser target is illuminated by the solar simulator which is monitored as it was during the solar calibration of the non-scanning instrument. It is suggested that the scanning instrument be designed for insertion of a 3° field of view cavity to view radiance from the diffuser during these calibrations. The sequence of calibration is as follows:

(1) Measurement of blackbody target with 3° X 6° cavity radiometer
(2) Calibration of scanning channels in scan mode
(3) Calibration of channels in stopped mode
(4) Remeasurement of blackbody target by cavity
(5) Calibration of inflight blackbody by Channel 7 in scan mode (as applicable)
(6) Calibration of inflight blackbody by Channel 7 in stopped mode (as applicable)
(7) Measurement of shortwave target with 3° x 6° cavity (lights on and off)
(8) Calibration of channels in scan mode
(9) Calibration of channels in stopped mode
(10) Remeasurement of shortwave target by cavity
(11) Calibration of diffuser target in scan mode (as applicable)
(12) Calibration of diffuser target in stopped mode (as applicable)

The entire sequence is then repeated at other target radiance levels. In vacuum, the instrument temperature is a variable for each complete sequence. During in-air testing, variable incidence angles should be used for the solar simulator radiance on the diffuser to characterize the reflectance of the diffuser.

5.4 GROUND CHECKOUT EQUIPMENT

The Ground Checkout Equipment (GCE) provides the spacecraft interface to the instruments. It also generates data products from raw data necessary to demonstrate instrument accuracy and precision.

5.4.1 Elements of the GCE

As a minimum, it is suggested that the GCE should include:

- Power supplies
- System clocks
- Command Panel
- TIP (TIROS Information Processor) Simulator
- TTY

- Mini-Computer
- Printer/Plotter
- Tape Recorder
- Cavity Radiometer Interfaces
- Target Monitor Interfaces
- Mechanism Controls
- Oscilloscope

Data products are corrected data, analysis results, command status', housekeeping telemetry data, field of view plots and limits status' of critical parameters.

Data reduction will be performed simultaneously with data recording and storage.

5.4.2 Software

As previously indicated, a prime function of the GCE is the reduction of instrument channel data through iterative processes. In practice the earth looking medium and wide field of view channel data is corrected as follows:

(1) Correction of total channel for aperture/detector coupling
(2) Subtraction of shortware from the total channel to determine, on a first look basis, the longwave value.
(3) Correction of shortwave for dome gradients, longwave and 3 to 5 micrometer leaks of emitted radiation.
(4) Redetermination of longwave component from corrected shortwave value.
(5) Final shortwave computation from redetermined longwave coupling to dome.

Final data products are thus provided for the MFOV and WFOV shortwave and longwave energy components. Corrections are made from lookup tables derived from test results, and housekeeping data and channel data algorithms. Final calibration data for a constant source are averaged and the standard deviation of the samples computed. The average values and the measured source radiances (by the cavity radiometers) are combined and a least squares best fit straight

line function determined to characterize the data. Other analysis programs should include solar and inflight calibration data correction, scanning channel earth looking data correction, scanning channel calibration data correction, field of view plots, solid angle field of view corrections and channel coregistration results.